United States
Environmental Protection
Agency

Washington
DC 20460

EPA 520/1-78-001A

EPA

Protective Action Evaluation Part I

The Effectiveness of Sheltering as a Protective Action Against Nuclear Accidents Involving Gaseous Releases

LEGAL NOTICE

This report was prepared as an account of work sponsored by the Environmental Protection Agency of the United States Government under Contract No. 68-01-3223. Neither the United States nor the United States Environmental Protection Agency makes any warranty, express or implied, or assumes any legal liability or responsibility for the accuracy, completeness or usefulness of any information, apparatus, product or process disclosed, or represents that its use would not infringe privately owned rights.

PROTECTIVE ACTION EVALUATION

PART I

THE EFFECTIVENESS OF SHELTERING AS A PROTECTIVE ACTION AGAINST NUCLEAR ACCIDENTS INVOLVING GASEOUS RELEASES

APRIL 1978

George H. Anno
Michael A. Dore

Prepared for

U.S. Environmental Protection Agency
Office of Radiation Programs
Washington, D.C. 20460

FOREWORD

The Office of Radiation Programs carries out a national program designed to evaluate the exposure of man to ionizing and nonionizing radiation, and to promote the development of controls necessary to protect the public health and safety and assure environmental quality.

Office of Radiation Programs technical reports allow comprehensive and rapid publishing of the results of intramural and contract projects. The reports are distributed to groups who have known interests in this type of information such as the Nuclear Regulatory Commission, the Department of Energy, and State radiation control agencies. These reports are also provided to the National Technical Information Service in order that they may be readily available to the scientific community and to the public.

Comments on this report, as well as any new information, would be welcomed; they may be sent to the Director, Environmental Analysis Division (AW-461), Office of Radiation Programs, U.S. Environmental Protection Agency, Washington, D.C. 20460.

W. D. Rowe, Ph.D.
Deputy Assistant Administrator
for Radiation Programs

PREFACE

The material contained in this report was sponsored by the U.S. Environmental Protection Agency under the technical guidance of Mr. J. Logsdon of the Office of Radiation Programs, Environmental Analysis Division. Based on a study to assess the application and utility of sheltering and evacuation as specific protective measures in the event of accidental releases of gaseous radioactive material from nuclear power plants, this report is the first of two that deal specifically with the effectiveness of public shelter structures.

The second report evaluates both sheltering and evacuation protection measures from the standpoint of providing technical guidance in formulating emergency planning procedures.

The purpose of this contract report is to provide a technical basis for EPA to develop guidance with regard to actions to protect the public from accidental airborne releases of radioactive material from nuclear power facilities. The information in this report should not be construed as guidance from EPA to State and local officials in development of their radiological emergency response plans. Such guidance will be published in the "Manual of Protective Action Guides and Protective Actions for Nuclear Incidents," currently under development by the EPA Office of Radiation Programs. The Environmental Protection Agency is making this report available as a source of technical information.

TABLE OF CONTENTS

PREFACE iii

LIST OF FIGURES vii

LIST OF TABLES ix

I. INTRODUCTION 1

II. ANALYSIS 3

RADIONUCLIDE SOURCES 3

SHELTER STRUCTURE MODEL 5

FALLOUT GAMMA-SOURCE ATTENUATION 19

TIME-FRAME MODEL 28

DOSE REDUCTION FACTOR 32

DOSE COMPONENTS--UNSHELTERED 35

DOSE COMPONENTS--SHELTERED 37

SHELTERING AND EVACUATION 43

III. RESULTS 51

IV. CONCLUSIONS AND RECOMMENDATIONS 85

Appendix A: Fallout Gamma Source 92

Appendix B: Dose Reduction Factor 94

REFERENCES 103

TABLE OF CONTENTS

Fig. 1--Attenuation Comparisons--Infinite Water Medium 14

2--Shelter-Structure, Cloud Gamma-Attenuation Geometry . . . 15

3--Attenuation for Structure Walls and Roof--Cloud Source 17

4--Finite Cloud, Gamma Dose-Correction Factors Versus Gamma Energy 20

5--Finite Cloud, Gamma Dose-Correction Factor Versus Effective Shelter Radius 21

6--Gamma Attenuation for Structures--Fallout Source 22

7--Finite Plane Source, Geometry-Correction Factor for 1 MeV Gammas 27

8--Sheltering-Model Time-Frame 29

9--Sheltering and Evacuation 45

10--Air Exchange and Infiltration Rates in Closed Passenger Compartment When Air Conditioning is Set at a Maximum . . 47

11--WB DRF Versus T_2, (T_1=0,T_a=1) 53

12--Thyroid DRF Versus T_2, (T_1=0,T_a=1) 56

13--WB DRF Versus T_a, (T_1=0,T_2=0), L = 1 57

14--WB DRF Versus T_a, Case A, (T_1=0,T_2=0), (T_1=0.25,T_2=0.5), L = 1 58

15--WB DRF Versus T_a, Case B, (T_1=0,T_2=0), (T_1=0.25,T_2=0.5), L = 1 59

16--WB DRF Versus T_a, Case C, (T_1=0,T_2=0), (T_1=0.25,T_2=0.5), L = 1 60

17--WB DRF Versus L, (T_1=0,T_2=0,T_a=1) 62

18--Thyroid DRF Versus L, (T_1=0,T_2=0,T_a=1) 63

19--WB DRF Versus L, Case A, (T_1=0,T_2=0), (T_1=0.25,T_2=0.5), T_a = 1 64

Fig. 20--WB DRF Versus L, Case B, (T_1=0,T_2=0), (T_1=0.25,T_2=0.5), T_a = 1 65

21--WB DRF Versus L, Case C, (T_1=0,T_2=0), (T_1=0.25,T_2=0.5), T_a = 1 66

22--Thyroid DRF Versus L, (T_1=0,T_2=0), (T_1=0.25,T_2=0.5), T_a = 1 67

23--WB DRF Versus T_2, Case B, LS, T_a = 1 69

24--WB DRF Versus T_2, Case B, SS, T_a = 1 70

25--Thyroid DRF Versus T_2, Case B, T_a = 1 71

26--WB DRF Versus T_2, Case B, SS (A=0.4,0.6,0.9,L=0.125, 1.0,2.0) 72

27--WB DRF Versus T_2, Case B, LS (A=0.05,0.1,0.2,L=0.125, 1.0,2.0) 73

28--WB DRF Versus T_1, Case B, (T_a=1,T_2=0), SS (L=0.5,1.0, 1.5), LS (L=2) 75

29--Thyroid DRF Versus T_1, Case B, (T_a=1,T_2=0), L = 0.5, 1.0, 1.5, 2.0 76

30--WB and Thyroid DRF Versus T_1, Case B, (T_a=1,T_2=0,L=0.125) 77

31--WB and Thyroid DRF Versus T_1, Case B, (T_a=1,T_2=0.25,L=1.0) 78

32--WB DRF Versus Iodine Ingress Fraction, Case B, (T_1=0,T_2=0,T_a=1) 79

33--Sheltering with Evacuation, WB, SS--Transit Time Versus Shelter Time (T_a=0.5) 81

34--Sheltering with Evacuation, WB, LS--Transit Time Versus Shelter Time (T_a=0.5) 82

35--Sheltering with Evacuation, Thyroid--Transit Time Versus Shelter Time (T_a=0.5) 83

LIST OF TABLES

Table 1. Radionuclide Source Data 4

2. Air Changes Taking Place Under Average Conditions in Residences, Exclusive of Air Provided for Ventilation . . . 8

3. Representative Cloud-Gamma Attenuation Factors 18

4. Representative Reduction Factors for Surface Source 24

5. Dose Components 34

6. Fixed Parameter Summary 52

I. INTRODUCTION

In the event of an airborne release of radioactive material from a nuclear power plant accident, sheltering of individuals is an important consideration in emergency protective action planning as it may be 1) an effective means of significantly reducing radiation dosages; 2) the only practical option in view of possible time and logistic constraints. Moreover, most people in urban areas, for example, spend 75 percent of their time indoors.

This report describes an analysis to estimate the effectiveness or benefit that might be derived from sheltering following a release of gaseous fission products from an operating nuclear power station. The objective of this effort is the development of sheltering effectiveness information that could provide general guidance to those responsible for formulating required emergency plans for nuclear power plant siting. Accordingly, the approach taken here does not lend itself to the specific evaluation of shelter structures involving detailed descriptions and operational scenarios; but rather focuses more broadly on what are deemed to be the essential parameters and their variations, and the general characteristics of small and large categories of shelter structures available to the public. Shelter effectiveness as referred to in this report is the ratio of the dose that may be incurred with sheltering conditions to that without sheltering in the open, specifically defined as the dose reduction factor (DRF). DRF estimates for different conditions of source release, shelter structure assumptions, and operational time parameters are made for both whole-body and thyroid doses separately, based on a single-compartment structural model of the time-varying outside and inside gaseous radionuclide sources of krypton, xenon, and iodine.

Design basis accident (DBA) assumptions are made for the gaseous radionuclide release to define the proportion of rare gases and radioiodines. The magnitude of the release and dose estimates are based on radionuclide data from *The Reactor Safety Study* (WASH-1400) [1]. However, inasmuch as the DRF, as defined above, is the key index used to characterize the effectiveness of sheltering, it is not sensitive to the

absolute source release magnitude insofar as an approximate proportionality is maintained among the individual radionuclide sources. Source release time and duration assumptions are related to release categories given in Ref. 1 as PWR 1, PWR 3, and PWR 4, for which release times range from 1.5 to 2.5 hr and the release duration ranges from 0.5 to 3 hr.

The basic shelter model characteristics considered are gamma ray attenuation, source geometry, gaseous fission-product ingress, and air change rate. Numerical values used for DRF calculations are based on a literature review and some assumptions that are made where data are sparse or lacking.

Temporal parameters considered are source release time and duration, cloud travel time, and time spent in the shelter structure. These parameters are used to illustrate the sensitivity of sheltering effectiveness to variations in parameter values. Also, the analysis of shelter effectiveness is based on a time-frame model, which can be conveniently related to other operational times important for emergency planning (e.g., information time-delay and reaction time) required to accomplish the protective action--in this case, sheltering. In addition to developing shelter-effectiveness estimates parametrically, the advantage of exiting and evacuating the vicinity of the shelter area after some initial time in the shelter is analyzed from the standpoint of the DRF and temporal considerations.

II. ANALYSIS

RADIONUCLIDE SOURCES

Table 1 gives the radionuclides and associated data used in this study to simulate a fission-product release of the rare gases (Xe and Kr) and the significant radioiodines. The Xe, Kr, and I radionuclide sources and parameters shown are essentially the same as those given in WASH-1400, Appendix VI [1], with the exception of Xe-133m and Xe-135m, which have been added for completeness only, since they would not affect results significantly.

Fission-product source inventory data based on ORIGEN Code calculations [2] were used to estimate the Xe-133m and Xe-135m sources listed in Table 1, based on a 550-day irradiation period (same as Ref. 1). Since the decay half-life of Xe-135m decaying to Xe-135 is short (15.6 min) considering the times of interest (hours) in this study, the estimated shutdown zero-time Xe-135m inventory was added to the Xe-135 source on a mass basis and converted to Xe-135 on an activity basis, which increases to 0.27 Ci instead of 0.26 Ci given for Xe-135 in Ref. 1. The metastable decay half-life for Xe-133 is by comparison appreciable, and no similar adjustment for the Xe-133 source inventory was made.

The average decay gamma energies listed in Table 1 for the metastable Xe radionuclides were taken from Ref. 3 (pp. 32-33); the whole-body (WB) cloud gamma-dose factors, from Appendix D, Ref. 1. These dose factors for the ground-γ (surface deposition source) do not take ground roughness into effect (such as a factor of 2). The estimated effectiveness values in terms of a dose-reduction factor would not be affected significantly whether or not the ground roughness adjustment were included.

An estimate of the average gamma decay energy was made for the source nuclides to serve as a guide in 1) estimating gamma ray attenuation factors for shelter structures and also in 2) making estimated adjustments for finite source geometries of cloud-source volume and contaminated floor-surface spaces inside the structure, since the dose factors for cloud-γ and ground-γ apply to infinite source geometries

Table 1

RADIONUCLIDE SOURCE DATA

Nuclide	Half-Life (hr)	Source (Curies ÷ 10^8) (Q)	Average Gamma Energy (MeV) (E)	Dose Factors			
				Cloud-γ $\frac{(rem/sec)}{(Ci/m^3)}$	Ground-γ $\frac{(rem/hr)}{(Ci/m^2)}$	WBD (50-yr) (rem/Ci)	Thyroid (50-yr) (rem/Ci)
Kr-85	93,600	0.006	0.0	0.0	0.0	0.0	0.0
Kr-85m	4.32	0.26	0.16	0.036	↓	↓	↓
Kr-87	1.27	0.52	0.82	0.36			
Kr-88	2.78	0.76	2.21	0.42			
Xe-133	127	1.7	0.08	0.007			
Xe-133m	55.2	0.04[a]	0.23[b]	0.0075[c]			
Xe-135	9.12	0.27[a]	0.26	0.06			
Xe-135m	0.27	0.27[a]	0.52[b]	0.0972[c]			
I-131	193	0.85	0.39	0.09	2.8	2,600	1.47×10^6
I-132	2.4	1.2	2.3	0.55	17	130	5.3×10^4
I-133	21	1.7	0.63	0.12	3.7	570	3.96×10^5
I-134	0.864	2.0	2.4	0.6	16	40	2.5×10^4
I-135	6.72	1.5	1.45	0.42	12	290	1.23×10^5

[a]Based on Refs. 1 and 2.

[b]Ref. 3.

[c]Ref. 4.

(discussed below, p. 13ff.). The average gamma decay energy was estimated to be ∿1.2 MeV, based on the following simple weighting relationship:

$$\langle E \rangle = \frac{\sum_j Q_j E_j \mu_e(E_j)}{\sum_j Q_j \mu_e(E_j)} ,$$

where Q_j and E_j are the radionuclide source activities and gamma energies, respectively, listed in Table 1, and $\mu_e(E_j)$ is the gamma-ray linear energy absorption coefficient as a function of energy for air given in Ref. 5. The estimate of the average gamma ray energy was based on a summation over all the radionuclides shown in Table 1, with the exception of Xe-135m--again because of its short half-life for the times of interest in this study. The gaseous radionuclide data in Table 1 are used to estimate shelter effectiveness in dose reduction by summing each nuclide contribution (assuming single radionuclide decay) to obtain the unprotected (outside shelter) and protected (inside shelter) dose. Design basis assumptions (DBA) are made for the source release--100 percent of the noble gases and 25 percent of the radioiodines available for release.

SHELTER STRUCTURE MODEL

A simplified approach rather than a detailed investigation was adopted to account for those factors that might contribute to the benefits of seeking structural shelter in the event of a gaseous, radioactive fission-product release from a nuclear power facility accident. The reasons for taking this approach are as follows:

1. Explicit consideration of all types of possible structures that may be available for shelter--single-family dwellings, apartment buildings, office buildings, subways, tunnels, factories, and vehicles, etc.--would require an analysis beyond the scope of this effort because of the large variability in the parameters that determine effectiveness.

2. In many instances, reliable parameter data are not available; e.g., the actual chemical/physical form of the "gaseous" constituents at some distant point from the source release and the ingress of, in particular, radioiodine into shelter structures.
3. The main purpose of this study is best served by providing overall technical guidance information as to the effectiveness of using a shelter structure based on some assumed conditions for shielding and ventilation rates without specifically focusing on detailed physical description and analysis of shelter structures.

After a review of the literature dealing with the key parameters of this study's simplified model (in keeping with the above reasons), calculations were performed using parameters selected to simulate what this study classifies as "small" and "large" structures (SS and LS) to illustrate the relative effectiveness of typical single-family dwellings and of larger structures such as office buildings, auditoriums, apartment complexes, etc. In developing the shelter model, consideration was given to account for the following possible avenues of exposure to shelter inhabitants:

- External WB dose from airborne radioactive material both outside (shielded) and inside (unshielded) the shelter structure.
- Inhalation WB and thyroid dose from airborne radioactive material inside the shelter structure.
- External WB dose from radioactive fallout material deposited both outside (shielded) and inside (unshielded) the shelter structure.

In this study, beta skin dose was not considered, as it is assumed to be of secondary importance as compared with WB and thyroid dose considerations. The external WB doses (cloud-γ and fallout-γ) are based solely on radionuclide-decay gamma radiation in which both shelter-structure attenuation and finite source geometry factors are included in the model as discussed below.

The entry of outside airborne radioactive cloud material is assumed to be dependent on the shelter-structure ventilation rate (forced, natural, or both) assuming constant homogeneous mixing based on simple one-compartment outside/inside air exchange. This type of stirred-tank mixing and ventilation model has been applied in studies of the relationship between indoor/outdoor pollutants (e.g., NO, NO_2, CO, and O_3) and has predicted concentration versus time profiles that are similar to those measured [6]. The radioiodine fallout deposition inside the shelter is then also assumed to be dependent on the ventilation rate as well as the fallout deposition velocity; these aspects are also discussed below.

Shelter Structure Ventilation

A review of literature on ventilation rates of homes and buildings indicates a wide variety of air change estimates ranging anywhere from ~0.1 to 6 per hour for single-family dwellings to ~1 to 9 changes per hour for large structures. The wide ranges are, of course, due to the various types of construction--whether the portals and windows were shut or sealed, and such environmental factors as wind speed, temperature differential, and humidity. Also, in some instances, it was not clear whether air change rates included internal forced-air systems.

A review by Handley and Barton [7] of published information on home ventilation rates resulted in their suggesting the use of the range from 0.5 to 1.5 air changes per hour for homes and 2.0 air changes per hour for modern high-rise apartment buildings. A check with commercial home air-conditioning and heating vendors seems to generally support those recommendations. For example, usually a 4-ton (1600 cfm) unit is recommended for a 1500-ft^2 single-family dwelling with from 10- to 20-percent outside air makeup. Such an installation results in from 0.8 to 1.6 air changes per hour with outside air. Of course, some systems are installed for complete internal recirculation with no outside air makeup other than normal expected structural leakage.

Municipal code requirements for building ventilation rates--for high-rise office buildings, large apartment complexes, auditoriums, etc.--also seem to support the value of two air changes per hour as suggested by Handley and Barton [7]. For example, a check with the

Health Division of the Los Angeles City Building and Safety Department [8] indicated internal air turnover time of from 5 to 10 min depending on occupancy requirements, with a representative value of about 7 min--with 15 percent outside air makeup as a comfort-level requirement--which corresponds to 0.9 and 1.8 air changes per hour and ∿1.3 air changes per hour. Considering the above data, the rates for single-family dwellings and large structures are generally comparable, assuming internal forced-air systems.

In the absence of forced-air ventilation systems, home and building air change rates would be expected to vary much more widely--as indicated by the published data examined by Handley and Barton [7]. This conclusion is also supported by observations of Yocom, *et al.* [9] who note that particulate pollutant levels are lower in public buildings than in homes. The *ASHRAE Handbook of Fundamentals* [10] points to the lack of published data on air change rates for different buildings, exclusive of air provided for ventilation, when utilizing the air change method for estimating infiltration* requires experience and judgment. Table 2 gives *ASHRAE Handbook* values that may be used with reasonable precision in making infiltration estimates for residences with different room conditions.

Table 2

AIR CHANGES TAKING PLACE UNDER AVERAGE CONDITIONS IN RESIDENCES, EXCLUSIVE OF AIR PROVIDED FOR VENTILATION

Kind of Room or Building	Number of Air Changes Taking Place per Hour [a]
Rooms with no windows or exterior doors	1/2
Rooms with windows or exterior doors on one side	1
Rooms with windows or exterior doors on two sides	1 1/2
Rooms with windows or exterior doors on three sides	2
Entrance halls	2

[a]For rooms with weatherstripped windows or with storm sash, use two-thirds these values.

*The other is the "crack method" based on measured leakage characteristics of the building components and selected pressure differences.

Another approach in making air change estimates due to natural ventilation for houses is given by Coblentz and Achenbach [11], who suggest the following empirical relationship in which the air change rate is proportional to the outside wind speed and inside/outside temperature differential (i.e., without inside forced ventilation):

$$I \text{ (changes/hr)} = A + BW + C\Delta T \quad ,$$

where

A = air change rate for $W = 0$, $\Delta T = 0$ (0.12 to 0.18),

$B = 0.013$,

$C = 0.005$,

W = wind speed, mph,

$\Delta T = T_{inside} - T_{outside}$, °F .

Assuming the upper limit of $A = 0.18$ and $\Delta T = 20°F$ gives air change rates of about 0.35 per hour for a 5-mph wind speed and about 0.5 for 15- to 20-mph wind speeds, which appears to be somewhat on the low side compared with other data reviewed. This difference, however, may be due to new, well-built houses that made up part of Coblentz and Achenbach's field samples. In contrast, measured air change rates given by Megaw [12] for a hut structure that were made in conjunction with radioiodine penetration experiments were substantially higher, ranging anywhere from about 2 per hour to 8 per hour (the latter, however, for open windows). An examination of Megaw's data reveals an indication of air-change-rate proportionality with outside wind speed that, roughly, was about 0.5 (changes/hr) per (mi/hr). This figure corresponds to only an "eyeball" estimate from Megaw's data, which are complicated by variations in wind direction. Such variations would give rise to different pressure differential distributions due to asymmetric flow patterns, which would affect the internal air change rate.

Based on the above review of air change rates that might be expected for single-family dwellings (small structures) and various building structures that could be used as temporary public shelters, values of from 0.125 to 3 air changes per hour were assumed in performing shelter-structure effectiveness calculations. It was felt that ~0.125 changes

per hour might represent relatively "tight" structures (either large or small) and that ∿3 air changes per hour might represent a practical upper limit of structural ventilation. Of course, as indicated, much larger values of 6 to 9 air changes per hour have been measured; but it was felt that these values would represent extreme cases (e.g., open windows or portals), which do not represent practical cases if good planning is assumed.

Gaseous Fission-Product Ingress

The extent to which radioiodine will penetrate a structural shielding facility is dependent on the gross tightness of the structure, the ventilation rate, filtration, and the chemical and physical properties of the released material and the interacting species. Many of these facets of a gaseous fission-product release from a nuclear accident are currently unknown, particularly for radioiodine, which leads to difficulty in accurately predicting the ingress of gaseous radioactive material into shelter structures. For the rare gases (Xe and Kr), most are willing to accept virtually no effective "structural filtering," because of their inertness and stability as gaseous forms. Accordingly, in this study no effective filtering action has been included in estimating their internal structure concentrations.

For the halogens, which are here assumed to be all radioiodines, the case is more complicated and suffers from scarcity of experimental work on indoor/outdoor pollutant-level relationships dealing with the ingress of radioiodine into various potential sheltering structures. The radioiodines are of course particularly important sources due to their large contribution to the WB dose, as well as being totally responsible for the thyroid dose.

Three known chemical forms of radioiodine present as airborne gaseous species in power-station areas during and after handling defective fuel elements are elemental iodine (I_2), hypoidous acid (HOI), and organic iodides (CH_3I). The ratio of the three species would depend on the conditions under which an accidental release might take place. Elemental iodine is thought to be the primary form released from uranium-oxide fuel. It hydrolyzes rapidly in water, generating HOI, or

it forms organic iodides through a slower reaction with organic compounds, with relative stability in air increasing in the following order [13]:

$$I_2 < HOI < CH_3I$$

The actual chemical/physical form of the radioiodine that would be present at some off-site point is yet another question; however, probably very little protection would be offered by a structure against the ingress of HOI and CH_3I, both unreactive gaseous forms like Xe and Kr [14]. *The Reactor Safety Study* [1] did consider other possible forms of radioiodine that could be released (e.g., HI, CsI, and ZrI), but concluded that these forms would not be major species as they had not been verified experimentally. In its dose calculations, Ref. 1 assumes, primarily, elemental iodine; and, to a much lesser extent, organic iodide (approximately a factor of 100 less). However, assuming elemental iodine release to the atmosphere, controlled field release tests [15] involving elemental iodine (I_2-131) indicated a rapid transformation in apparent particle size from the source--in that the field sampling results for the released gaseous product (effective MMD ≈ 2Å) revealed a much broader spectrum of sizes, closely resembling the normal distribution by size, of particles in the atmosphere (with an MMD ≈ 0.4 microns). The above would suggest some effectiveness of shelter structures in reducing radioiodine ingress released in the elemental form, depending, of course, on overall integrity, ventilation, filtering, etc.

Estimates of radioiodine ingress into structures for this study are primarily based on the observations and work of Megaw [12], which represents essentially the only source of published information applicable to this study; other related, but not applicable, work [16] has been sponsored by the Office of Civil Defense (Defense Civil Preparedness Agency). Megaw's work originated from the accidental Wind scale incident in which it was estimated that dose rates inside buildings may be from about 14 to 25 percent of those outside. Subsequent experimental measurements were made by Megaw involving radioiodine

releases and a reasonably tight wooden hut; and he concluded that the time integral of the inside concentration (dose) may be from 20 to 80 percent of that outside, depending on wind velocity and direction.

An examination of Megaw's published data [12] does not suggest any correlation of the inside-to-outside dose ratio with either outside wind velocity or ventilation rate, probably because of the varying conditions under which measurements were made; e.g., measurements were made for unique sets of wind direction and velocity. A simple statistical analysis of the data indicates a protection factor (ratio of inside to outside dose) of 0.51 ± 0.12 (pooling the data from two experiments described). From Megaw's work, however, it is not possible to identify precisely the extent of the radioiodine filtering action or resistance to ingress for use in a simple mixing model such as is assumed for this study, even for the test structure used in the experiment, because of the absence of experimental information regarding source release time and intensity distribution and the absence of any correlation of the inside-to-outside dose ratio with ventilation rate. The dose reduction factors given by Megaw are therefore effective values that would include any filtering or ingress action of the shelter structure used in the experiment plus the specific test conditions and parameters. However, to take into account what is felt to amount to some gross filtering action for radioiodine--whether assumed to be due to trapping or deposition in small cracks or openings--the above-mentioned value of 0.51 has been tacitly assumed in approximating the explicit filtering action for shelter structures.

Radioiodine Deposition

Shelter effectiveness estimates in this study take into account external WB dosages from outside and inside radioiodine source deposition, using estimates for the deposition velocity, V_g. Values ranging from 0.1 to 1 cm/sec were obtained from controlled environmental radioiodine tests made at the National Reactor Testing Station in Idaho [15]. For outside radioiodine deposition velocity, the *Reactor Safety Study* [1] used a value of 0.5 cm/sec, which is also assumed in this study for surfaces outside a shelter structure.

Inside a shelter, a value of 0.025 cm/sec was assumed for the radioiodine deposition velocity for the floor surface, based on Megaw's work in which he estimated the inside deposition velocity to be only about 5 percent of the outside deposition velocity [12].

Cloud-Gamma Attenuation

The attenuation of cloud-gamma radiation that might be afforded by building structures has been estimated by Burson and Profio [17]; the results of their analyses served as a guide for estimating the cloud-gamma attenuation factors used in this study. The source basis for the attenuation calculations that were performed applies to the PWR Category 2 accident [17] ten miles from the plant, under average dry meteorological conditions. Figure 1 shows comparison of mass-path attenuation for different energies based on dose buildup and exponential attenuation in water. Since, for the source energies of interest, most of the attenuation will be due to Compton scattering--where Z/A remains relatively constant at about 0.5--water data (mass-path) are suitable for application to the usual structural materials such as wood, concrete, brick, and even steel [17]. As shown in Fig. 1, for mass-path thicknesses of interest up to $\sim$45 gm/cm^2, attenuation values--particularly, for reactor-accident spectra (ground and cloud source) and Co-60--are all quite close. Moreover, slight variations in the spectrum are not considered significant, since the higher-energy gamma rays would be the most penetrating and any differences in attenuation would not amount to any major source of uncertainty considering the other assumptions made in this study.

Burson and Profio's attenuation factors [17] used in this study are based on calculations assuming a simple hemispherical shell model (Fig. 2). Estimates were made of the gamma attenuation (with the dose point at the origin) for the portion of radioactive cloud material outside the shelter, based on numerical evaluation of the attenuation, A(x), given by a relationship of the form

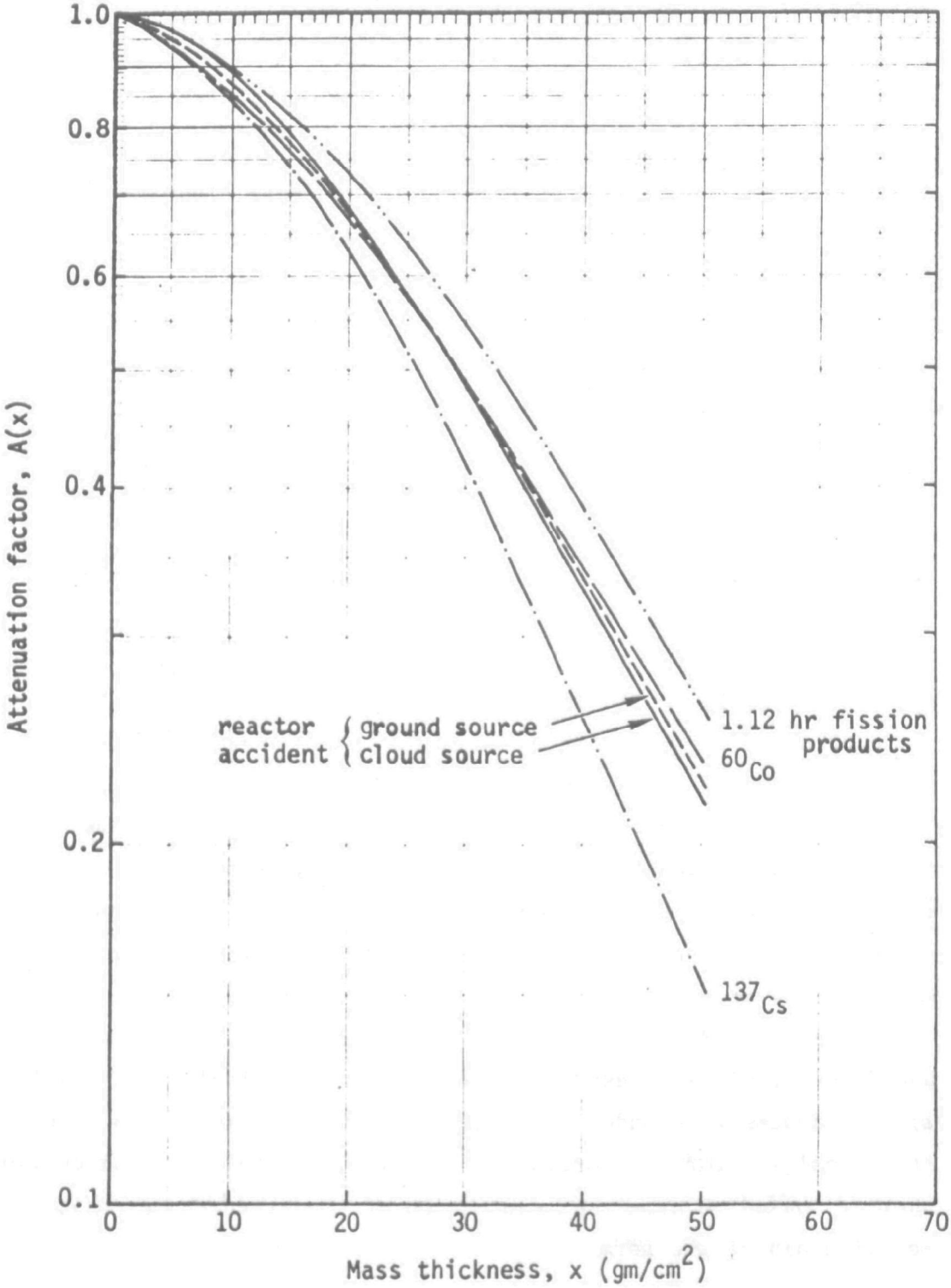

Fig. 1--Attenuation comparisons--infinite water medium

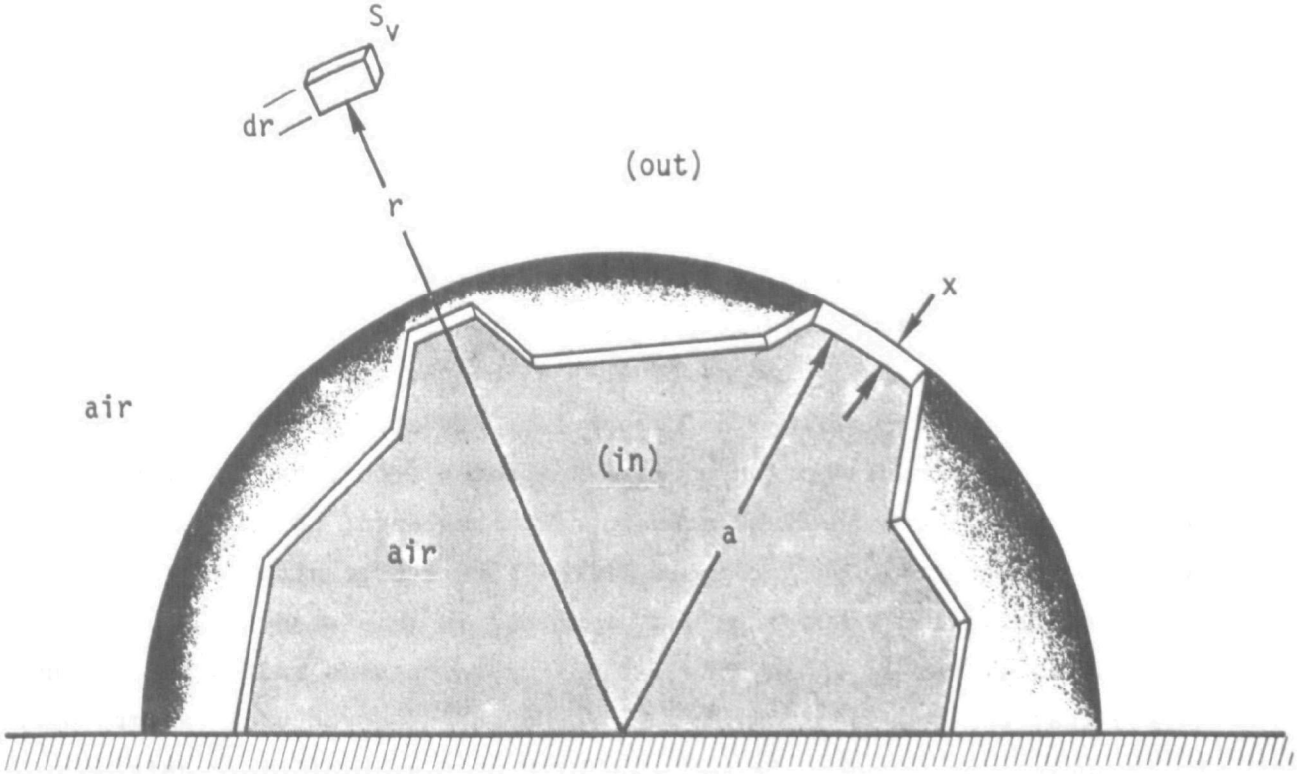

Fig. 2--Shelter-structure, cloud gamma-attenuation geometry

$$A(x) = \frac{\sum_{\substack{\text{gamma}\\ \text{energies}}} KS_v \int_a^R B(\mu_a r+\mu_w x)\, e^{-(\mu_a r+\mu_w x)}\, dr}{\sum_{\substack{\text{gamma}\\ \text{energies}}} KS_v \int_a^R B(\mu_a r)\, e^{-\mu_a r}\, dr} ,$$

where μ_a and μ_w are the energy-dependent gamma-ray absorption coefficients for air and water, respectively; and K and S_v are the energy-dependent dose-conversion and volume-source terms, respectively; and B is the dose buildup factor. Figure 3, a plot of the gamma ray attenuation for accident spectra for a = 3 m and μR = 3, is applicable for estimating gamma ray attenuation for structures of a wide variety of enclosure sizes (effective radii, a), since A(x) is relatively insensitive to a, because of the low density of air (1.293×10^{-3} gm/cm^3) as compared to structural material. Also, very little dose contribution would be expected from cloud sources beyond about three mean-free paths in air; therefore, μR = 3 is a reasonable approximation for an infinite cloud source with regard to the gamma-radiation transport considerations in this study.

The estimates of gamma attenuation for an outside radioactive cloud source that can be made from Fig. 3 depend on the structural assumptions. For example, for a wooden frame house with roof and ceiling consisting of 1/4-in. wood or asphalt shingles, 3/4 in. of wood sheathing and rafters, and 1/2 in. of gypsum board, the mass thickness would be

$$1.5 \text{ (in.)} \times 2.54 \text{ (cm/in.)} \times 0.84 \text{ (gm/cm}^3\text{)} \approx 3.2 \text{ gm/cm}^2$$

where A(x) ≈ 0.9. Better protection would be afforded by a small house with a wooden roof and masonry walls. For example, assuming half the 2π solid angle (Fig. 2) to be subtended by the walls and the other half by the roof, the overall attenuation factor would be

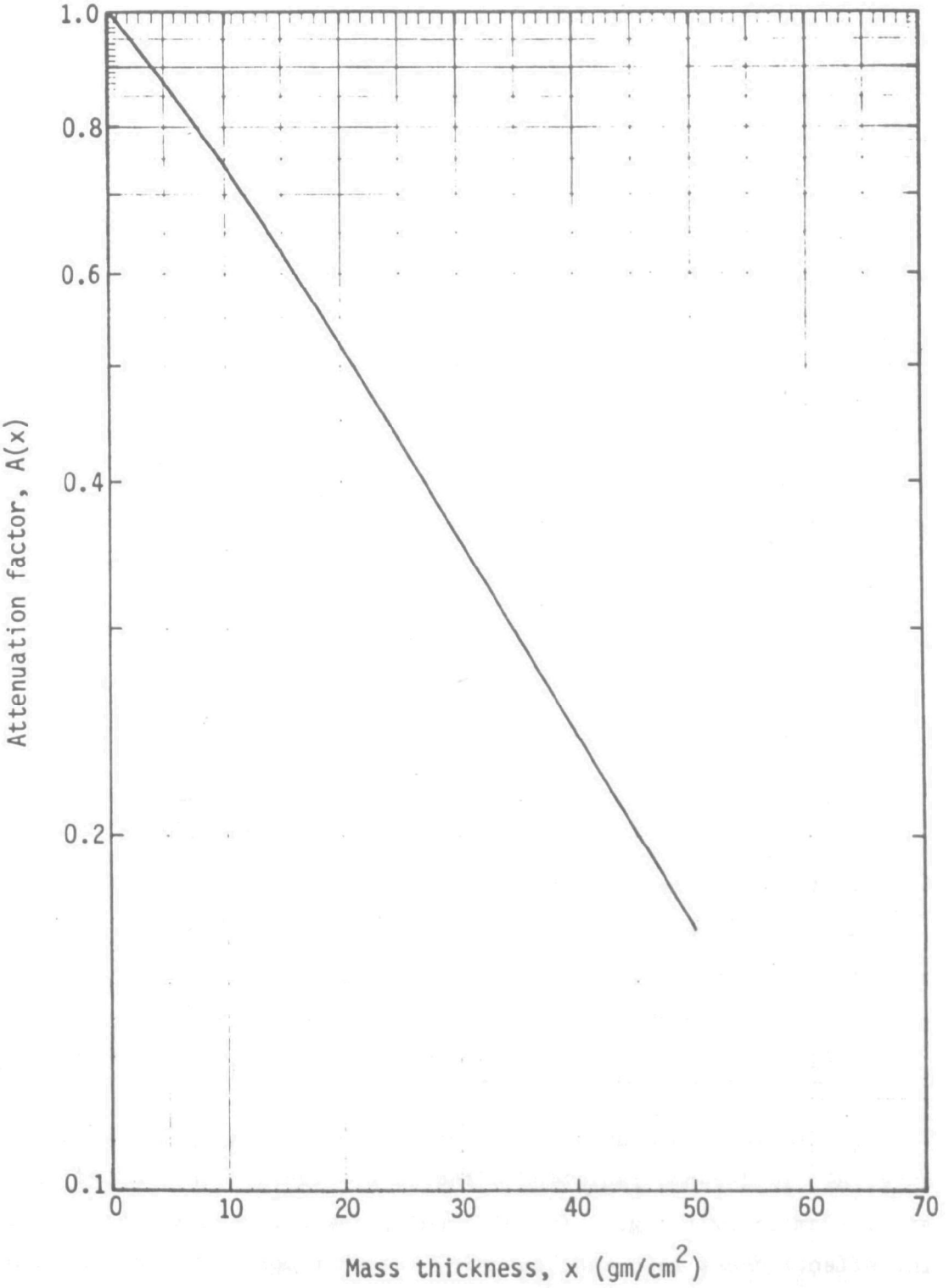

Fig. 3--Attenuation for structure walls and roof--cloud source

$$0.5 \times (0.9) + 0.5(0.38) = 0.64 \quad ,$$

where the attenuation for the walls (0.38) is based on a wall-mass thickness of

$$4 \text{ (in.)} \times 2.54 \text{ (cm/in.)} \times 2.7 \text{ (gm/cm}^3\text{)} \approx 28 \text{ gm/cm}^2 \quad ,$$

(assuming 8-in. concrete bricks with a 50-percent void volume).

Attenuation of cloud-gamma radiation for large structures such as office buildings and multistory structures could be significantly more than for simple structures such as single-family dwellings. Attenuation of 8-in.-thick solid concrete, either exterior walls or interior walls (e.g., fire-resistant stairwells) may be equivalent to mass thickness of around 45 to 50 gm/cm^2, corresponding to attenuation factors of 0.2 to 0.17 (Fig. 3). Table 3 summarizes representative cloud-gamma attenuation factors for the types of structures noted.

Table 3

REPRESENTATIVE CLOUD-GAMMA ATTENUATION FACTORS

Structure	Attenuation Factor
Wood frame house, no basement	0.9
Masonry house, no basement	0.6
Basement of wood house	0.6
Basement of masonry house	0.4
Large office or industrial building	0.2 or less

The above values do not suggest any substantial protection from external cloud-gamma radiation afforded by lightly constructed, frame single-family dwellings. In this study, however, estimates of sheltering effectiveness were made assuming somewhat more substantial gamma-attenuation protection, A(x) = 0.4 to 0.9 for small structures. For large

structures, shelter effectiveness estimates were made for $A(x) = 0.05$ to 0.2; gamma attenuation could be even greater, amounting to values much less than 0.05 for well-protected areas within large multistory structures.

The estimated external WB gamma-dose contribution from airborne gaseous radioactive material that enters a shelter structure is based on a finite cloud-source geometry correction factor, since infinite cloud-dose conversion factors (Table 1) are used in estimating shelter effectiveness. The source geometry correction factor is defined as

$$G(E,R) = D(E,R)/D(E,\infty) \quad ,$$

where $D(E,R)$ and $D(E,\infty)$ are gamma doses at the origin of a hemispherical cloud source for finite and infinite radii, respectively. Values for $G(E,R)$ based on point-kernel integration over a hemispherical source volume in air, assuming Berger's expression for a dose buildup factor, are given in Ref. 18 for various energies and source radii; values of $G(E,R)$ are plotted in Fig. 4. Figure 5 gives finite cloud-geometry correction factors for a couple of gamma energies of interest in this study, where very little difference is seen between 1 and 1.25 MeV gammas.

Simulation of small and large shelter structures in this study assumes effective hemispherical radii of 3.4 and 10.3 m to represent shelter enclosures of approximately 400 and 3600 ft^2 of floor area, respectively. From Fig. 5, estimated small- and large-shelter-structure-geometry correction factors are 0.01 and 0.034, respectively. These values are assumed in estimating the effectiveness of shelter structures.

FALLOUT GAMMA-SOURCE ATTENUATION

Considerable analytical and experimental work has been done to determine the protection against fallout-source gamma radiation afforded by various types of building structures, primarily for civil defense applications. Burson and Profio [17] reviewed much of this work for application to nuclear power plant accidents, and performed additional calculations using the method given in Ref. 19 to estimate attenuation factors for some simple rectangular structures (Fig. 6). Experimental results [20-24] generally indicate protection factors (PF), often

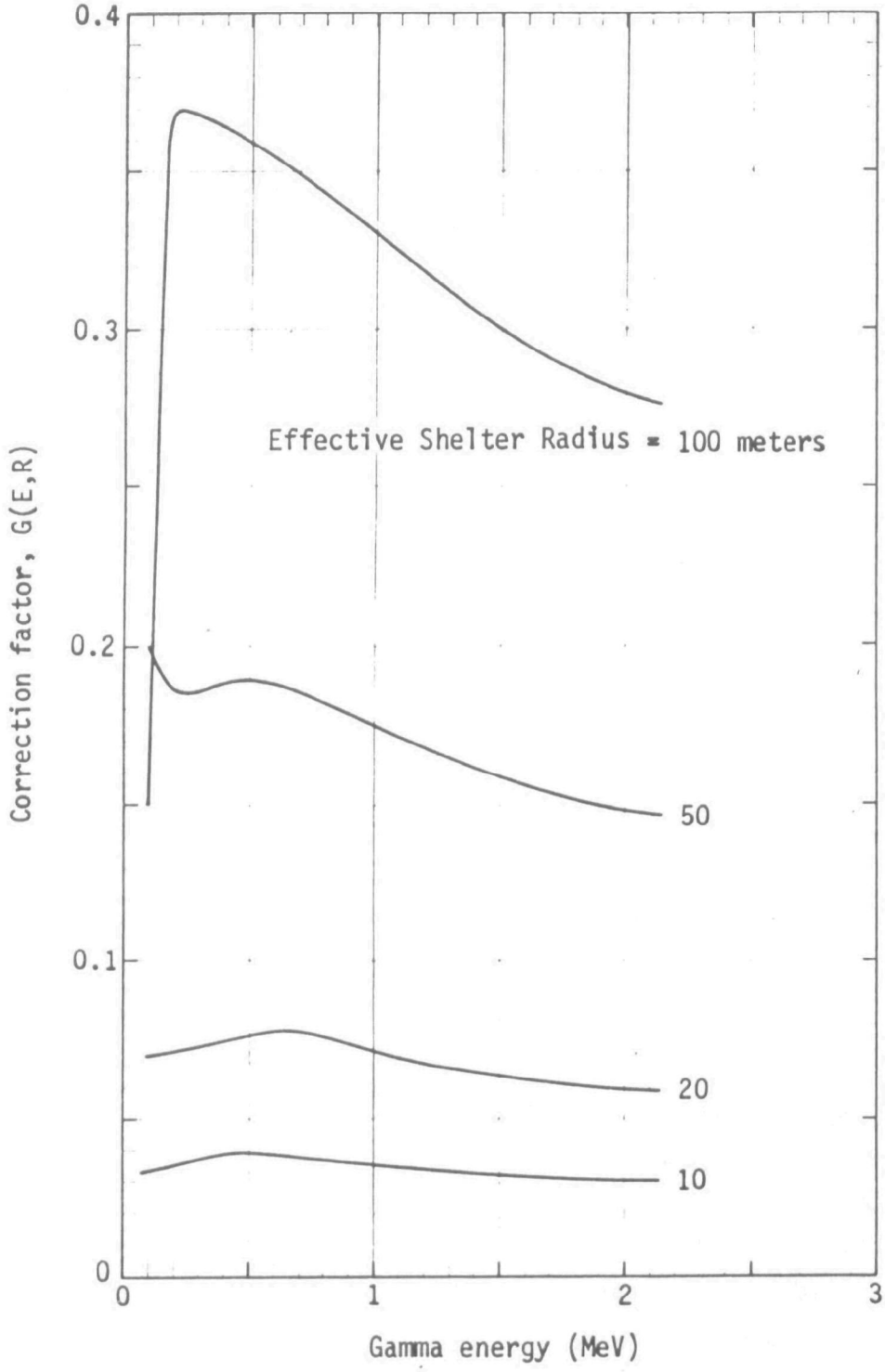

Fig. 4--Finite cloud, gamma dose-correction factors versus gamma energy

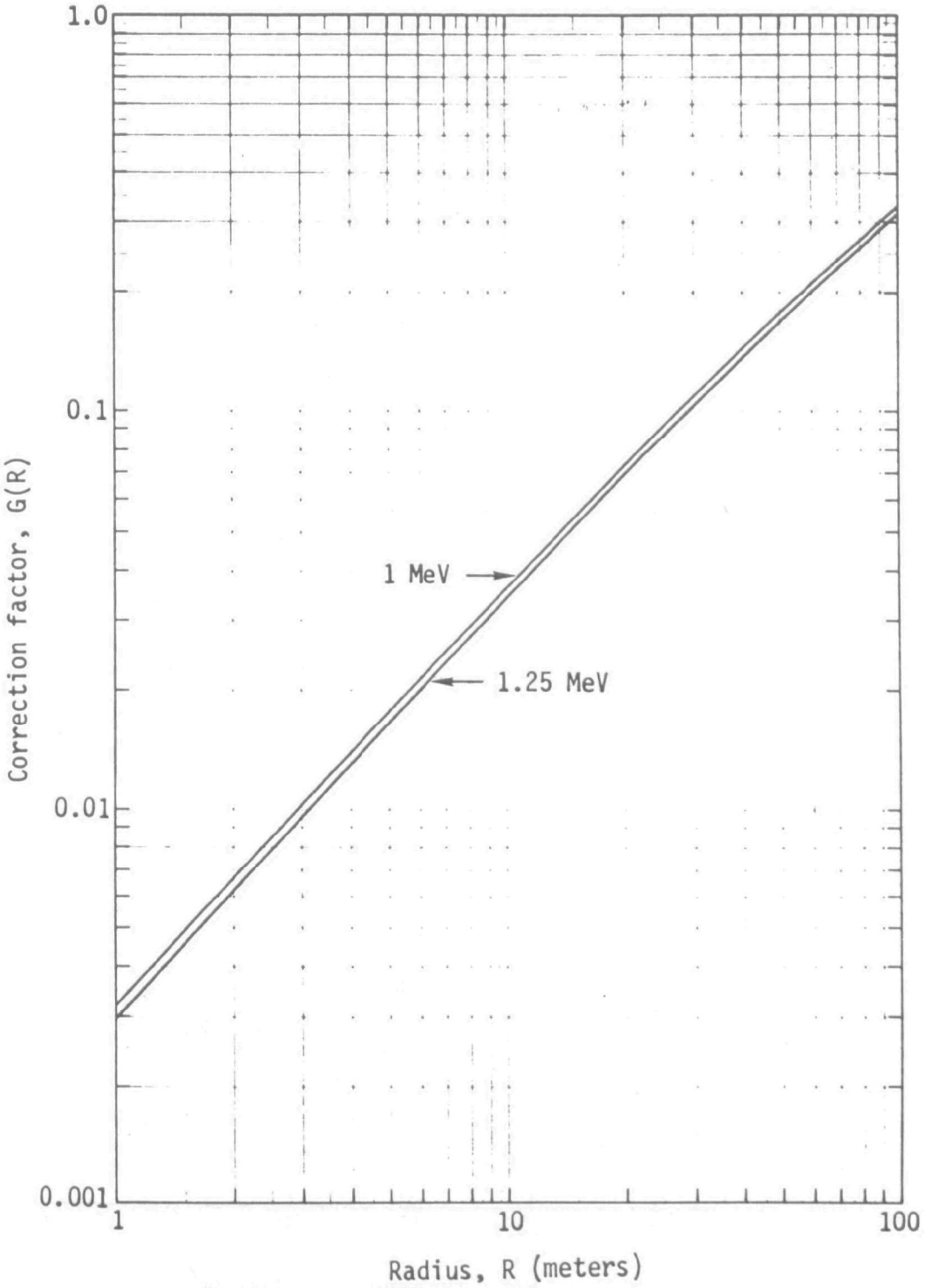

Fig. 5--Finite cloud, gamma dose-correction factors versus effective shelter radius

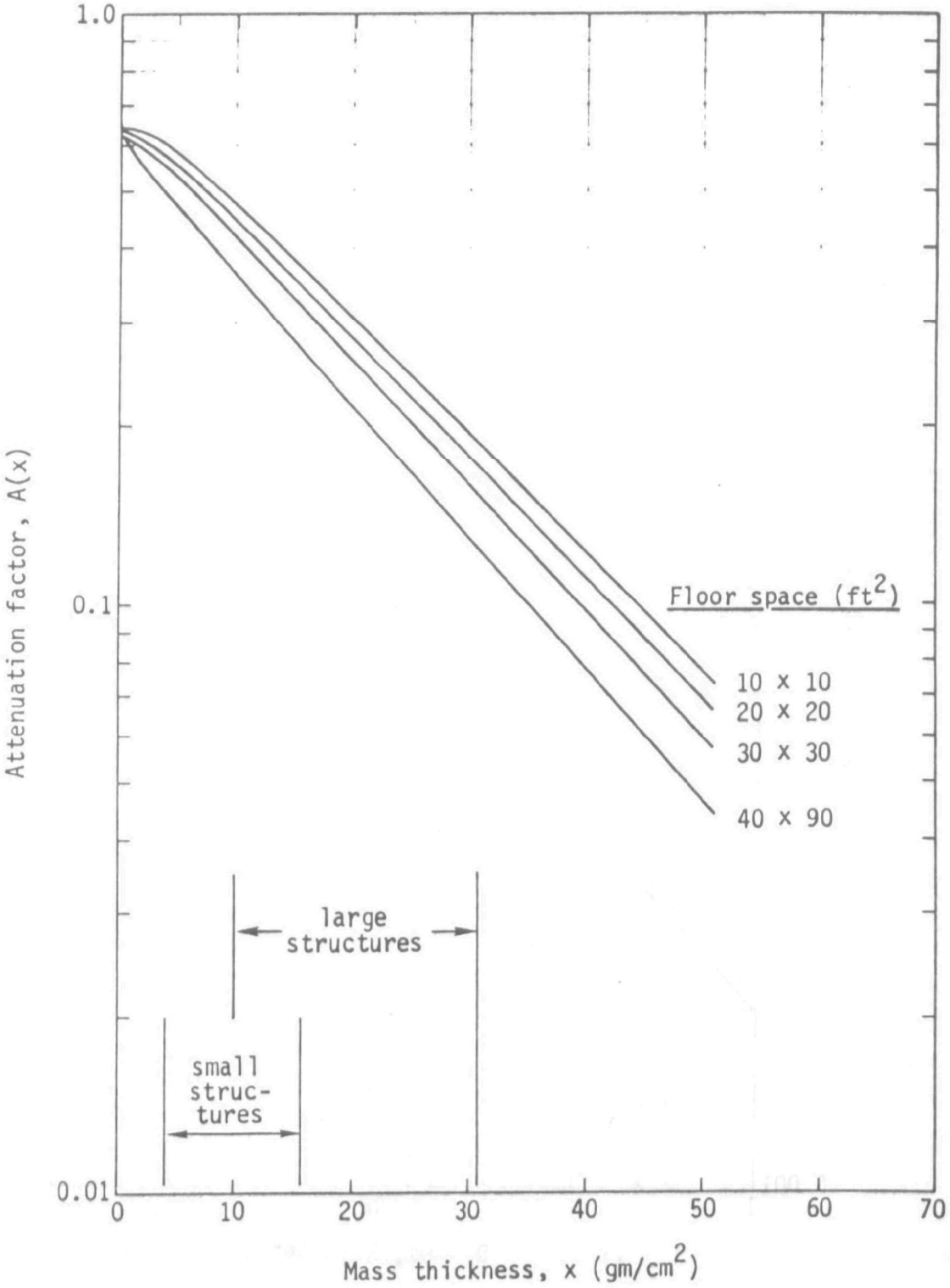

Fig. 6--Gamma attenuation for structures--fallout source

referred to as the reciprocal-of-attenuation factor, from 2 to 5 for a wood frame home (without basement) and from 3 to 10 for block and brick homes. Most attenuation-factor estimates for fallout gamma sources include the effect of ground roughness, which can vary accordingly as tabulated below by the Defense Civil Preparedness Agency [19].

Ground Roughness Condition	Reduction Factor
Smooth plane (hypothetical)	1.00
Paved areas	1.00 to 0.85
Lawns	0.85 to 0.75
Gravelled areas	0.75 to 0.65
Ordinary plowed field	0.65 to 0.55
Deeply plowed field	0.55 to 0.47

Many other aspects affect protection against fallout sources, including structural materials, wall-exposure areas (taking into consideration basements and multilevel dwellings), topographical variations (hillside or flat ground level), mutual shielding offered by nearby buildings and structures, and the internal location within a shelter structure. For example, protection factors for basements may be from 10 to 50; and material shielding of nearby buildings may offer protection factors of from about 1.7 to 2.5 [25]. Complex structures such as multistory office and apartment buildings offer protection factors of 20 or more (away from doors or windows); this factor is supported by experimental measurements [26-28]. Table 4 summarizes recommended attenuation or reduction factors for some representative shelter structures and also vehicles [17].

The reduction values in Table 4 are relative to 1 meter above a hypothetical, uniform infinite plane of homogeneous source concentrations. The values given are only representative and not to be taken as exact; and as indicated above, different values will result because of wide variations in constructional details and topography.

Estimates of the external WB dose from radioiodine fallout inside a shelter structure are based on a dose detector point 1 meter above

Table 4

REPRESENTATIVE REDUCTION FACTORS FOR SURFACE SOURCE

Structure and/or Location	Reduction Factors
1m above a hypothetical, infinite, smooth plane	1.00
1m above ordinary ground	0.70
1m above center of 50-ft roadway half contaminated	0.55
Cars, pickups, buses, and trucks on 50-ft road:	
Road fully contaminated	0.5
Road fully decontaminated	0.25
Trains	0.4
1- and 2-story wood frame homes (no basement)	0.4
1- and 2-story block or brick homes (no basement)	0.2[a]
Home basement--1 or 2 walls fully exposed:	0.1[a]
1 story, less than 2 ft of basement walls exposed	0.05[a]
2 story, less than 2 ft of basement walls exposed	0.02[a]
3- or 4-story structures, 5000 to 10,000 ft^2 per floor:	
First and second floors	0.05[a]
Basement	0.01[a]
Multistory structures, >10,000 ft^2 per floor:	
Upper floors	0.01[a]
Basement	0.005[a]

[a]Away from doors and windows.

a circular area for small and large shelter structures in which infinite-plane dose-conversion factors were used (see Table 1, p. 4). Therefore, a finite-plane geometry correction factor was applied in calculating dosages, defined as

$$G'(R) = D(R)/D(\infty) \quad ,$$

where $D(R)$ and $D(\infty)$ are the finite plane (radius, R) and infinite-plane doses for d = 1m above the surface. $G'(R)$ may also be expressed as

$$1 - D(R,\infty)/D(0,\infty) \quad ,$$

where $D(R,\infty)$ is the plane-source dose for source radial dimensions from R to ∞, and $D(\infty) = D(0,)$. The dose $D(R)$ for a flat plane source is given by

$$D(R) = \frac{k}{2} S_a \int_{\sqrt{R^2+d^2}}^{\infty} \frac{B(\mu r)\, e^{-\mu r}\, dr}{r}$$

where

S_a = source strength per unit area,

k = dose-conversion constant,

R = distance from source plane (1 m),

= gamma-ray absorption coefficient in air,

$B(\mu r) = 1 + C\mu r e^{D\mu r}$ (Berger buildup factor).

Integrating the above over the appropriate source-plane upper limits (see Appendix A) yields

$$D(R) = \frac{kS_a}{2} \left[E_1\left(\mu \sqrt{R^2+d^2}\right) + \frac{C}{(1-D)} e^{-(1-D)\mu\sqrt{R^2+d^2}} \right]$$

and

$$D(\infty) = \frac{kS_a}{2}\left[E_1(\mu d) + \frac{C}{(1-D)}\, e^{-(1-D)\mu d}\right] ,$$

where $E_1(x)$ is the first-order exponential integral function, and C and D are the Berger buildup factor coefficients for air given in Ref. 29. Assuming 1.293×10^{-3} gm/cm^3 for air, calculations of G'(R) were made for 0.5, 1.0, and 2.0 MeV gamma rays for various values of R using the following data from Ref. 29.

Energy (MeV)	C	D	$\frac{\mu}{\rho}\left(\frac{cm^2}{gm}\right)$
0.5	1.6001	1.0094	0.088
1.0	1.1571	0.05749	0.063
2.0	0.8363	0.0243	0.046

Some results are given below for R = 10 and 30m:

Energy (MeV)	G'(R)	
	10m	30m
0.5	0.413	0.620
1.0	0.414	0.624
2.0	0.419	0.622

As indicated above, very little variation exists from 0.5 to 2.0 MeV; the 1-MeV values plotted in Fig. 7 are assumed to be representative for this study. Again, assuming 3.4 and 10.3 m as effective radii applicable for small and large shelter structures, yields finite-source geometry correction factors of 0.28 and 0.43, respectively, which are used in the shelter model calculations.

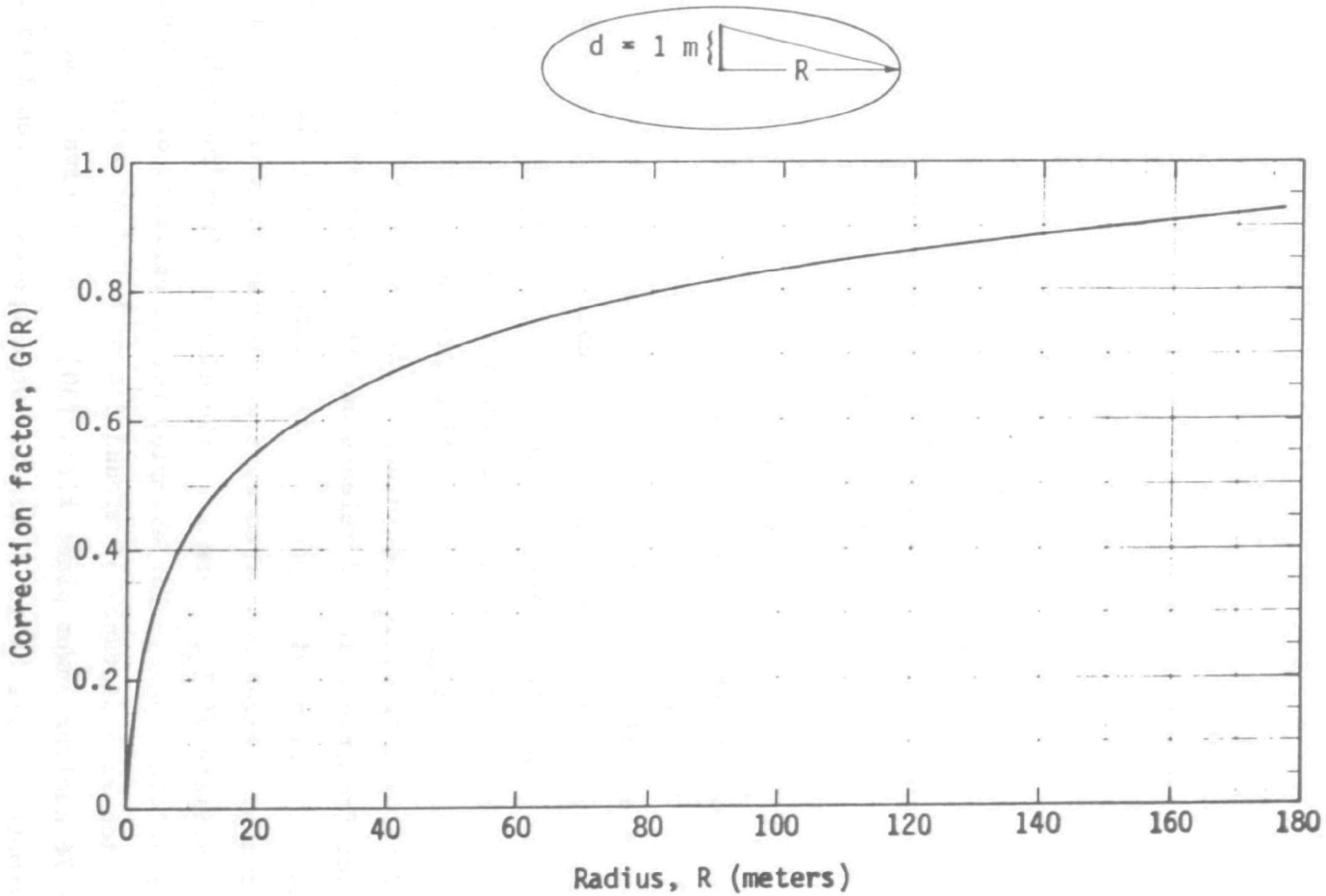

Fig. 7--Finite plane source, geometry-correction factor for 1 MeV gammas

TIME-FRAME MODEL

The question of shelter protection effectiveness from airborne radioactive material accidentally released from a nuclear power plant is dependent upon the time required for individuals to gain entry into a protective structure; and the length of time they remain, as compared with the time of cloud arrival and passage. The required entry time assumes that individuals are transferred from either unprotected or protected locations to another location affording maximum protection, considering logistic constraints, etc. On the other hand, individuals could also be located in houses and buildings already providing adequate shelter so that effectiveness would not depend on access time.

Figure 8 shows the time-frame model assumed in estimating the effectiveness of sheltering, as well as other times of interest (to put them in perspective). Measured from initiation of a possible incident, (T_R+T_a) is the estimated time-of-arrival of the assumed lead portion of a radioactive cloud. The time from source release, T_R, measured from incident initiation, may vary from about 1.5 to 9 hr for the more severe accident categories [1]; although in one instance (PWR 4 Category), a value of 28 hr was indicated. Source release times of from 1.5 to 3 hr were considered to be of more interest in this study, since protective evacuation action might very well be more appropriate, considering the greater time that would be available.

Cloud arrival time, T_a, would depend completely on the location of a shelter from the point of release and the prevailing meteorological conditions (primarily, wind speed and direction) during cloud travel time. Assuming a given sustained average wind speed (and direction), $x/\bar{u}$ is an estimate of T_a, where x is the distance from the release and $\bar{u}$ the average wind speed. For example, for an estimate of the average low-population zone distance of around 3.4 mi based on siting data given for 76 nuclear power plant sites [30], cloud arrival time would be approximately 1-1/2 hr to 20 min for wind speeds of from 2 to 11 mph, respectively. The effective time for sheltering from incident initiation is shown in Fig. 8 as (T_D+T_T), where T_D is the delay time for the initiating event to the sheltering order, and T_T is the actual time spent in taking

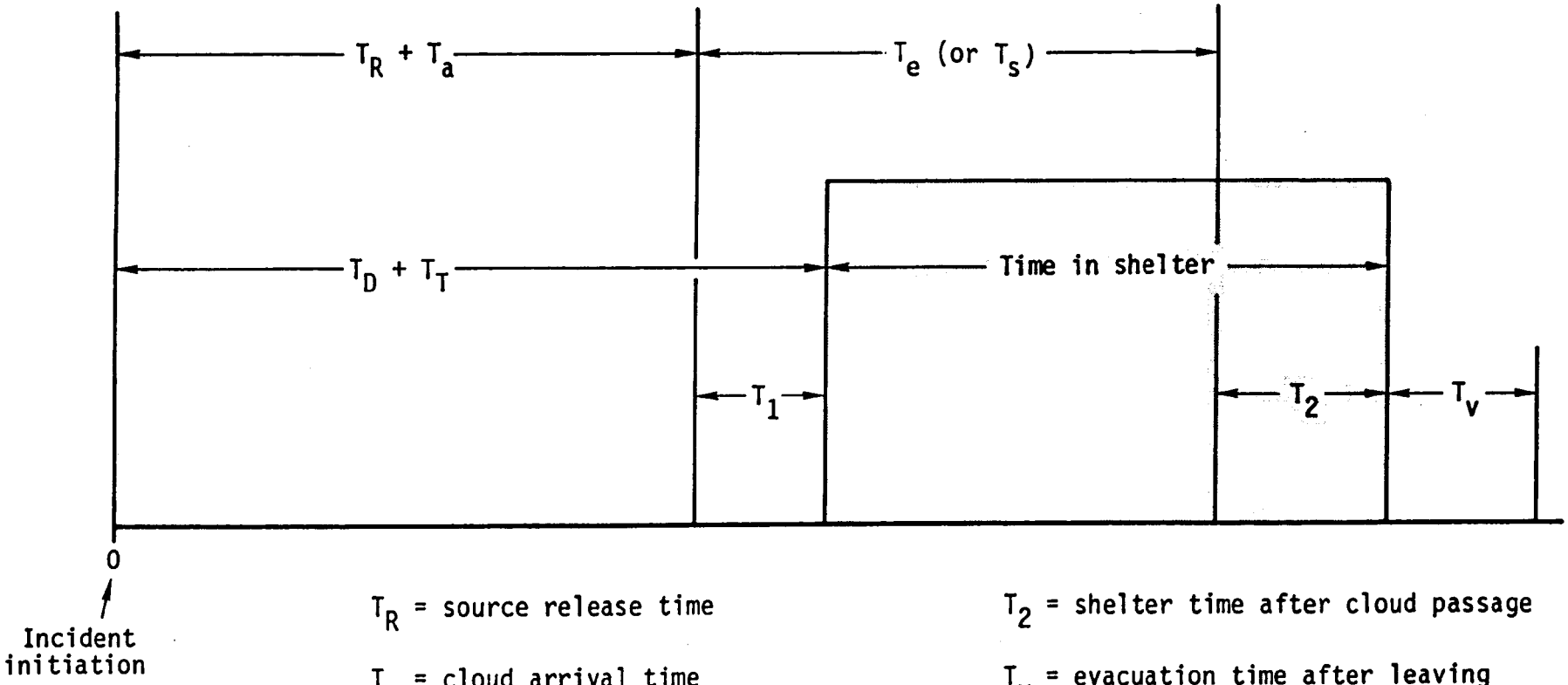

T_R = source release time

T_a = cloud arrival time

T_e = cloud passage time

T_s = cloud-source release duration (for $T_e \geq T_S$, $T_e = T_S$)

T_1 = shelter entrance-delay time after cloud arrival

T_2 = shelter time after cloud passage

T_v = evacuation time after leaving shelter

T_D = delay time from initiating event to sheltering alert

T_T = actual time spent taking shelter

Fig. 8--Sheltering-model time-frame

shelter (assuming individuals are not already in a suitable shelter). Delay time estimates (T_D) have been discussed by the EPA [31] with regard to evacuation that may be somewhat applicable to sheltering, since the time components of T_D are similar or may in fact be one and the same in terms of a local decision process. As assumed here, T_D represents the total delay time from initiation of an event to onset of physical movement to a shelter. For evacuation, the EPA estimates this delay time as being from 0.9 to 4.5 hr [31]. Also, for evacuation, the EPA estimate for T_T is from 0.2 to 1.5 hr, which may be excessive for sheltering on the high end. That is, reasonable sheltering times may be anywhere from a few minutes to half an hour.

Allowance is made in the time-frame model for a shelter-entrance delay time measured from time of cloud arrival, which would be dependent upon T_R, T_a, T_D, and T_T. The shorter T_1 is, the better is the sheltering effectiveness with the maximum advantage for T_1 equal to zero, $(T_D+T_T) \leq (T_R+T_a)$. Normally, T_1 would be expected to be either zero or small except for relatively high sustained wind speeds and/or for locations relatively close to a release.

The cloud passage time, T_e, would depend on source release duration (T_s) and wind persistence time (direction and speed). T_s may range from 0.5 to 4 hr, depending on the accidental release events [1] that would be of interest for seeking shelter. Estimates of wind persistence time should be based on particular site meteorology. In terms of protective action by the public (i.e., taking shelter or evacuating), the wind persistence time estimates made at the time of and during postincident phases of an accident are among the most important parameters affecting the effectiveness of the protective action. Ideally, the most useful type of information on persistence, when making protective action decisions, would be an estimate of the mean or expected wind-direction persistence time--given a particular time of the day and that a particular direction has been maintained up to that point. Such predictive ability would have to be formulated from a detailed statistical analysis of site meteorological data of record requiring frequent observations (perhaps every 15 min) over an adequate period of time. A means of

computing source-cloud trajectory based on real-time analysis of site and regional meterological data is described as a feature of the ARAC program currently being developed at the Lawrence Livermore Laboratory [32]. This kind of capability would obviously be very useful in planning emergency public actions such as sheltering.

In this study, the persistence time is simply related to the cloud exposure time designated in Fig. 8 as T_e; such that, if τ is an estimate of the persistence time, then $T_e = T_s$ for $T_s \leq \tau$, otherwise, $T_e = \tau$.

The time-frame model for sheltering also considers the time that individuals may have remained in a shelter after passage of the radioactive cloud. For example, although exiting a shelter may afford more protection and thus avoid exposure to accumulated internal contamination, precise exiting with regard to cloud passage may not be practical, and the overall time spent in a shelter could be as indicated by the shaded portion of Fig. 8. This shaded portion, then, designates an "internal receptor" with respect to radioactive gaseous fission-product sources. That is, during T_1, after cloud arrival, unprotected individuals may be exposed to airborne radioactive material by means of direct WB gamma radiation from both airborne and ground-source fallout material and from radioactive material entering the body via inhalation. During the interval inside the shelter, $(T_R+T_a+T_e) - (T_D+T_T)$, the internal receptor is exposed to WB radiation from airborne and surface-source (fallout) material, both inside and outside the structure, and internal radioactive material entering the body via inhalation. During T_2, after cloud passage, the internal receptor is assumed to undergo the same type of exposure with the exception of that due to airborne gaseous fission products outside the structure.

Finally, after T_2, the time-frame model makes allowance for the time that may be required for leaving the area (where an individual may be exposed to outside fallout in transit either on foot or by vehicle). If vehicles are used for transport, simulation can include the effect of shielding attenuation of the fallout-source gamma radiation. In terms of the time-frame model, the shielding effectiveness is defined as the ratio of the dose received under unprotected and

protected conditions to that received under unprotected conditions over the interval $(T_e+T_2+T_v)$ due to the exposure modes mentioned above. The time-frame model is thus formulated to indicate the effects of the time parameters on shelter effectiveness. The effectiveness estimates in this study are mainly concerned with times commencing at cloud arrival, (T_R+T_a), in which simple radioactive decay by each source isotope is considered over (T_R+T_a). Note also that the time-frame model assumes an abrupt boundary at both the leading and trailing edges of the radioactive cloud material. Of course, in reality, this is not true, as it is well-known that turbulent diffusion in the atmosphere gives rise, on the average, to continuously changing airborne source boundaries--whose dimensional scales, however, are such that the above model would be a reasonable approximation, considering the source release intervals of interest (excluding an instantaneous puff).

DOSE REDUCTION FACTOR

The estimated measure of effectiveness afforded by a shelter structure--based on the models and assumptions discussed above--is referred to here as the dose reduction factor (DRF). This value is given by the ratio of the dosage received during shelter protection to that which would be received in the open. DRF values are estimated for both thyroid and WB exposures. The DRF for WB gamma dose is given as

$$(DRF)_\gamma = \frac{EC + IC + FD}{EC_o + IC_o + FD_o} ,$$

where

EC = External gamma airborne source dose, sheltered,

EC_o = External gamma airborne source dose, unsheltered,

IC = Inhalation airborne source dose, sheltered,

IC_o = Inhalation airborne source dose, unsheltered,

FD = External gamma surface source dose, sheltered,

FD_o = External gamma surface source dose, unsheltered.

The DRF for thyroid gland dose is given as

$$(DRF)_{Thyroid} = \frac{TC}{TC_o} \quad ,$$

where

TC = Thyroid inhalation dose, sheltered,

TC_o = Thyroid inhalation dose, unsheltered.

Table 5 summarizes the dose components given above, relating the source, receptor, and time-frame conditions that were considered in performing DRF calculations. For example, EC and FD values include estimates of external gamma WB dose for sources both inside and outside a shelter structure for the exposure times (defined in Fig. 8, p. 29) indicated. Shelter dose components (EC, FD, IC, and TC) also include a portion of unsheltered dose contributions accumulated over the exposure period, T_1, to simulate the effects of shelter-access delay times that assume no protection during that interval. The remainder of this section describes the development of these dose components used in the calculation of the DRF values.

Doses downwind from an accidental release of airborne gaseous fission products are dependent upon the concentration of the airborne radioactive material that can be expressed as follows for continuous source release conditions:

$$\chi(r,t) = (\chi(r)/\dot{Q})\ \dot{Q}(t) \qquad (Ci/m^3) \quad ,$$

where $\chi(r)/\dot{Q}$ (sec/m^3) is the ratio of the concentration $\chi(r)$ (Ci/m^3), at a distance r from the release to the source release rate $\dot{Q}$ (Ci/sec); and $\dot{Q}(t-x/\bar{u})$ (Ci/sec) is the time-dependent source-release rate function. In general, the dose at r is given by the integral of the concentration over the period of exposure, T_e,

$$D(r) = \int_0^{T_e} K_D\ \chi(r,t)\ dt \qquad rem \quad ,$$

Table 5

DOSE COMPONENTS

Dose Component	Source		Receptor		Exposure Times
	In	Out	In	Out	
EC, FD		X		X	T_1, T_v [a]
		X	X		$(T_e-T_1) + T_2$ [a]
	X		X		$(T_e-T_1) + T_2$
IC, IC		X		X	T_1
	X		X		$(T_e-T_1) + T_2$
EC_o, FD_o IC_o, TE_o		X		X	$(T_e+T_2+T_v)$

[a] T_v and T_2 are post-outside airborne cloud times and apply to the fallout dose (FD) only.

where K_D is a dose conversion factor. For this study, calculations were performed assuming $\chi(r)/\dot{Q}$ unity (i.e., a unit dilution factor), since it is a common multiplier for all dose components and therefore does not affect DRF values. Accordingly, the dose component estimates described here are based on integrations of the time-dependent sources both inside and outside the shelter structure. The release rate at the source is assumed to be constant with a correction for simple radioactive decay over a release period, T_s,

$$\dot{Q}(t) = \frac{f_r Q_o}{T_s} e^{-\lambda t} \qquad \text{(Ci/sec)} \quad ,$$

where Q_o is the initial radionuclide activity inventory in the reactor at the time of an accident (Table 1, p. 4), f_r is the radionuclide release fraction (DBA assumptions), and λ is the radioactive decay constant. For ease of illustration, the development of the following dose components does not use subscripts designating each radionuclide source, and it should be understood that summations over radionuclide sources are performed in making computations.

The calculations are obtained from differential rate equations and integration over the time-dependent sources. Derivation of these dose component relationships are detailed where necessary in Appendix B.

DOSE COMPONENTS--UNSHELTERED

Whole-body cloud and thyroid dose components assuming no shelter protection are given as

$$\begin{bmatrix} EC_o \\ IC_o \\ TC_o \end{bmatrix} = \begin{bmatrix} K_1 \\ K_2 \cdot B \\ K_3 \cdot B \end{bmatrix} \quad e^{-\lambda(T_R+T_a)} \int_0^{T_e} \dot{Q}(t)\, dt$$

$$= \begin{bmatrix} K_1 \\ K_2 \cdot B \\ K_3 \cdot B \end{bmatrix} \frac{f_r Q_o \, e^{-\lambda(T_R+T_a)}}{T_s \lambda} (1-e^{-\lambda T_e}) \quad \text{rem} \quad ,$$

where K_1, K_2, and K_3 are the dose conversion factors given for WB cloud gamma, WB inhalation, and the thyroid inhalation dose, respectively, and B is the breathing rate assumed to be 3.4×10^{-4} (m^3/sec). In the above, the source release duration, T_s, is assumed to be the downwind exposure time, T_e.

The local fallout deposition rate outside the shelter is assumed to be $V_g \chi(r,t)$ (Ci/sec-m^2), and the depletion rate to be due to only radioactive decay. Expressing the airborne concentration as $\chi(r,t) = \chi_o \, e^{-\lambda t}$, where χ_o includes the exp $[-\lambda(T_R+T_a)]$ term, the outside ground-fallout deposition, F(t) (Ci/m^2), is obtained from the following equation:

$$\frac{dF(t)}{dt} = V_g \chi_o \, e^{-\lambda t} - \lambda F(t) \quad .$$

Integrating,

$$F(t)_{out} = V_g \chi_o t \, e^{-\lambda t} \qquad (\text{Ci}/m^2) \quad .$$

The fallout dose component is given by integration of $F(t)_{out}$ over the time of cloud passage, T_e, plus the contribution from the fallout source after cloud passage integrated over the reference time, (T_2+T_v).

$$FD_o = K_4 \left[\int_0^{T_e} F(t)_{out} + F(T_e) \int_0^{T_2+T_v} e^{-\lambda t} \, dt \right]$$

$$= V_g \chi_o K_4 \left\{ \frac{1}{\lambda^2} \left[1 - (\lambda T_e + 1) \, e^{-\lambda T_e} \right] + \frac{T_e \, e^{-\lambda T_e}}{\lambda} \left[1 - e^{-\lambda(T_2+T_v)} \right] \right\} \text{rem} \quad ,$$

where K_4 is the ground-source gamma-dose conversion factor.

DOSE COMPONENTS--SHELTERED

Airborne Source--Inside

The source intake rate for a shelter structure is assumed to be $\varepsilon L \chi_o e^{-\lambda t}$, where ε is the ingress fraction (discussed above); and L (time)$^{-1}$ is the air change rate that is (f/v), where f is the volumetric air-inflow rate and v is the enclosure volume. The internal concentration $C(t)$ is assumed to be reduced by air outflow, radioactive decay, and internal radioiodine surface deposition at the rates given by $(L+\lambda)\ C(t)$ and $(V_g'/\ell)\ C(t)$. For internal surface deposition, V_g' is the deposition velocity inside the shelter (discussed above) and ℓ is the mean fall distance for iodine fallout material in the shelter enclosure, assumed to be one-half the average floor-to-ceiling distance or about 1.5 meters. The significance of this coefficient as compared with $(L+\lambda)$ per hour can be seen from

$$(V_g'/\ell) = \frac{0.00025\ (\mathrm{m/sec})\ \times\ 3600\ (\mathrm{sec/hr})}{1.5\ (\mathrm{m})} = 0.6\ \mathrm{hr}^{-1} \quad ,$$

where (as indicated above) a range of 0.125 to 3 hr^{-1} for L was chosen for the DRF calculations, and λ can range from about 0.0036 to 0.8 hr^{-1} for the radioiodines. Since $V_g' = 0$ for the rare gases, the (V_g'/ℓ) coefficient is zero for determination of the internal noble-gas concentrations. Based on the above, the internal structure concentrations are determined from the following differential equation:

$$\frac{dC(t)}{dt} = \varepsilon L \chi_o e^{-\lambda t} - K\ C(t) \quad ,$$

where

$$K = L + \lambda + K_f \quad , \quad \text{and} \quad K_f = V_g'/\ell$$

Integrating,

$$C(t) = \frac{\varepsilon \chi_o L}{L + K_f} \left(e^{-\lambda t} - e^{-Kt}\right) \qquad (\mathrm{Ci/m^3})$$

The dose accumulated in the shelter structure over the time interval (T_1, T_e) is

$$D = G\, K_D\, B \int_{T_1}^{T_e} C(t)\, dt$$

$$= \frac{G\, K_D\, B\, \varepsilon \chi_o L}{(L+K_f)} \left[\frac{1}{\lambda} \left(e^{-\lambda T_1} - e^{-\lambda T_e} \right) - \frac{1}{K} \left(e^{-KT_1} - e^{-KT_e} \right) \right] \quad \text{rem} \quad .$$

Specific dose components are given by the above equation, depending on the values of the dose conversion factor, K_D, the breathing rate, B, and the finite cloud-geometry correction factor, G, as listed below:

	K_D	B	G
EC_1	K_1	1	<1
IC_1	K_2	3.4×10^{-4}	1
TC_1	K_3	3.4×10^{-4}	1

After the cloud has passed the vicinity of the structure, the internal concentration is

$$C'(t) = C(T_e)\, e^{-Kt} \quad ,$$

and the dose accumulated in the shelter due to the internal airborne source is

$$D = G\, K_D\, B \int_0^{T_2} C'(t)\, dt$$

$$= \frac{G\, K_D\, B}{K}\, C(T_e)\, (1 - e^{-KT_2}) \quad \text{rem} \quad ,$$

where

$$C(T_e) = \frac{\varepsilon\chi_o L}{L + K_f}\left(e^{-\lambda T_e} - e^{-KT_e}\right) \quad .$$

The dose components EC_2, IC_2, and TC_2 are obtained in the manner given above for EC_1, IC_1, and TC_1. Dosages due to airborne gaseous fission-produced sources inside the structure are given by $(EC_1+EC_2) + (IC_1+IC_2)$ for the WB and (TC_1+TC_2) for the thyroid.

Airborne Source--Outside

During the time interval T_1, it is assumed that individuals are unprotected and dose components are similar to those given for unprotected exposures over the exposure interval to the cloud, T_e, i.e.,

$$\begin{bmatrix} EC_o' \\ IC_o' \\ TC_o' \end{bmatrix} = \begin{bmatrix} K_1 \\ K_2 \cdot B \\ K_3 \cdot B \end{bmatrix} \frac{f_r Q_o\, e^{-\lambda(T_R+T_a)}}{T_e \lambda}\left(1 - e^{-\lambda T_1}\right) \quad \text{rem} \quad .$$

The attenuated WB gamma-ray exposure in the shelter structure from the outside airborne cloud source over the internal (T_1,T_e) is given by

$$EC_1' = A(1-G)\, K_1 \chi_o \int_{T_1}^{T_e} e^{-\lambda t}\, dt$$

$$= \frac{A(1-G)K_1\chi_o}{\lambda}\left(e^{-\lambda T_1} - e^{-\lambda T_e}\right) \quad \text{rem} \quad ,$$

where A is the cloud gamma-ray attenuation, (1-G) is the source-geometry correction factor for the outside cloud, and χ_o--the reference concentration per unit $\chi/\dot{Q}$--is

$$\chi_o = \frac{f_r Q_o \, e^{-\lambda(T_R+T_a)}}{T_e}$$

Surface Source--Inside

The differential equation for the surface deposition rate for radioiodine in the shelter structure is

$$\frac{dF(t)}{dt} = V_g' C(t) - \lambda F(t) \quad ,$$

where C(t) is the internal concentration. Integrating the above yields the fallout surface source, $F(t)_{in}$, which is in turn integrated over the interval (T_1, T_e) to yield the WB external gamma-dose component (see Appendix B) given by

$$FD_1 = \frac{V_g' G' \varepsilon \chi_o L K_4}{K'} \left\{ \frac{1}{\lambda^2} \left[(\lambda T_1 + 1)\, e^{-\lambda T_1} - (\lambda T_e + 1)\, e^{-\lambda T_e} \right] - \frac{1}{K'\lambda} \left(e^{-\lambda T_1} - e^{-\lambda T_e} \right) + \frac{1}{K'K} \left(e^{-KT_1} - e^{-KT_e} \right) \right\} \quad \text{rem}$$

After cloud passage, the WB dose from internal radioiodine surface deposition that accumulated during cloud passage is given by

$$FD_2 = F(T_e)_{in} \int_0^{T_2} e^{-\lambda t} \, dt$$

$$= \frac{V_g' G' \varepsilon \chi_o L K_4}{K'} \left[\frac{T_e \, e^{-\lambda T_e}}{\lambda} - \frac{1}{\lambda K'} \left(e^{-\lambda t} - e^{-Kt} \right) \left(1 - e^{-\lambda T_2} \right) \right] \quad \text{rem} \quad ,$$

where $F(T_e)_{in}$ is the internal fallout level at T_e.

After cloud passage, internal radioiodine fallout deposition continues to take place owing to the residual airborne source inside the shelter structure. The rate of internal fallout deposition is

$$\frac{dF(t)}{dt} = V'_g C(T_e)\ e^{-Kt} - \lambda F(t) \quad .$$

Integrating the above yields the fallout deposition from the post-cloud passage internal-airborne source in the shielding structure, which is in turn integrated to yield the WB dose written as (see Appendix B)

$$FD_3 = \frac{V'_g G' \varepsilon \chi_o L K_4}{K'} \left(e^{-\lambda T_e} - e^{-KT_e}\right) \left[\frac{1}{K'\lambda}\left(1 - e^{-\lambda T_2}\right) - \frac{1}{K'K}\left(1 - e^{-KT_2}\right)\right] \text{ rem} \quad .$$

The WB external gamma dose from internal radioiodine fallout in the shelter structure is given by $(FD_1+FD_2+FD_3)$.

Surface Source--Outside

During the time interval T_1, the accumulated WB dose while seeking shelter (unprotected) from outside ground fallout deposition is

$$FD'_o = K_4 \int_0^{T_1} F(t)_{out}\ dt$$

$$= \frac{V_g \chi_o K_4}{\lambda^2} \left[1 - (\lambda T_1 + 1)\ e^{-\lambda T_1}\right] \qquad \text{rem} \quad .$$

During the time interval (T_1, T_e), the WB gamma dose inside the shelter structure from outside ground-fallout deposition is

$$FD_1' = A'K_4 \int_{T_1}^{T_e} F(t)_{out}\, dt$$

$$= A'V_g\chi_o K_4 \left\{ \frac{1}{\lambda^2} \left[(\lambda T_1+1)\, e^{-\lambda T_1} - (\lambda T_e+1)\, e^{-\lambda T_e} \right] \right\} \quad \text{rem} \quad ,$$

where A' is the shelter-structure attenuation of gamma rays from the ground-fallout source.

The WB gamma dose accumulated inside from residual outside ground-fallout deposition is

$$FD_2' = A'K_4\, F(T_e)_{out} \int_0^{T_2} e^{-\lambda t}\, dt$$

$$= A'V_g\chi_o K_4 \frac{T_e\, e^{-\lambda T_e}}{\lambda} (1 - e^{-\lambda T_2}) \quad \text{rem} \quad .$$

After T_2, the time interval assumed during which people may continue to be in the shelter structure after outside cloud passage, the computational model assumes that individuals leave the vicinity of the shelter over a time interval, T_v, either unprotected (e.g., on foot) or protected from residual ground-fallout source gamma radiation while leaving the contaminated area in a vehicle with a shielding attenuation factor of A_v'. Accordingly, the WB gamma dose is

$$FD_3' = A_v'K_4\, F(T_e)_{out} \int_{T_2}^{T_2+T_v} e^{-\lambda t}\, dt$$

$$= A_v'V_g\chi_o K_4 \frac{T_e\, e^{-\lambda T_e}}{\lambda} \left[e^{-\lambda T_2} - e^{-\lambda (T_2+T_v)} \right] \quad \text{rem} \quad .$$

The external WB dose from shielded gamma radiation emanating from ground-fallout deposition outside the shelter structure (with the exception FD'_o, where the receptor is assumed outside) is $FD'_o + FD'_1 + FD'_2 + FD'_3$. Note that for FD'_1, FD'_2, and FD'_3 (receptor inside) a geometry factor--i.e., (1-G')--is not assumed, which is consistent with the attenuation values, A', for ground-source fallout deposition. That is, the fallout source on the roof of a simple structure would approximate the ground-fallout source deposition in terms of source geometrical effects for the reference dose point 1 meter above an idealized ground-plane source, (see sketch below).

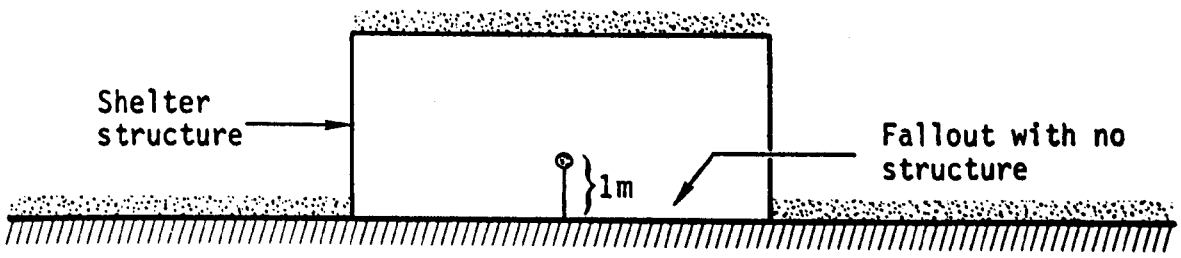

SHELTERING AND EVACUATION

An investigation was made to determine the utility of the combined protective action of sheltering and evacuation. That is, both from the standpoint of time constraints and the DRF, the combined protective-action measures may offer an advantage over sheltering only. For example, for individuals located relatively close to the point of the accidental release in terms of either distance or cloud-arrival time, sheltering may be the only option. Furthermore, if the duration of the source release were to continue longer than expected because of, e.g., wind persistence or miscalculation, exit and evacuation from the shelter structure may be advantageous in terms of dose savings as opposed to remaining inside over the whole cloud-passage time. The important considerations in addressing this question are exit-time from the

shelter structure, T_S, evacuation transport time, T_T, and cloud exposure time, T_e; and protection characteristics of the shelter structure (see above) and any evacuation vehicle(s) that may be used from transporting people out of a radiocontaminated area.

The analysis of the above situation is based on a simple model (Fig. 9) assuming ideal sheltering conditions where both shelter-entrance delay time and residence time after cloud passage are zero ($T_1 = 0$, $T_2 = 0$; see Fig. 8). Figure 9 is a plot of accumulated dose as a function of shelter time up to the cloud passage time, T_e, where the dose is D_S. Values D_1 and D_2 are to suggest possible accumulated dosages for shelter exit at T_S and evacuation time T_T. During the interval T_T, the model assumes that individuals are exposed to airborne and ground-fallout source radioactive material while in an evacuation vehicle that offers some degree of protection discussed below. The decision is simplified to making a comparison of the estimated dose values. That is, for $D_1 < D_S$, exit from the shelter structure and evacuation would be a serious consideration; whereas, for $D_2 > D_S$, it would be more advantageous to remain inside from the standpoint of dose savings.

An equivalent means of deciding whether to effect shelter exit and evacuation is based on DRF comparison. The actual numerical approach taken in this analysis is based on the question of for what values of T_S, T_T, and T_e is the relationship $(DRF)_{S/E} \leq (DRF)_S$ satisfied, where

$$(DRF)_S = \frac{D(T_e)_{in}}{D(T_e)_{out}} \qquad \text{(shelter only)}$$

and

$$(DRF)_{S/E} = \frac{D(T_e)_{in} - D(T_S,T_e)_{in} + D(T_S,T_T)_{ev}}{D(T_e)_{out}} \qquad \text{(shelter and evacuation)} \quad ,$$

where

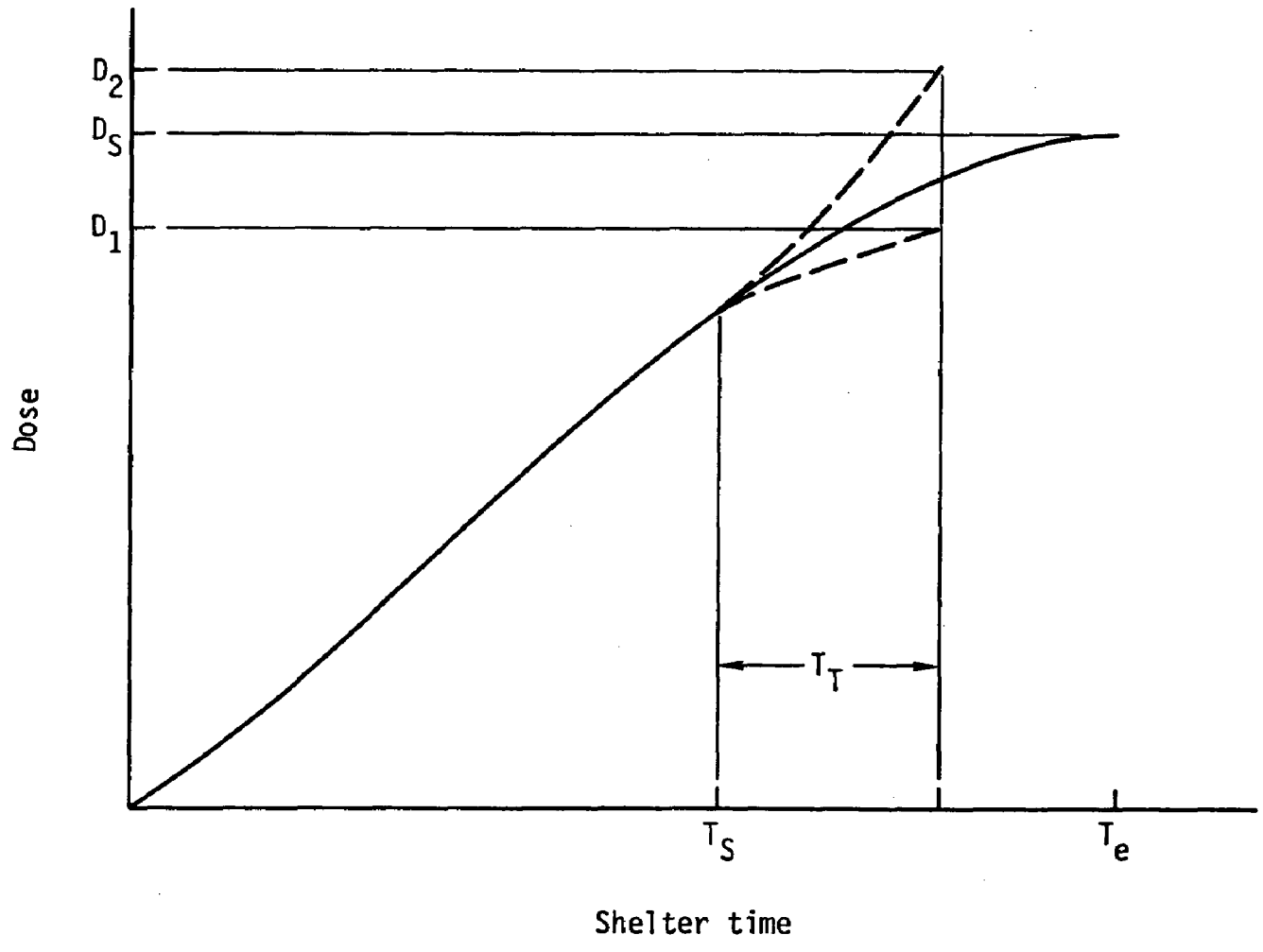

Fig. 9--Sheltering and evacuation

$D(T_e)_{out}$ = dose outside shelter structure,

$D(T_e)_{in}$ = dose inside shelter structure,

$D(T_S,T_e)_{in}$ = dose inside shelter structure over interval (T_e-T_S),

$D(T_S,T_T)_{ev}$ = dose accumulated during evacuation over interval T_T commencing at T_S.

Assuming an evacuation vehicle, Burson and Profio [17] estimated that steel and glass in automobiles and small trucks correspond to an average of roughly 2 gm/cm^2 of shielding thickness for gamma radiation from an airborne cloud source. From Fig. 3 (p. 17), this thickness corresponds to an attenuation of only about 0.95 (the value assumed in this analysis). For heavier vehicles (e.g., large commercial buses), the gamma attenuation may be 0.8 to 0.9—still not appreciable. Also, assuming an effective vehicle enclosure radius of around 1 meter gives a source-geometry correction factor of around 0.003 (Fig. 5, p. 21) for the contaminated airborne material in the vehicle.

Gamma ray attenuation in automobiles and small trucks is 0.5 for contaminated 50-ft-wide roads (Table 4, p. 24). Values estimated by Burson, based on experimental measurements [33] were from 0.5 to 0.67. An average value of 0.6 was assumed in this analysis.

Air change rates for automobiles under various conditions of operation have been determined by Peterson and Sabersky [34]. Their results (Fig. 10) are from measurements made of pollutants (O_3, CO, NO, and NO_X) inside a stock Chevrolet automobile with an air-conditioning unit. The exchange rate is relatively high. In fact, the passenger compartment is not intended to be airtight; and even in the maximum air-conditioning mode, a small fan draws outside air into the compartment. Without this ventilation, the rates can probably be reduced by a factor of 5 without difficulty. The single point marked by an arrow (Fig. 10) was taken when, with windows closed, the vehicle's air conditioning was turned off but the engine left running. Under these conditions, a fan also draws in

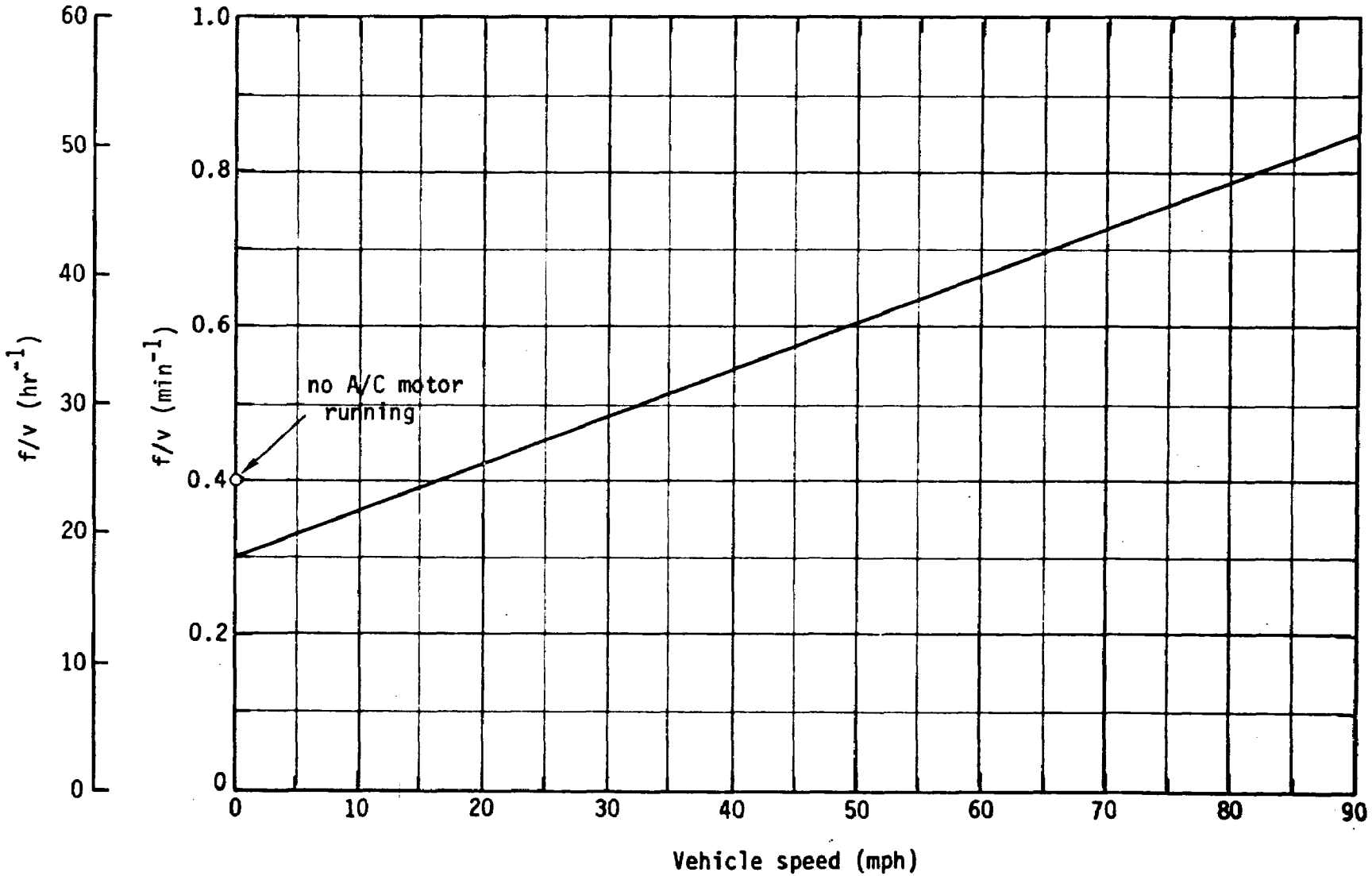

Fig. 10--Air exchange and infiltration rates in closed passenger compartment when air conditioning is set at a maximum

outside air. At higher speeds and with the same settings, Q/V (air change rate) would be expected to approach the values obtained with the air-conditioning unit in operation. This expectation is based on the assumption that general leakage rather than the fan is the dominant factor determining f/v at these speeds. A value of 0.5 min^{-1} (30 hr^{-1}) was chosen for this analysis, which corresponds to ∿35 mph when general leakage is the dominant factor for f/v. Penetration of gaseous fission products into evacuation vehicles was assumed to be 100 percent for the rare gases and 80 percent for radioiodines, which corresponds to the upper limit of the estimates of Megaw [12] based on simple shelter structure experiments.

For sheltering, the DRF and dose component relationships are as given above (p. 28ff.); where, for $D(T_S,T_e)_{in}$ above, $T_S = T_1$ and $T_2 = 0$. For evacuation, the vehicle is assumed to be analogous to a shelter structure, and dose estimates for $D(T_S,T_T)_{ev}$ for the exposure-evacuation time, T_T, are based on the same dose components considered for shelters--with the exception of radioiodine deposition inside the vehicle, which is assumed to be insignificant and, moreover, cannot be modeled accurately without some experimental verification.

External WB cloud-dose accumulation from gamma-ray penetration of the evacuation vehicle is

$$EC_{out} = A_v(1-G_v)K_1\chi_o \int_{T_S}^{T_S+T_T} e^{-\lambda t}\, dt$$

$$= A_v(1-G_v)K_4\chi_o\, e^{-\lambda T_S} \frac{1}{\lambda}\left(1 - e^{-\lambda T_T}\right) \qquad \text{rem} \quad ,$$

where A_v is the vehicle attenuation for cloud-source gamma radiation, G_v the finite cloud-source geometry factor, and K_1 the dose conversion factor.

Inside the evacuation vehicle, the rate of concentration change is

$$\frac{dC(t)}{dt} = \varepsilon\chi_o L_v e^{-\lambda t} - K_v C(t)$$

where $K_v = L + \lambda$.

Integrating the above for $C(0) = 0$ gives

$$C(t) = \varepsilon\chi_o \left(e^{-\lambda t} - e^{-K_v t}\right) \qquad (Ci/m^3)$$

for the concentration in the vehicle. The dose accumulated in the vehicle over the period T_T is given as

$$D_{in} = G_v \varepsilon\chi_o K_D \int_{T_S}^{T_S+T_T} C(t)\, dt$$

$$= G_v \varepsilon\chi_o B K_D e^{-\lambda T_S} \left[\frac{1}{\lambda}\left(1 - e^{-\lambda T_T}\right) - \frac{1}{K_v}\left(1 - e^{-K_v T_T}\right)\right] \qquad \text{rem}$$

Specific dose components are obtained based on the values for the constants as given below:

	K_D	B	K_v
EC_{in}	K_1	1	<1
IC_{in}	K_2	3.4×10^{-4}	1
TC_{in}	K_3	3.4×10^{-4}	1

The ground-fallout deposition given above is $F(t)_{out} = V_g \chi_o t\, e^{-\lambda t}$. The external WB dose from ground-fallout source gamma-ray penetration of the vehicle during evacuation is

$$FD_{out} = A_v' K_4 \int_{T_S}^{T_S+T_T} F(t)_{out}\, dt$$

$$= \frac{A_v' V_g \chi_o K_4}{\lambda^2} \left[(\lambda T_S+1)\, e^{-\lambda T_S} - (\lambda T_S + T_T + 1)\, e^{-\lambda (T_S+T_T)} \right] \quad \text{rem} \quad .$$

The dose accumulated during evacuation, $D(T_S,T_T)_{ev}$, corresponds to either the WB or thyroid. For the WB, the dose is $(EC_{in}+EC_{out}+IC_{in}+FD_{out})$; for the thyroid, TC_{in}. Note that internal exposures for EC_{in} and IC_{in} are assumed to accrue only when the evacuation vehicle is in the vicinity of the airborne radioactive gaseous material over the period T_T, which is a very good approximation considering the large values of L_v. That is, in actuality, once the vehicle leaves the vicinity of the airborne radioactive material, χ_o in the differential equation above is zero and the internal vehicle concentration drops very rapidly within a few minutes--which would not give rise to any significant dosage as compared with conditions when the vehicle is assumed to be in the vicinity of the airborne radioactive material, provided of course T_T is more than a few minutes. That is, the equilibrium concentration that would be reached in the vehicle within a few minutes is given as

$$C_{eq} = \frac{\varepsilon \chi_o L_v\, e^{-\lambda t}}{L_v + \lambda} = \frac{\varepsilon \chi_o\, e^{-\lambda t}}{1 + \frac{\lambda}{L_v}} \approx \varepsilon \chi_o\, e^{-\lambda t} \quad ,$$

which would be approximately that outside the vehicle. Then, after leaving the vicinity of airborne contamination, the concentration of gaseous radioactive material in the vehicle falls off as $\exp[-(L_v+\lambda)t]$, where L_v is $\sim 0.5\ \text{min}^{-1}$ ($30\ \text{hr}^{-1}$).

III. RESULTS

Estimates of shelter effectiveness have been made using the DRF calculational model and assumptions discussed in Sec. II. It is, of course, impossible within the scope of this effort to develop information comprehensive enough to anticipate what might be expected for all practical situations. Accordingly, assumptions are made regarding input parameters and ranges of variables in order 1) to demonstrate the degree of shelter effectiveness in a general sense, and 2) to indicate sensitivity variations for some specific situations.

Input values used in the sheltering calculations fall under two categories. First, a set of fixed parameters were selected (summarized in Table 6). These values are in part based on study ground rules (DBA gaseous-release assumptions), review and analysis of existing data, and an attempt to develop representative information that can also be related to the *Reactor Safety Study* [1]. The notion of "fixed parameters" obviously applies only to this particular analysis; in reality, there may be appreciable variations in shelter characteristics and, for example, iodine deposition velocity. The second input category consists of the temporal and ventilation rate variables selected to indicate the sensitivity and degree of sheltering effectiveness over their range of values. In some cases, extrapolation can be made (with care) to estimate shelter effectiveness beyond the specific range limits used in making the calculations.

Shelter effectiveness results are given in terms of the DRF in Figs. 21 through 31. Enough data are given in Figs. 11 through 31 to enable a fair amount of cross-plot extrapolation. All the time variables have units of hours and are identified in Fig. 8 (p. 29). The ventilation rate, L, is in units of hr^{-1}; and SS and LS designate the small and large shelter structure categories, respectively. The plotted results in Figs. 11 through 31 are discussed below.

Figure 11 gives WB DRF as a function of time (T_2) in the shelter structure after passage of the airborne cloud source, assuming no delay (T_1=0) in shelter access after initial cloud arrival and 1-hr cloud

Table 6

FIXED PARAMETER SUMMARY

SOURCE TIMES

Case	Release Time T_R, Hr	Release Duration T_S, Hr
A	1.5	0.5
B	2.0	1.0
C	2.5	3.0

GASEOUS FISSION PRODUCTS

	Release Fraction	Ingress Fraction
Kr and Xe	1.0	1.0
I	0.25	0.51

SHELTERS

	Small Structures (SS)	Large Structures (LS)
Cloud gamma attenuation, A	0.6 (0.4, 0.9)[a]	0.1 (0.05, 0.2)[a]
Fallout gamma attenuation, A'	0.2	0.01
Finite cloud factor, G	0.01	0.034
Finite fallout factor, G'	0.28	0.43

DEPOSITION

V_g(outside) = 0.005 m/sec

V'_g(inside) = 0.00025 m/sec

[a]Variations

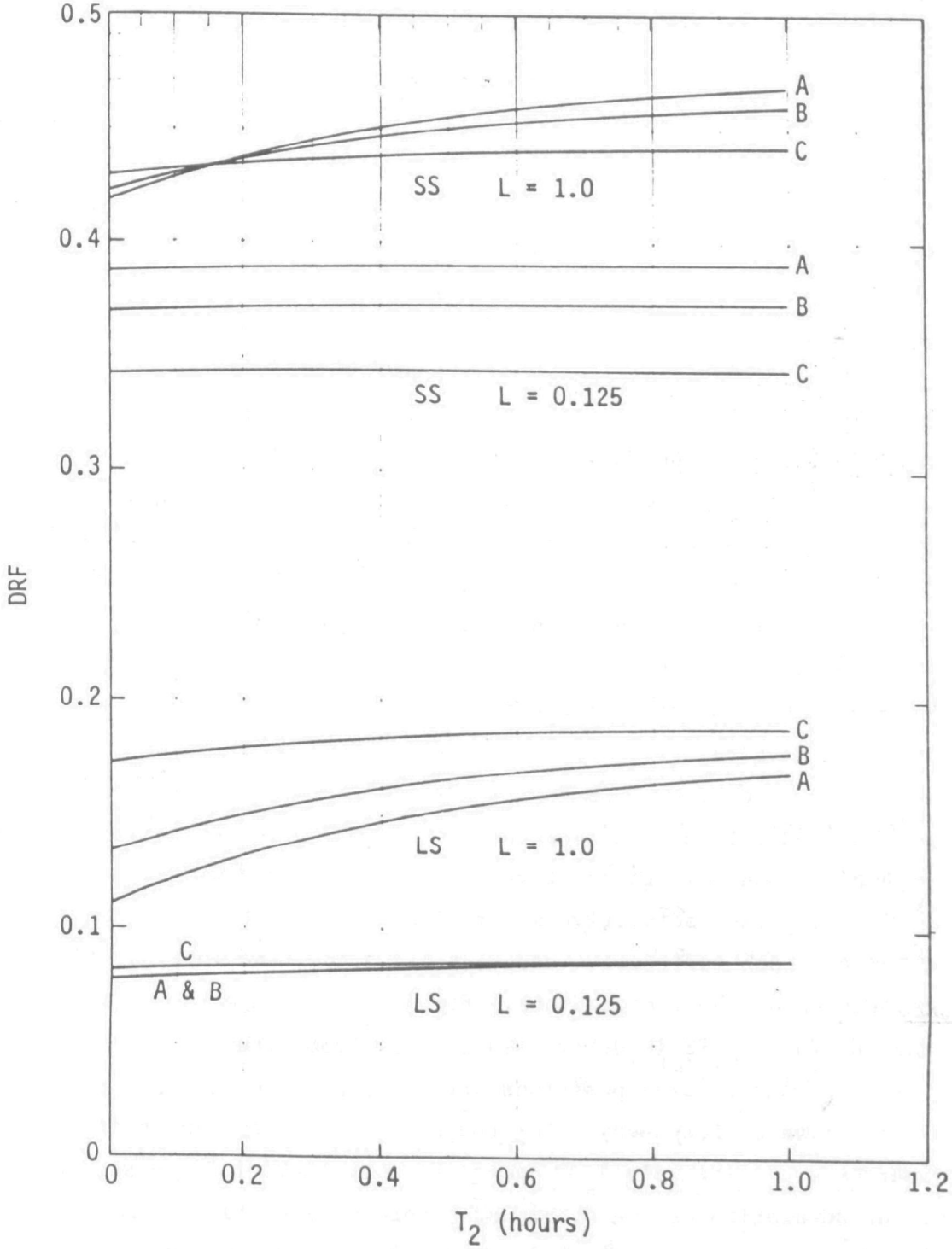

Fig. 11--WB DRF versus T_2, (T_1=0,T_a=1)

travel time (T_a=1) from the point of source release. Significantly, more protection is afforded by the large shelter structure (LS) than the small one (SS). The effect of ventilation rate is also more important for the LS than the SS, primarily because of the difference in cloud-gamma attenuation. That is, a larger portion of the dose in the SS is due to gamma ray penetration of the shelter from the outside airborne cloud source than in the LS; that portion of the dose does not depend on the air change rate. A value of L = 1 hr^{-1} may be somewhat representative, whereas 0.125 hr^{-1} represents a fairly low value associated with a relatively tight structure with very little or no forced air circulation. The relative positions of the A, B, and C categories of release duration are also determined by the combination of cloud-gamma attenuation and ventilation rate. For the SS, the relatively larger dose component from outside cloud-gamma ray penetration is sufficient to offset the dose component from internal airborne radioactive material. For example, for T_2 = 0 and L = 1, the relative positions of A, B, and C are the same for both SS and LS; but the spread is larger for the LS than the SS, indicating the effect of a relatively larger number of air changes with respect to release duration (0.5, 1, and 3 for A, B, and C, respectively) for the LS as compared with the SS. The crossover point at T_2 ≈ 0.2 for the SS is due to the increasing importance of the outside ground-fallout dose component, assumed to be reduced at a rate dependent upon only radioactive decay, as compared with the dose from inside airborne radioactive material assumed to be reduced at a rate dependent upon radioactive decay, ventilation, and internal fallout deposition of the radioiodines. For low air-change rates (L=0.125 hr^{-1}), the DRF for the SS is determined largely from external sources, where the A, B, and C curve positions primarily reflect the differences in radioactive source decay. For the LS, the dose components from outside sources are relatively less important than those for the SS; and a clear separation of the A, B, and C release-duration categories is not seen when both inside and outside dose components are relatively more comparable.

Figure 12 gives DRF plots for the thyroid for the same conditions assumed for Fig. 11, which apply to both SS and LS. In general, the DRF values indicate somewhat more protection for the thyroid than for the WB, and are more sensitive to T_2; particularly for $L = 1\ hr^{-1}$, since there are no competing outside-source dose components. The relative positions for A, B, and C are due to the different number of air changes associated with each source release duration. Since the DRF values in Fig. 12 correspond to a radioiodine ingress fraction of 0.51, they scale accordingly.

Calculated results of the WB DRF sensitivity with cloud-source arrival time are given in Figs. 13 through 16. The DRF variations for the thyroid, not plotted here, are insignificant as a function of cloud arrival time, T_a. In Fig. 16, the DRF decrease with T_a for the SS is due to the relatively decreasing importance of the WB-dose component from the outside airborne cloud source. That is, the model includes only simple radioactive decay and predicts that the relative contribution of the noble-gas sources to the WB dose decreases more with time than does that of the radioiodines. In reality, that decrease with T_a may not be quite as prevelant, particularly for times longer than a few hours. The countereffect, however, is indicated for the LS, since the significance of the external gamma WB-dose component from the outside airborne source is masked by the greater gamma-shielding attenuation assigned to the LS as compared with the SS. The relative positions of the A, B, and C curves are, as indicated above, due to the increasing number of air changes, respectively, during cloud passage.

Figure 14 shows WB DRF as a function of T_a for case A, assuming late shelter access (T_1=0.25) coupled with extended residence time (T_2=0.5) after passage of the airborne cloud. Ideal shelter timing (T_1=0, T_2=0) is also shown for comparison to indicate the significant loss of protection for non-ideal shelter-access timing. Figure 14 also shows loss of inherent LS protection advantage (due to shielding), as compared with the SS, because of shelter-timing considerations.

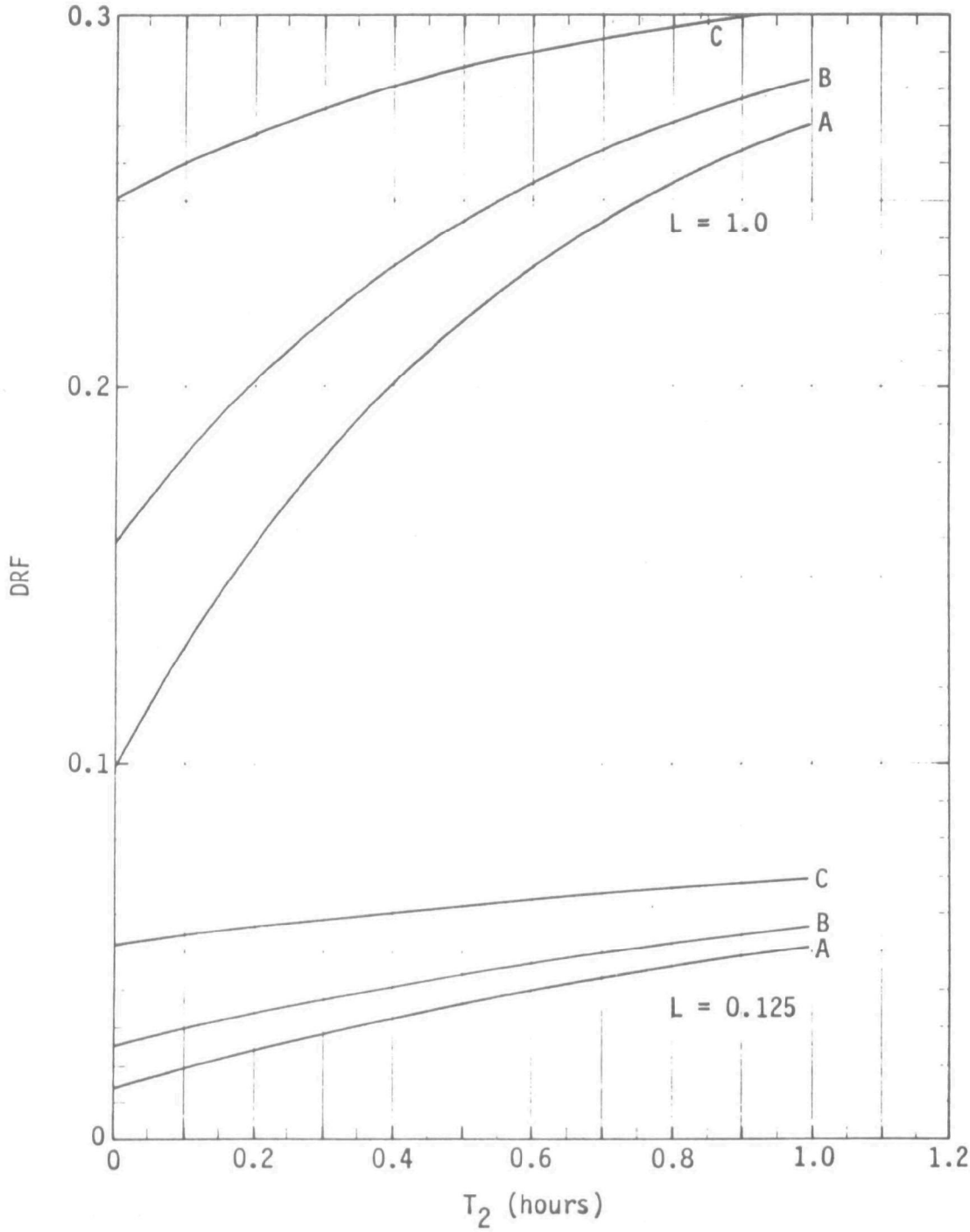

Fig. 12--Thyroid DRF versus T_2, (T_1=0,T_a=1)

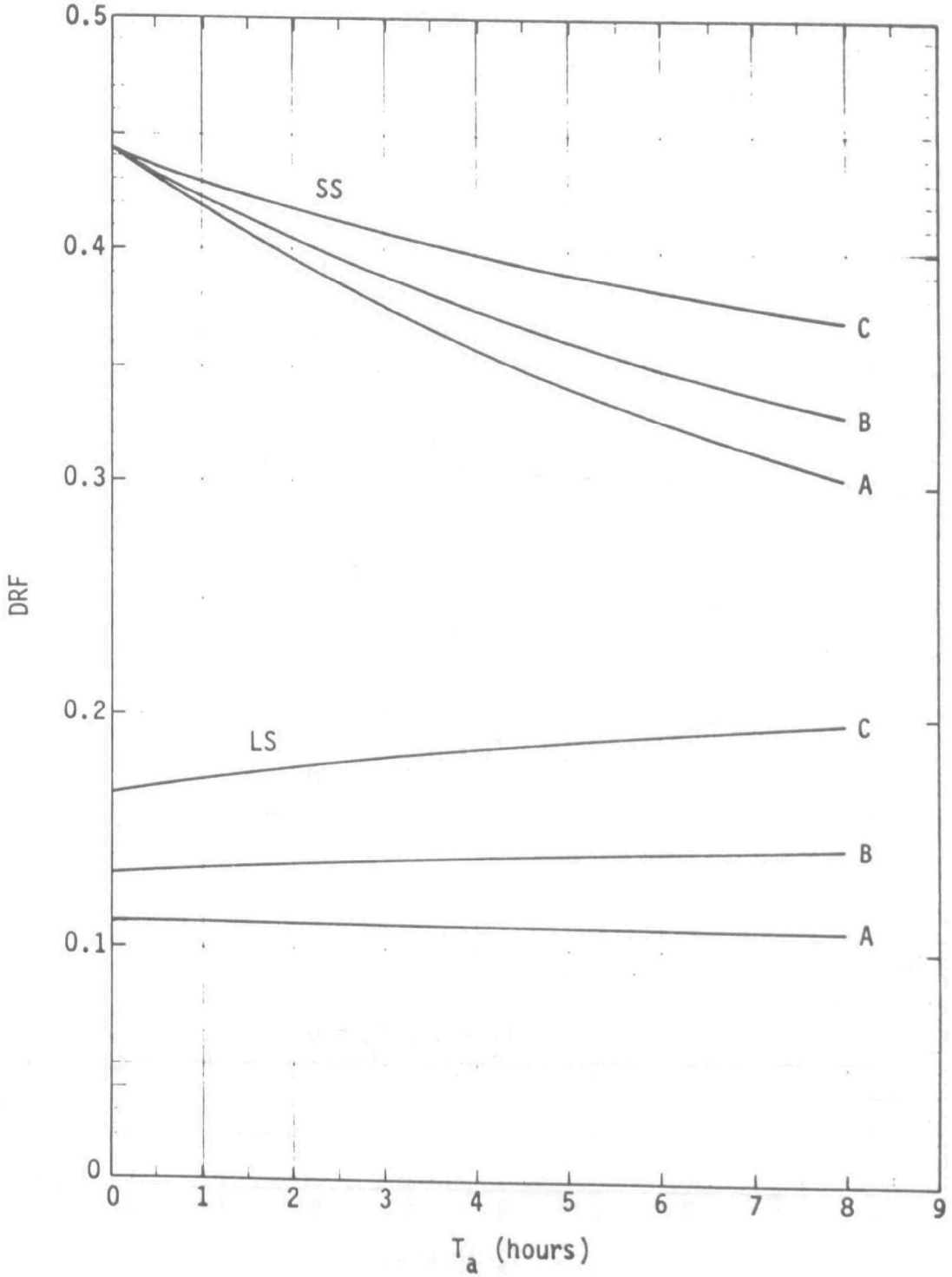

Fig. 13--WB DRF versus T_a, (T_1=0,T_2=0), L = 1

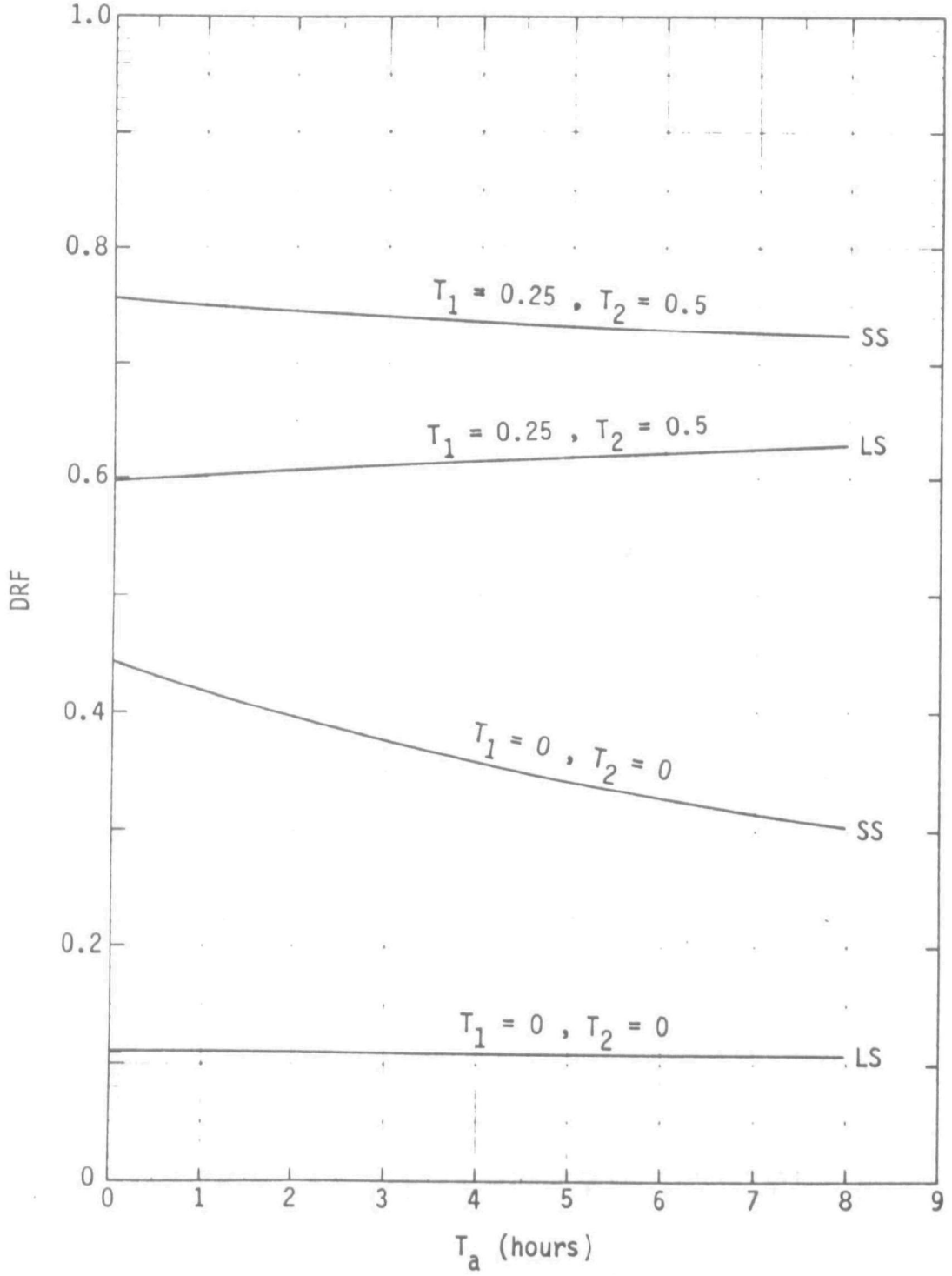

Fig. 14--WB DRF versus T_a, case A, (T_1=0,T_2=0), (T_1=0.25,T_2=0.5), L = 1

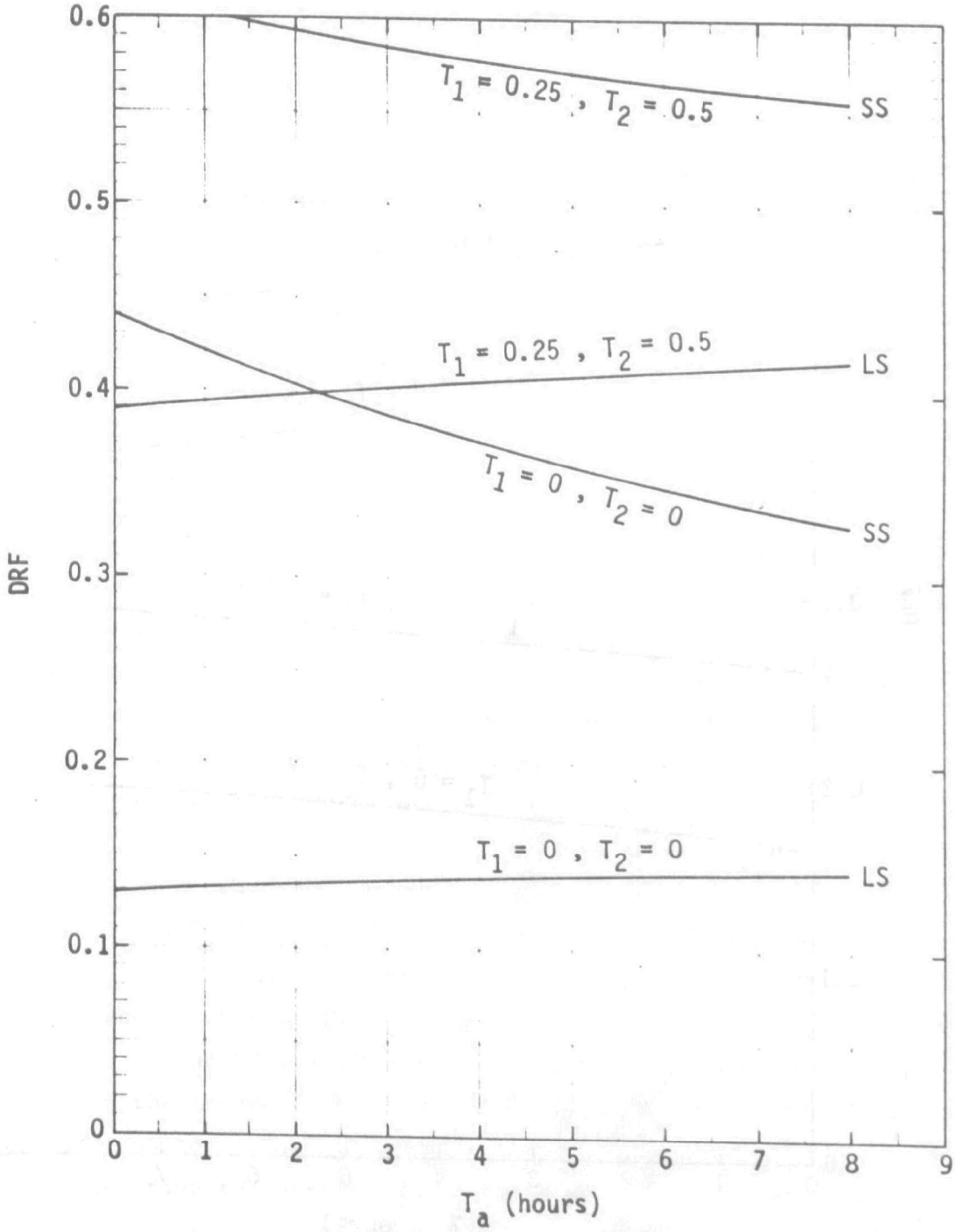

Fig. 15--WB DRF versus T_a, case B, (T_1=0,T_2=0), (T_1=0.25,T_2=0.5), L = 1

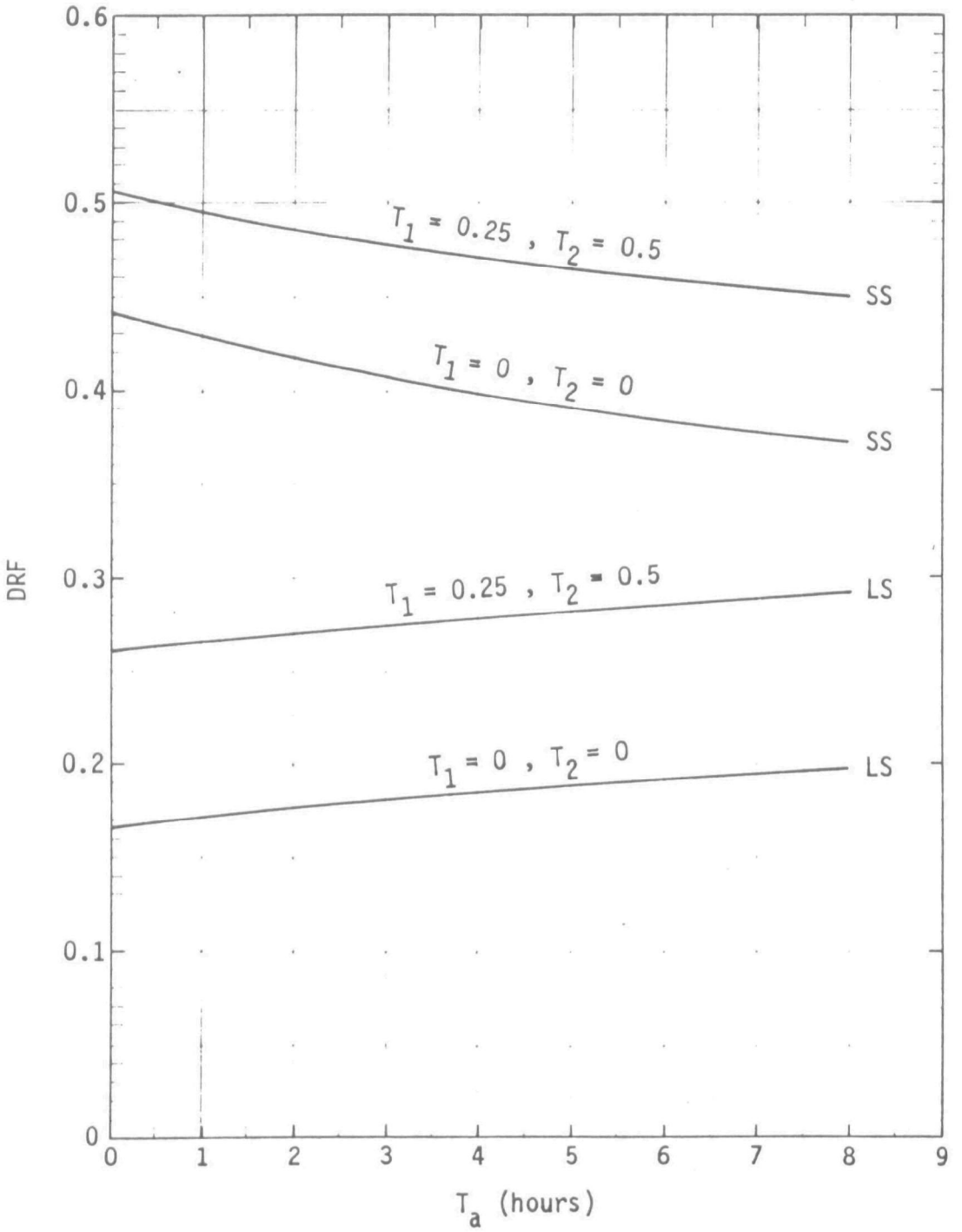

Fig. 16--WB DRF versus T_a, case C, (T_1=0,T_2=0), (T_1=0.25,T_2=0.5), L = 1

Figures 15 and 16 are similar plots for cases B and C, respectively, where timing (T_1 and T_2) is relatively less important, because of longer exposure to the cloud source.

Calculated DRF results in Figs. 17 through 22 show the effects of shelter-structure ventilation rate. Figure 17 gives the WB DRF as a function of air change rate, L hr^{-1}, for ideal shelter timing (T_1=0, T_2=0). For L less about one air change per hour, the SS DRF is based on a relatively larger external gamma-dose contribution from the outside airborne cloud source; for L greater than about one air change per hour, the DRF is based on a relatively larger dose component from internal airborne radioactive material. The LS DRF, on the other hand, is based primarily on the relatively larger WB-dose component from internal airborne gaseous radioactive sources for all values of air change rate, L.

Figure 18 gives the thyroid DRF dependence on the ventilation rate for ideal shelter timing. Compared with the WB DRF values in Fig. 17, the thyroid DRF functional dependence on L is much more pronounced, since the thyroid dose is based solely on internal airborne radioiodine. The advantage of low air-change rates less than about one-half per hour is quite apparent for protection against inhalation doses.

Figures 19 through 22 show the comparative effects of ideal and nonideal shelter timing. Figure 19 gives WB DRF values as a function of L for case A, showing considerable overlap of SS and LS protection for ideal (T_1=0, T_2=0) and nonideal (T_1=0.25, T_2=0.5) shelter timing, respectively. Figure 20 gives WB DRF for case B as a function of L when the SS and LS overlap is much less than in case A (Fig. 19), and Fig. 21 shows no SS and LS overlap for the longer source release duration category (C) when the inherent LS protection advantage over the SS is maintained, even for nonideal shelter timing. Figure 22 gives plots of the thyroid DRF, comparing the effects of nonideal and ideal shelter timing. The inversion in the order of the A, B, and C release-duration categories for nonideal shelter timing is primarily due to the fraction of time an individual is assumed to remain unprotected during cloud passage for shelter-access delay time, T_1; i.e., the fraction of time an individual is unprotected is larger for A than for C.

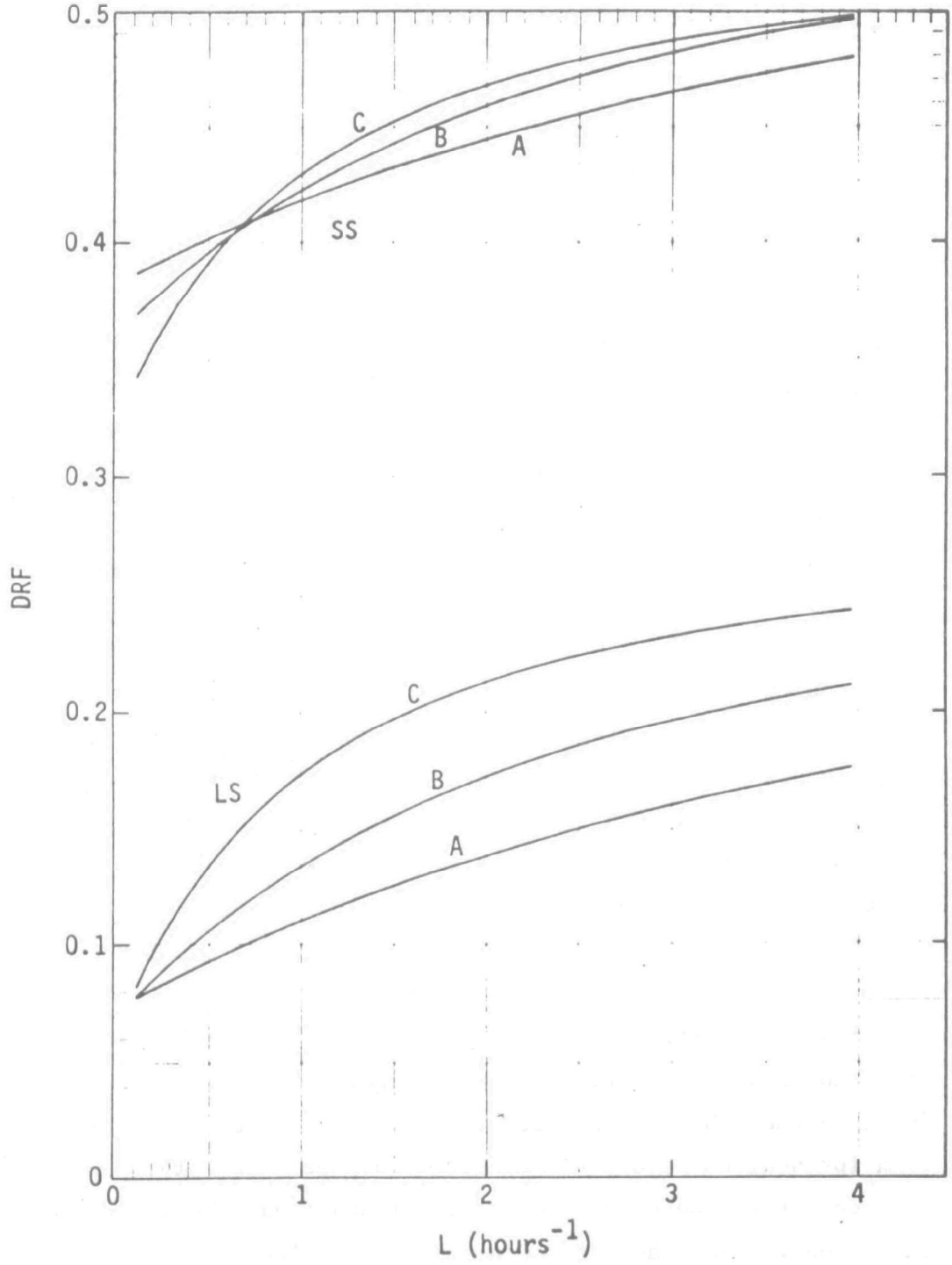

Fig. 17--WB DRF versus L, (T_1=0,T_2=0,T_a=1)

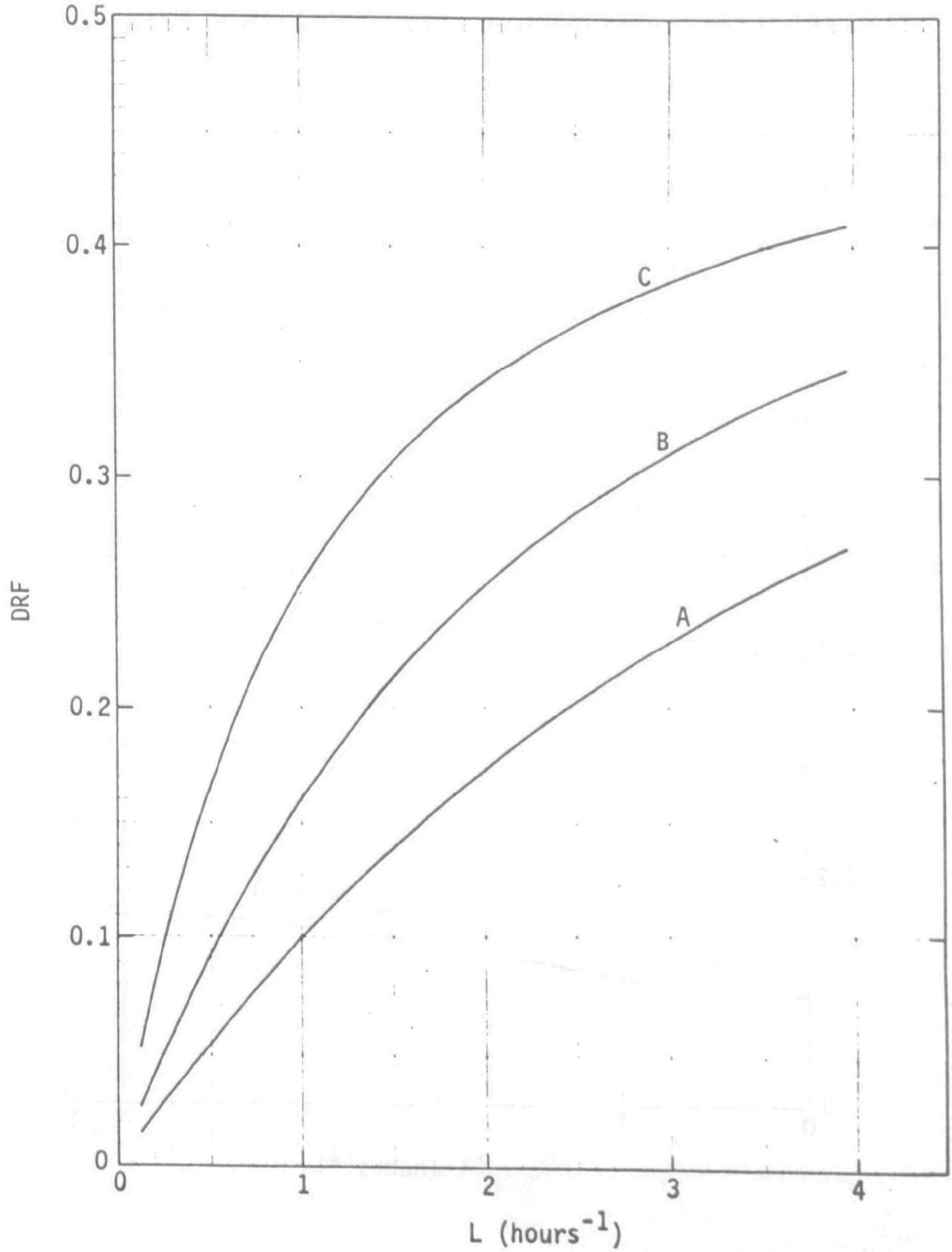

Fig. 18--Thyroid DRF versus L, (T_1=0,T_2=0,T_a=1)

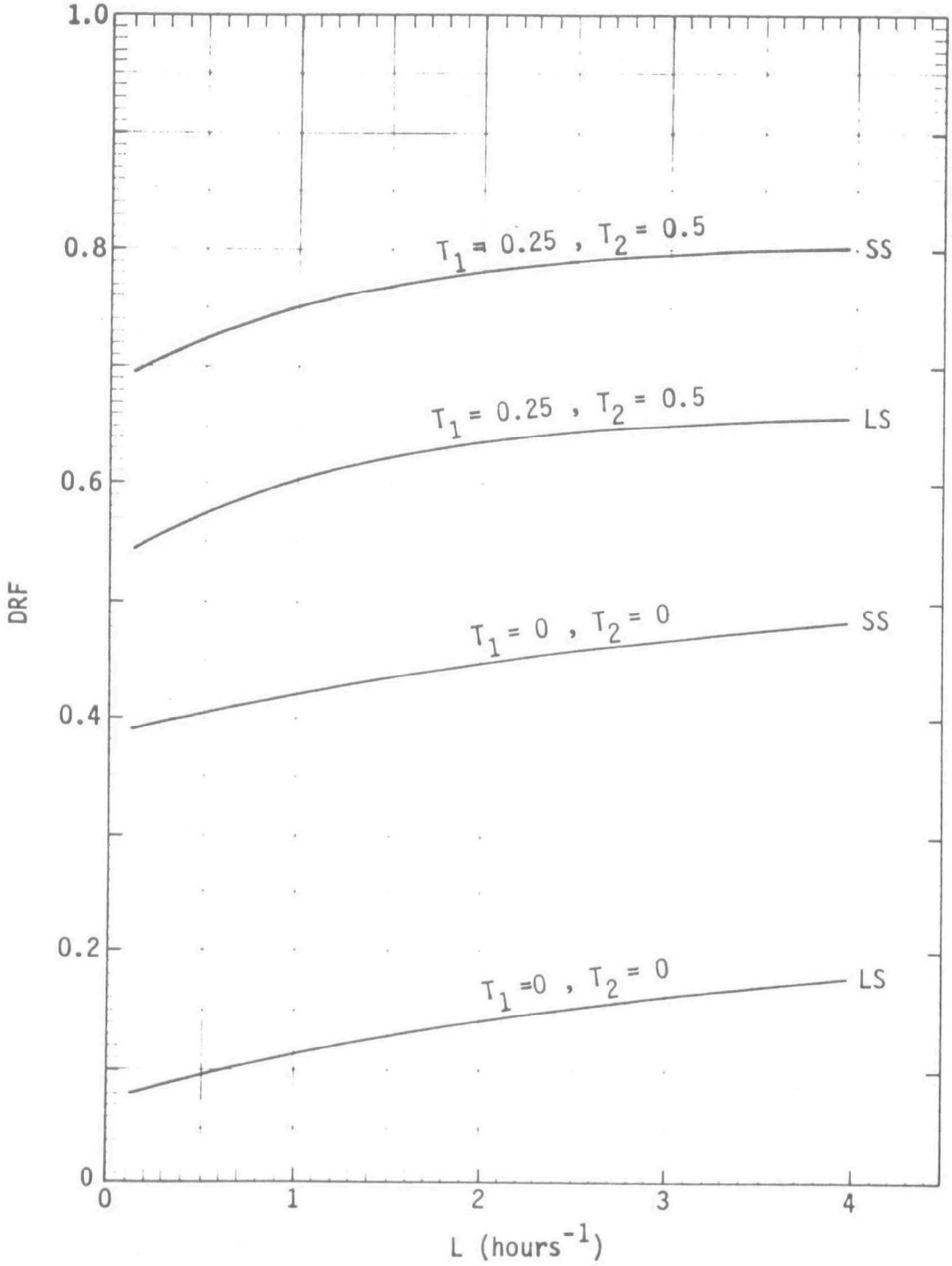

Fig. 19--WB DRF versus L, case A, (T_1=0,T_2=0), (T_1=0.25,T_2=0.5), T_a = 1

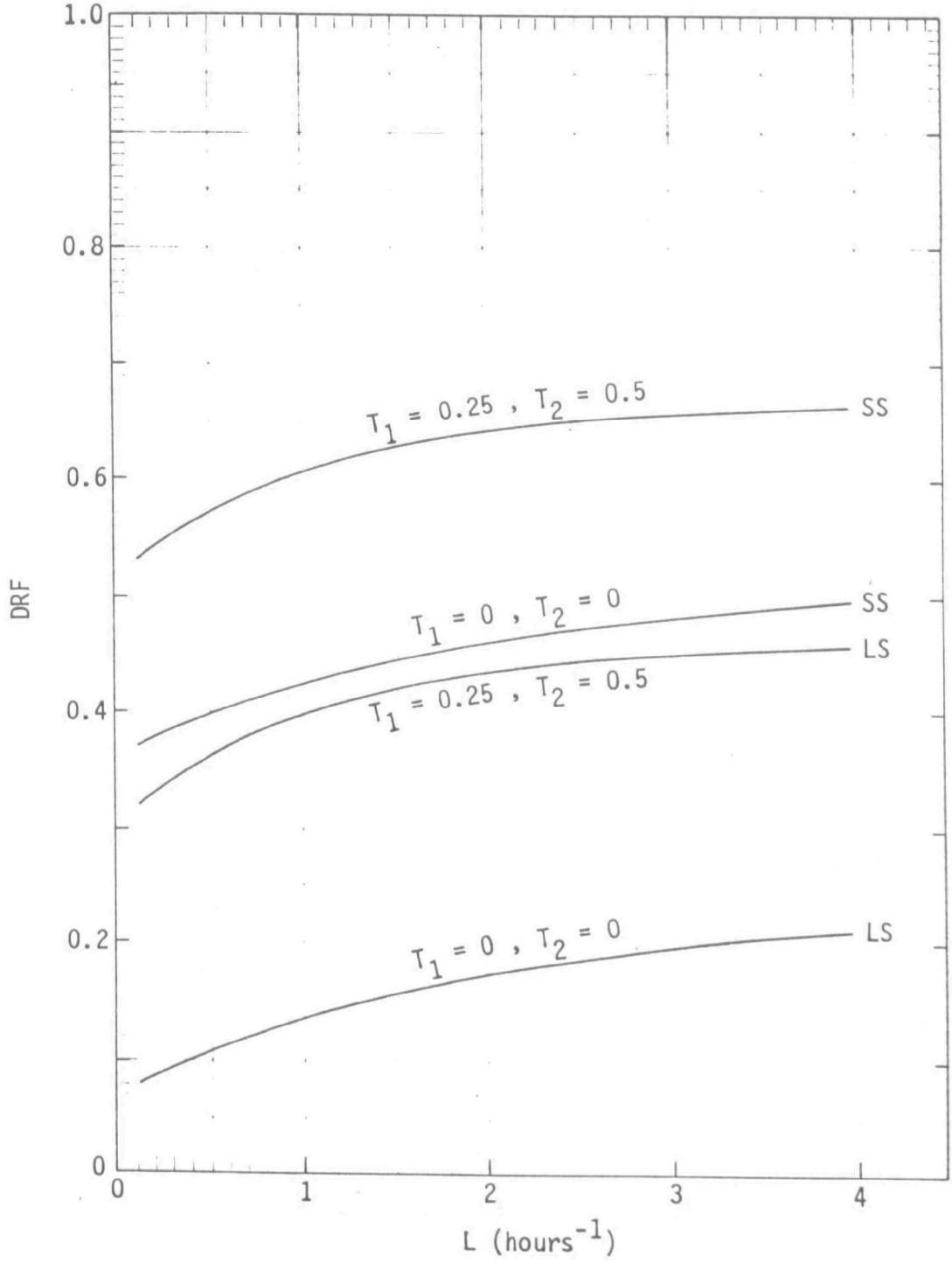

Fig. 20--WB DRF versus L, case B, (T_1=0,T_2=0), (T_1=0.25,T_2=0.5), T_a = 1

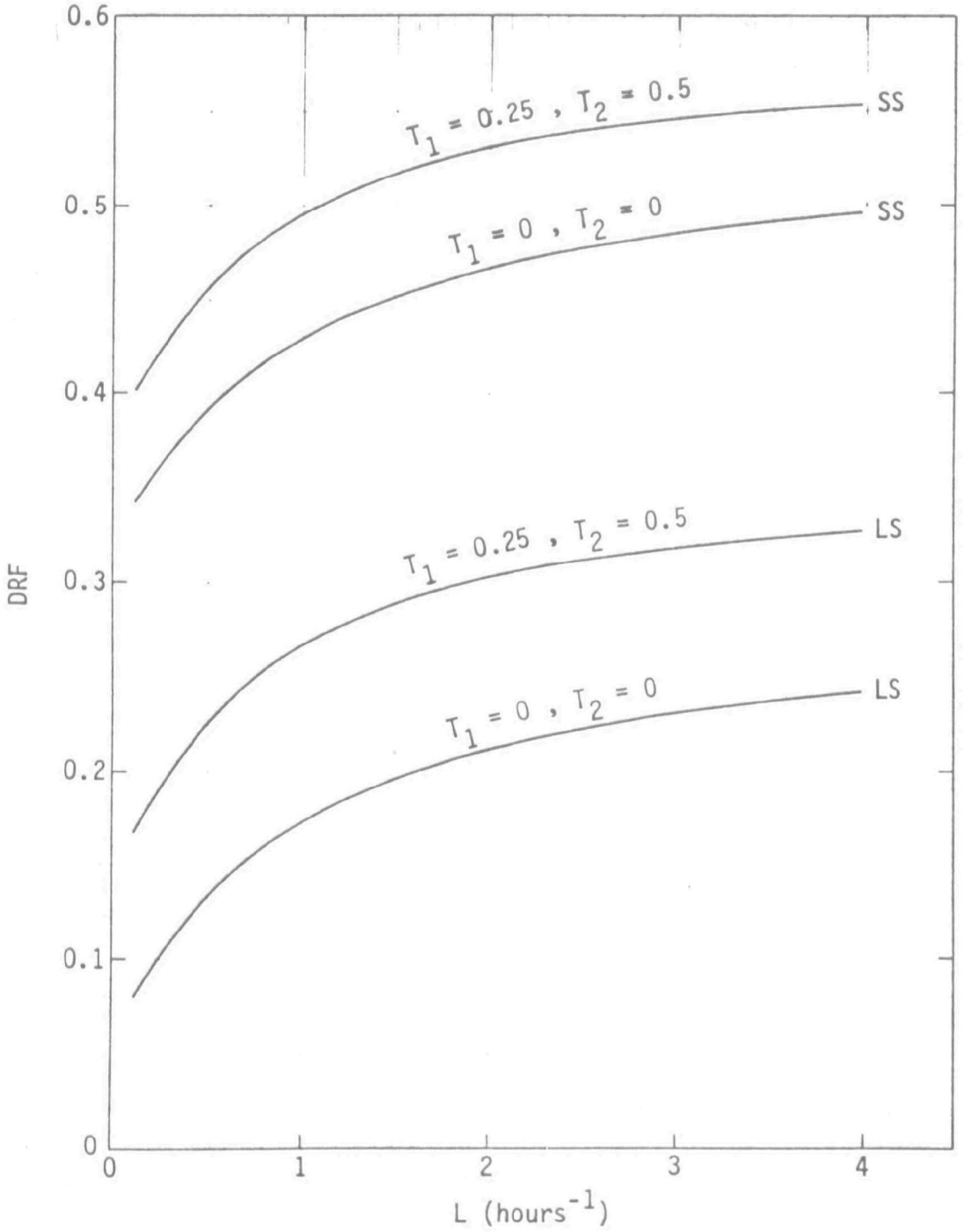

Fig. 21--WB DRF versus L, case C, (T_1=0,T_2=0), (T_1=0.25,T_2=0.5), T_a = 1

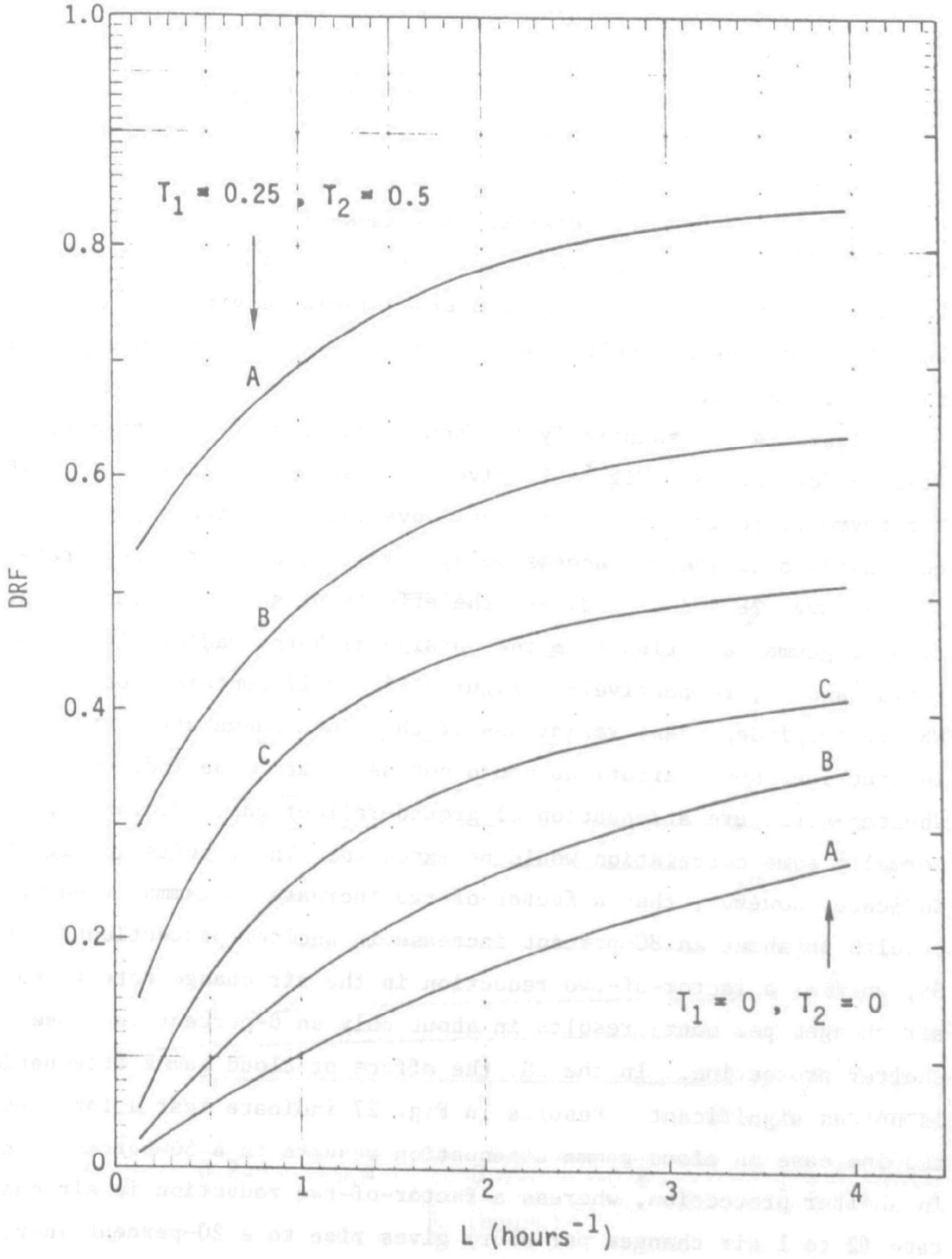

Fig. 22--Thyroid DRF versus L, (T_1=0,T_2=0), (T_1=0.25,T_2=0.5), T_a = 1

Figures 23 through 25 show WB and thyroid DRF values in terms of T_1 and L in parametric perspective. WB DRF values are shown in Fig. 23 for case B and for LS. DRF values for $T_1 = 1$ (also the cloud passage time for case B) can exceed unity for the larger values of L; this situation corresponds to entering a shelter after cloud passage, which gives rise to additional dose from lingering internal contamination for $T_2 > 0$, although the relative loss in shelter protection as a function of T_2 is insignificant for all values of T_1 and L. Also, calculations performed during this study indicate virtually no protective advantage in seeking shelter after unprotected exposure to a passing radioactive cloud.

Figure 24 is essentially the same parametric perspective plot as Fig. 23 for the SS. Figure 25 gives corresponding plots of the DRF for thyroid, indicating considerable overlap for certain parameter combinations of shelter-access delay time, T_1, and air change rate, L.

Figures 26 and 27 indicate the effects of shelter-structure attenuation of gamma radiation from the outside airborne radioactive cloud for the SS and LS, respectively. Figures 26 and 27 contain plots of the WB DRF for independent variations of the cloud gamma attenuation, A. In practice, such variations would not necessarily be independent of the shelter-structure attenuation of ground-fallout gamma radiation, as normally some correlation would be expected. The results in Fig. 26 indicate, however, that a factor-of-two increase in gamma attenuation results in about an 80-percent increase in shelter protection for the SS, whereas a factor-of-two reduction in the air change rate (2 to 1 air changes per hour) results in about only an 8-percent increase in shelter protection. In the LS, the effect of cloud gamma attenuation is not as significant. Results in Fig. 27 indicate that a factor-of-two increase in cloud gamma attenuation results in a 50-percent increase in shelter protection, whereas a factor-of-two reduction in air change rate (2 to 1 air changes per hour) gives rise to a 20-percent increase in shelter protection.

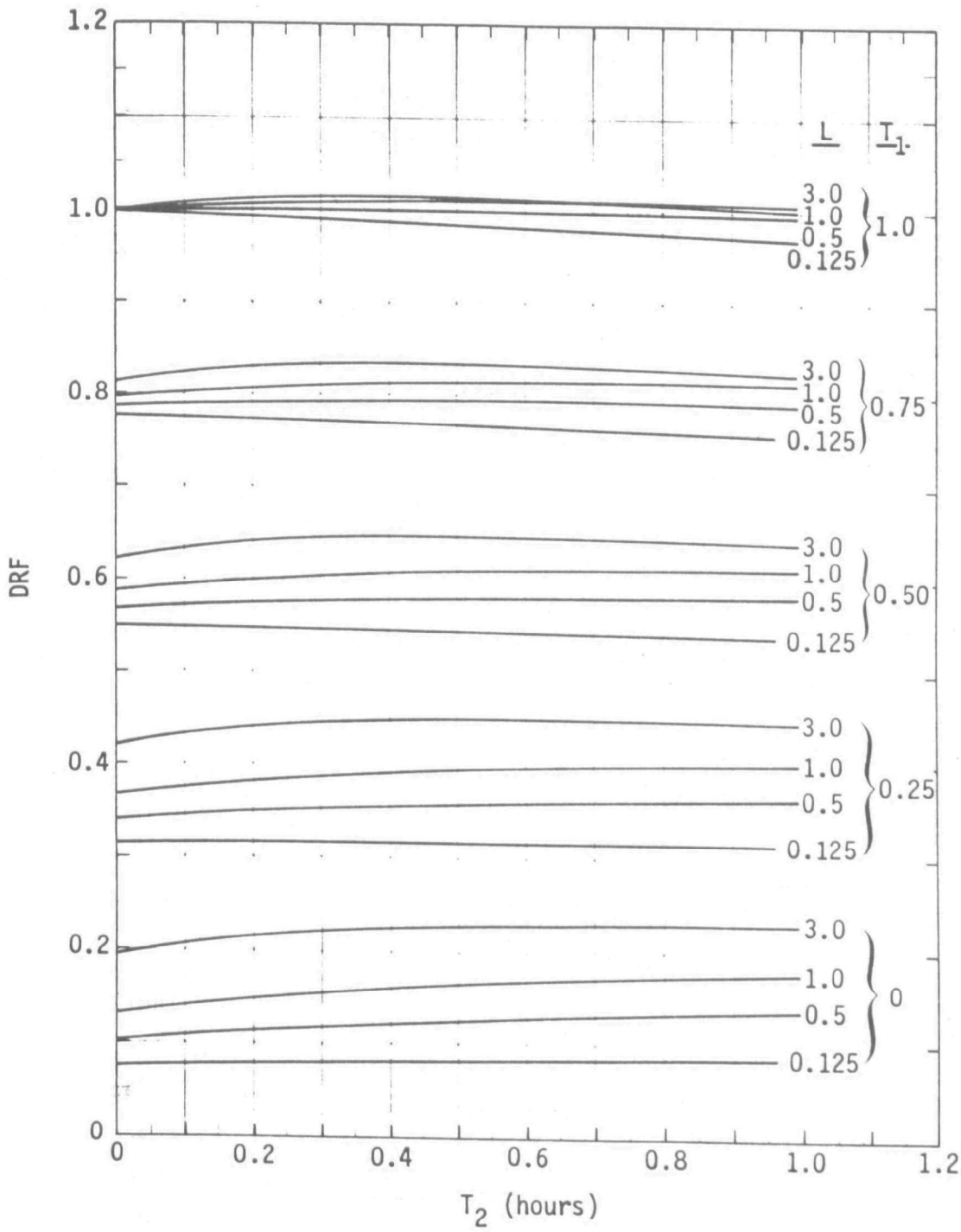

Fig. 23--WB DRF versus T_2, case B, LS, T_a = 1

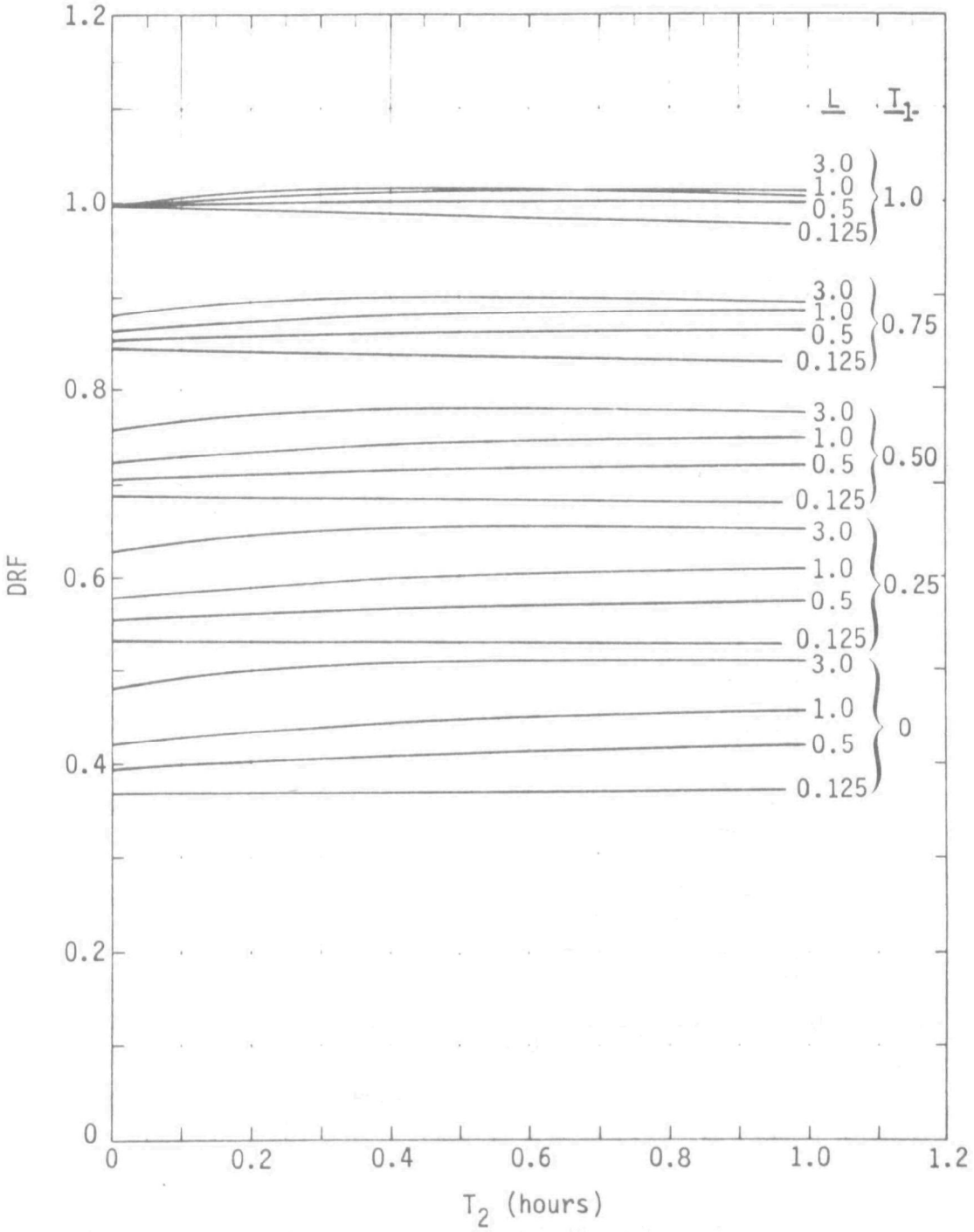

Fig. 24--WB DRF versus T_2, case B, SS, T_a = 1

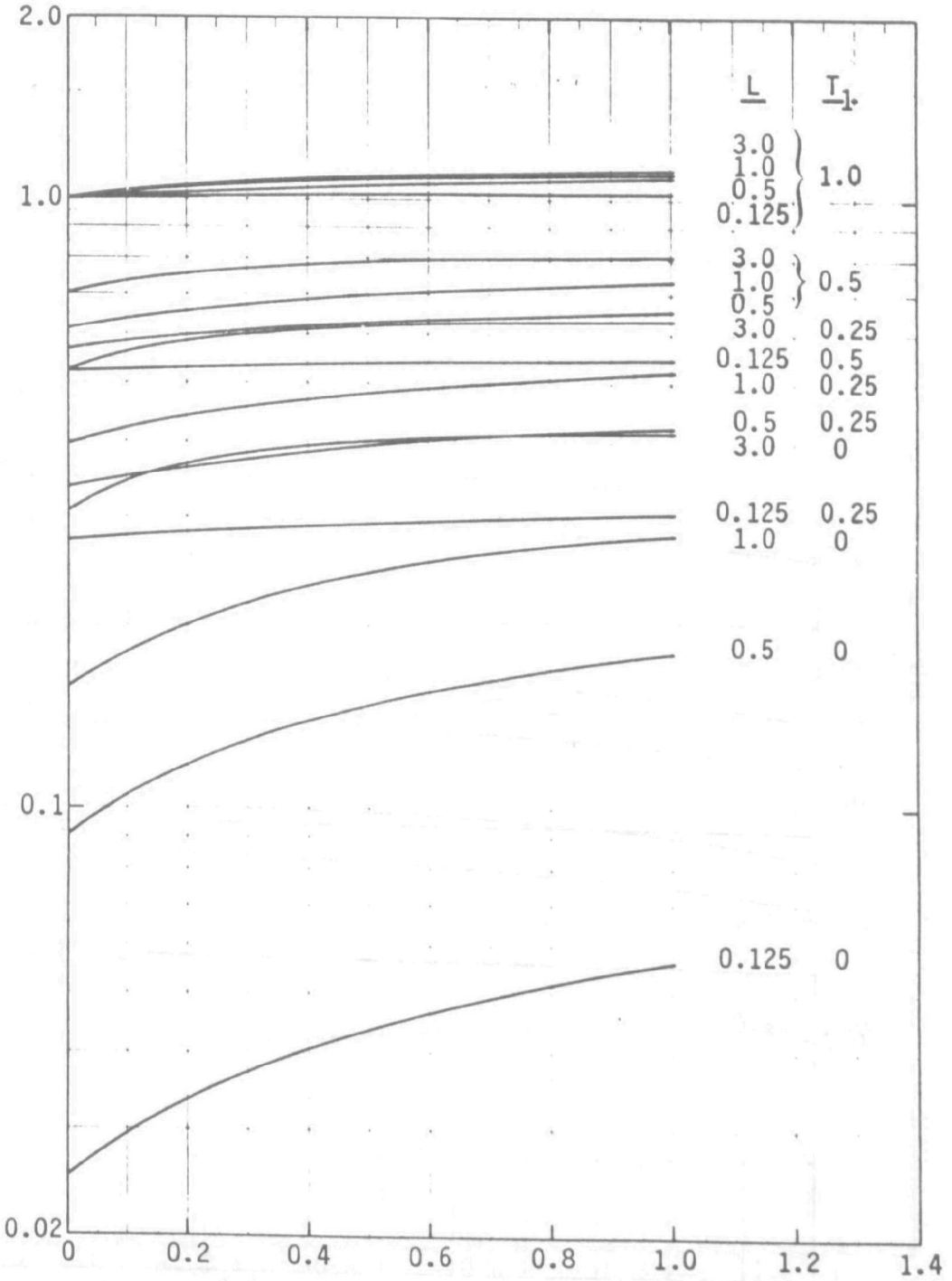

Fig. 25--Thyroid DRF versus T_2, case B, $T_a = 1$

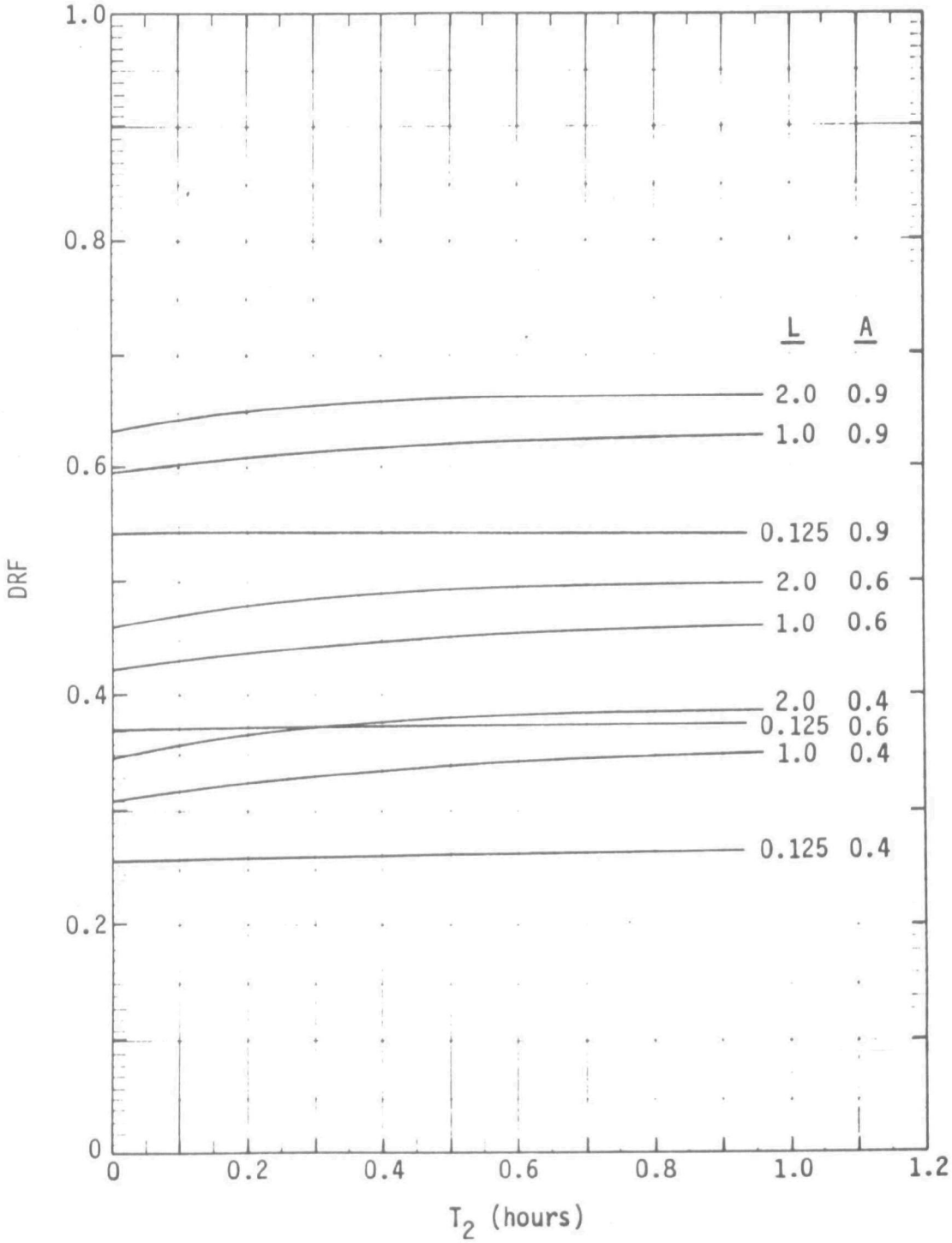

Fig. 26--WB DRF versus T_2, case B, SS (A=0.4,0.6,0.9,L=0.125,1.0,2.0)

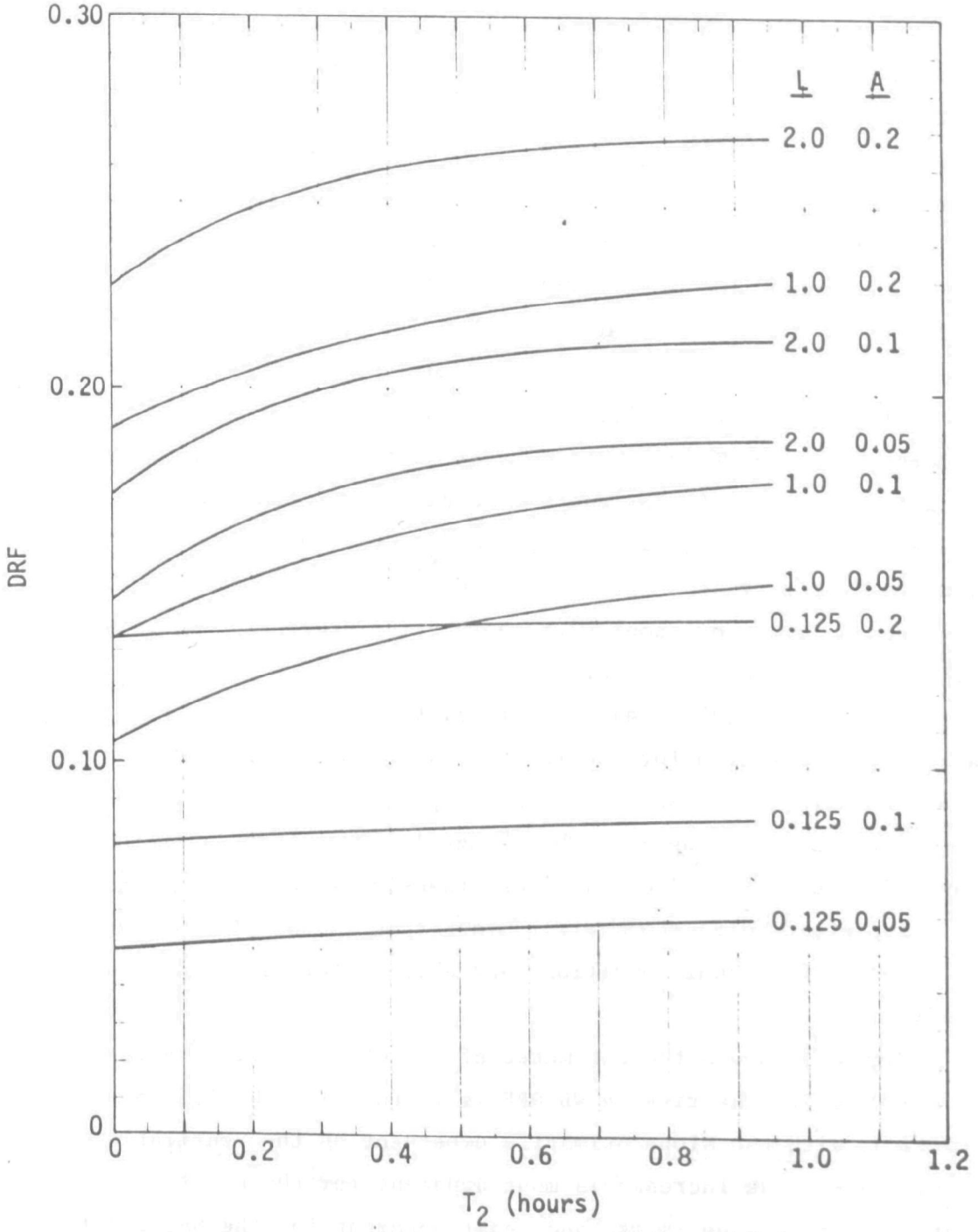

Fig. 27--WB DRF versus T_2, case B, LS (A=0.05,0.1,0.2,L=0.125,1.0,2.0)

Figures 28 and 29 are plots of shelter DRF as a function of shelter-delay access time, T_1, for the WB and thyroid, respectively. Figure 28 plots are given for a range of 0.5 to 1.5 air changes per hour, which is recommended by Handley and Barton [7] as applicable to single-family dwellings. The value of two air changes per hour for the LS is also consistent with their recommendations for larger structures and apartment buildings. For ideal shelter timing, $T_1 = 0$, and $T_2 = 0$, the LS provides about twice the protection as the SS, which decreases with increasing access delay time. Figure 29 gives thyroid DRF plots for the same conditions as Fig. 28; since the thyroid dose is dependent only on the ventilation rate, somewhat less protection is afforded by the LS than by the SS, because of the difference in ventilation rate.

Figures 30 and 31 illustrate the difference in shelter protection afforded for the WB and thyroid under ideal and less-than-ideal conditions. In Fig. 30, DRF values are given as a function of T_1 for a low air-change rate (0.125 hr^{-1}) and $T_2 = 0$. For $T_1 = 0$, the SS provides a factor of about 2.8 for WB-dose protection; whereas the LS provides a factor of about 12.5--a relative protective advantage of 4.5--for the LS over the SS. In Fig. 31, for less-than-ideal sheltering conditions (T_2=0.25 and L=1 hr^{-1}), the SS provides a factor of about 2.2 protection for the WB dose; whereas the LS provides a WB protective factor of $\sim$6.7--a relative protective advantage of about 3--for the LS over the SS. The change in the protection for the thyroid dose between ideal and less-than-ideal sheltering conditions is about eight-fold; the shelter protection factor of the thyroid dose is about 40 for ideal conditions and about 5 for less-than-ideal conditions.

Figure 32 shows the estimated effect of the iodine ingress fraction on the WB DRF. The rise in WB DRF is linear with the iodine ingress fraction, with the slope primarily dependent on the ventilation air-change rate. The increase is most apparent for the LS, for representative air change rates, and least apparent for the SS, for low air-change rates. Again, this difference is due to the relative contribution of the dose components from radioactive sources outside and inside the

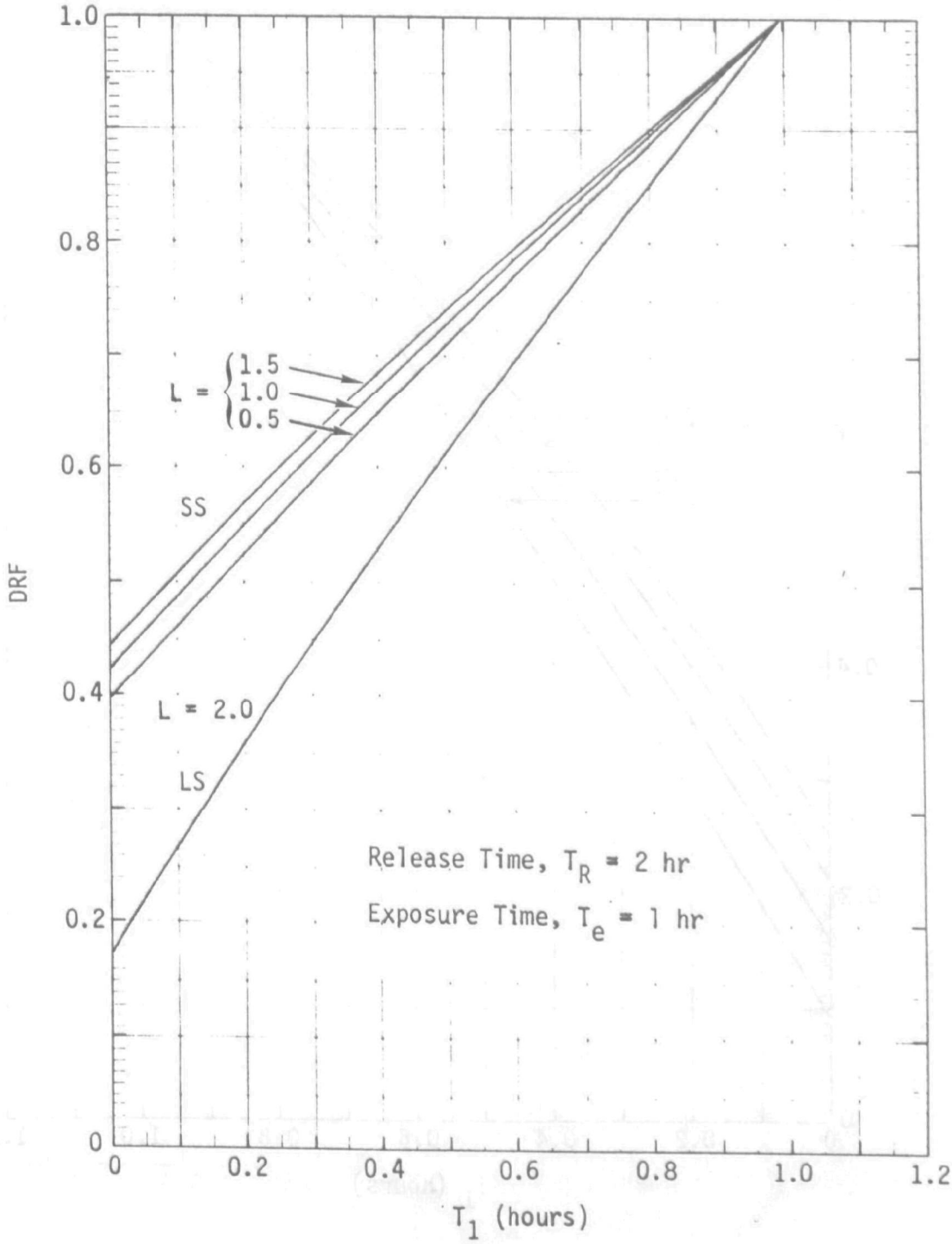

Fig. 28--WB DRF versus T_1, case B, (T_a=1,T_2=0), SS (L=0.5,1.0,1.5), LS (L=2)

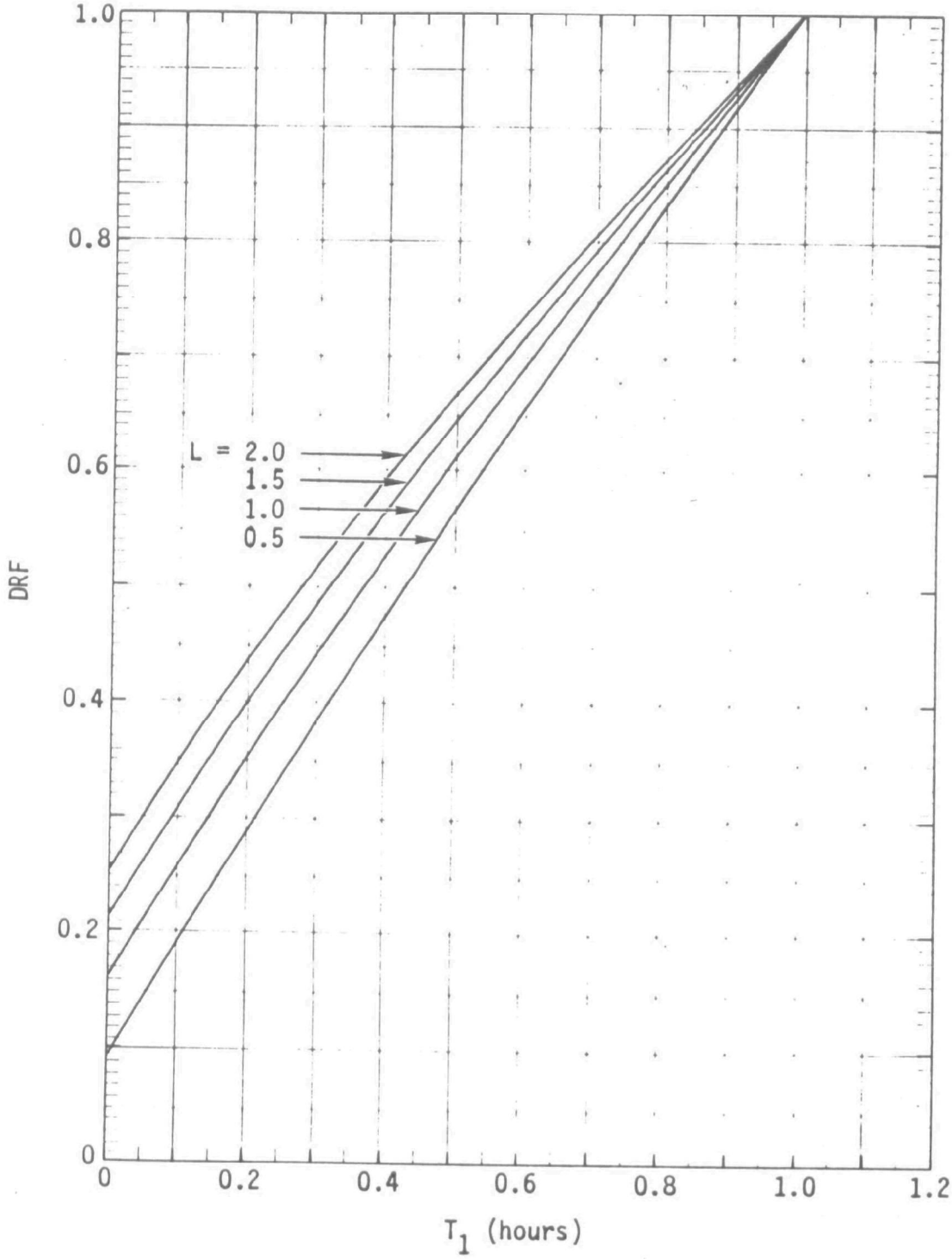

Fig. 29--Thyroid DRF versus T_1, case B, (T_a=1,T_2=0), L = 0.5, 1.0, 1.5, 2.0

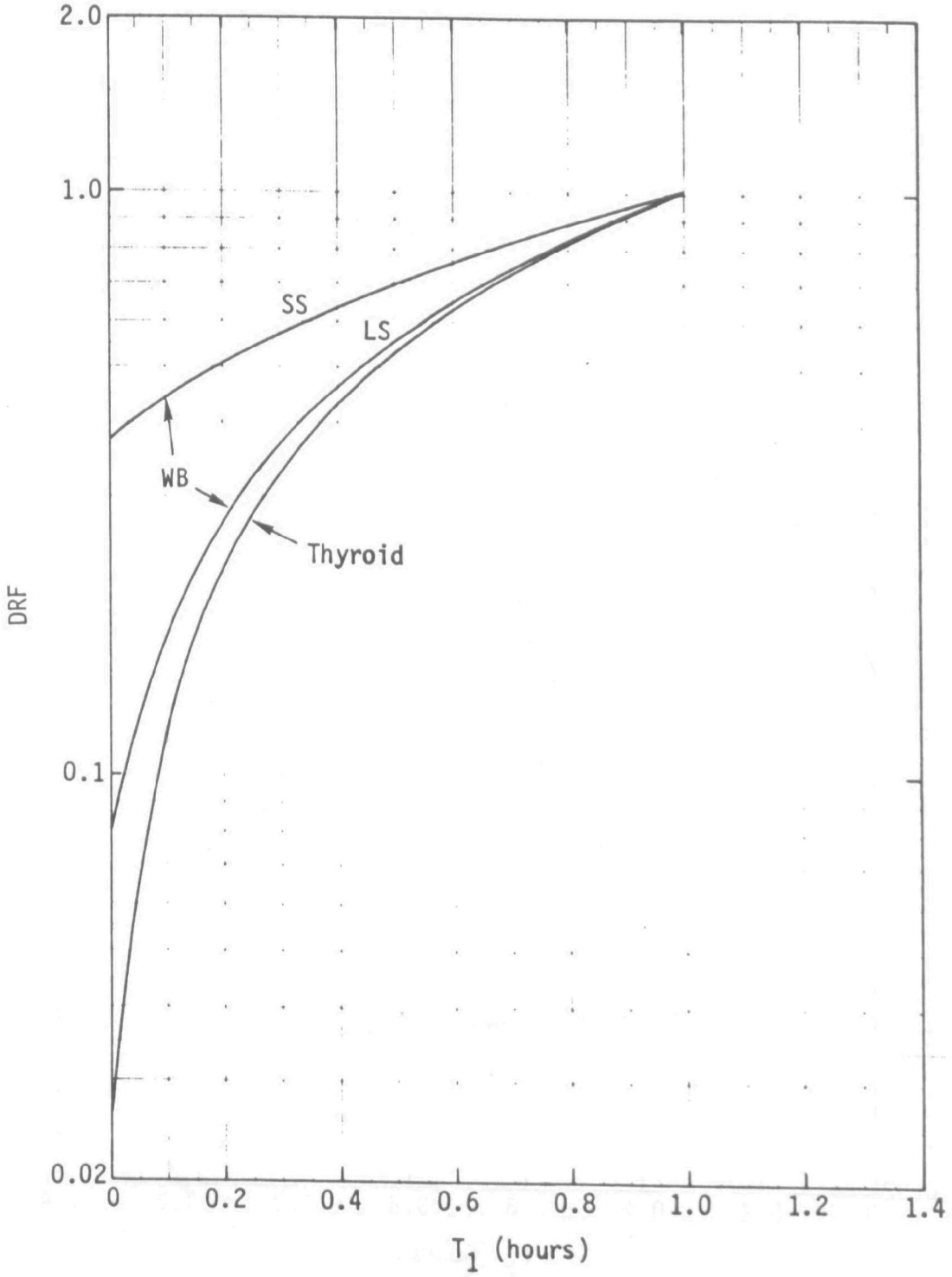

Fig. 30--WB and thyroid DRF versus T_1, case B, (T_a=1,T_2=0,L=0.125)

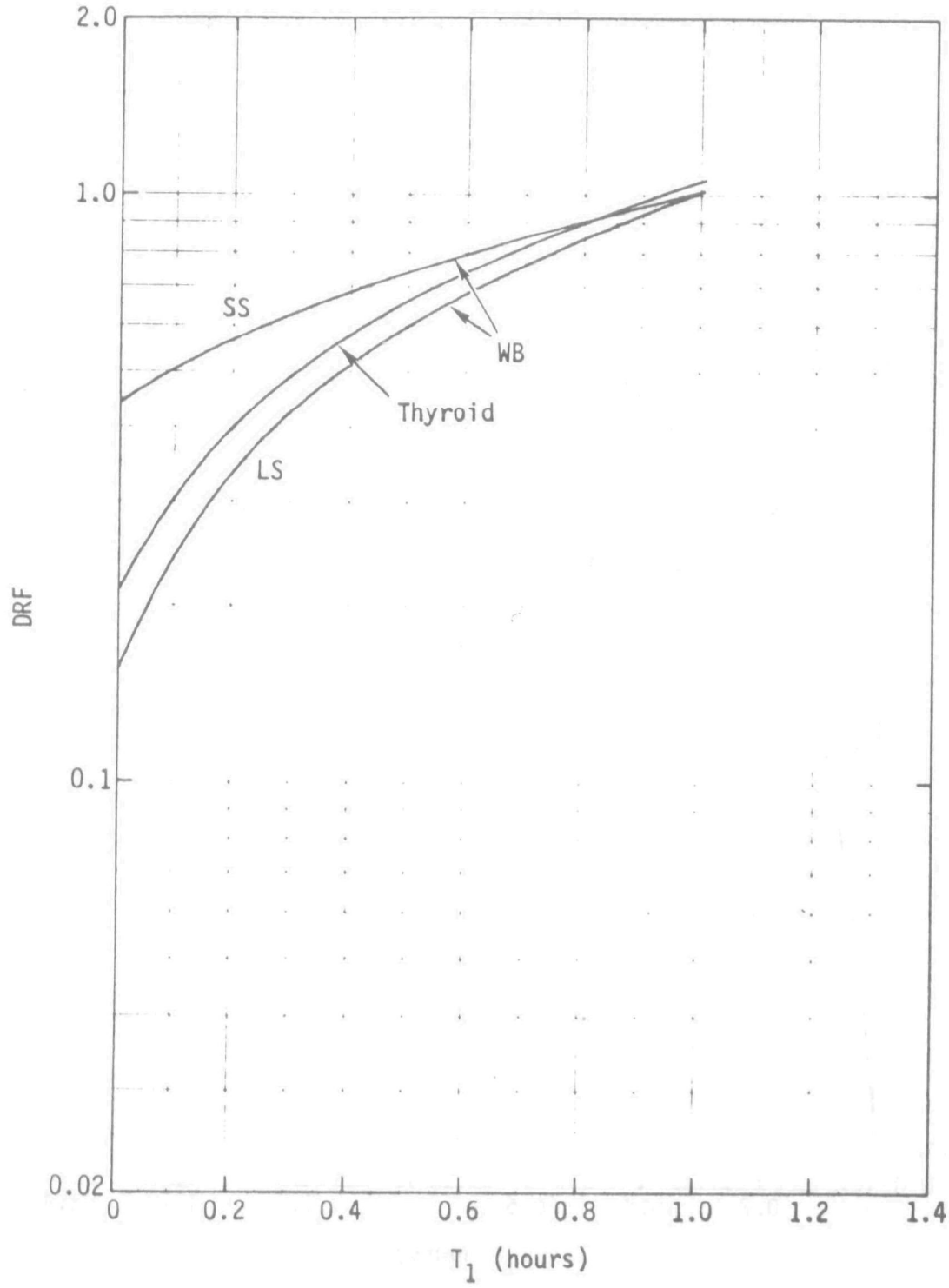

Fig. 31--WB and thyroid DRF versus T_1, case B, (T_a=1,T_2=0.25,L=1.0)

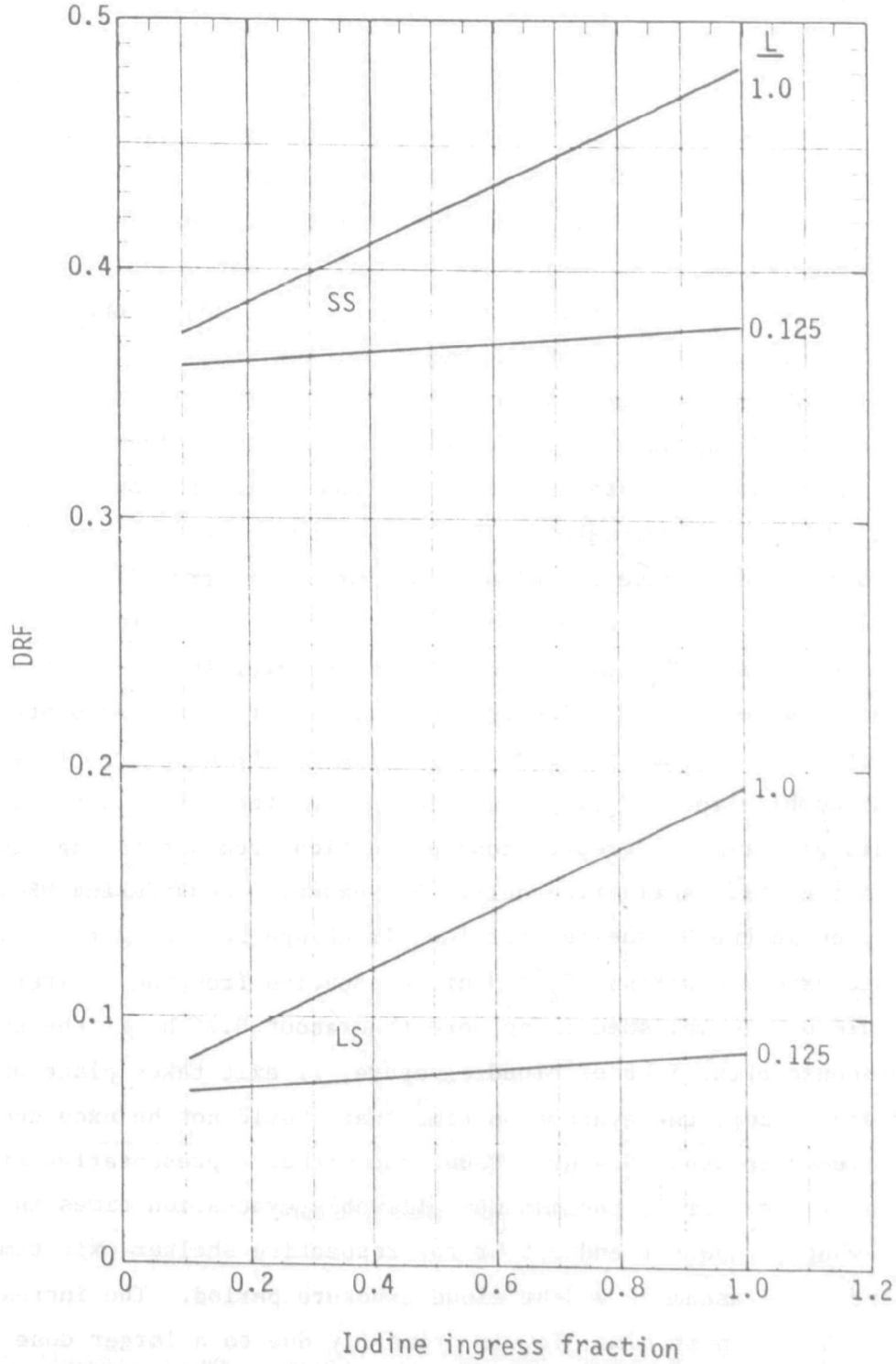

Fig. 32--WB DRF versus iodine ingress fraction, case B, (T_1=0,T_2=0,T_a=1)

shelter. As indicated above, a value of 0.51 was used in the calculations for estimating the DRF. If iodine ingress were 100 percent, the DRF may be from about 1.4- to 14-percent higher for SS and from about 16- to 46-percent higher for LS. Of course, for the thyroid dose, the DRF could be nearly double (assuming ideal shelter-access timing).

Figures 33 through 35 are based on calculations for the combined protective action of sheltering and evacuation. The results shown are for the shelter time, T_S, and the evacuation transport time, T_T, which together would provide protection equal to that of sheltering alone during the period of cloud exposure, T_e. The conditions of sheltering are consistent with ideal timing; i.e., individuals are assumed to be in the shelter at the time of cloud arrival (T_1=0) and exit immediately after cloud exposure (T_2=0). The combined protective actions of sheltering and evacuation assume that individuals exit the shelter after a period, T_S, and evacuate during the period T_T, while exposed to the airborne radioactive cloud material during its transit away from the shelter area. Accordingly, if the structure were exited after a shelter period, T_S, evacuation out of the vicinity of cloud exposure should not exceed the time period, T_T, to effect a dose protection at least equal to that provided by staying in the shelter. Therefore, time combinations (T_S,T_T) that lie between the curves and the axes would give rise to greater dose protection from sheltering plus evacuation than from sheltering only. For example, considering WB-dose protection in the SS shelter for low air-change rate conditions and a cloud exposure period, T_e = 3 hr, evacuation from the shelter vicinity should be accomplished in no more than about 0.75 hr if the shelter is abandoned after 1 hr of cloud exposure; if exit takes place after 2 hr of sheltering, the evacuation time that should not be exceeded is shortened to about 0.4 hr. Under the higher representative air change rate of L = 1 hr^{-1}, the maximum allowable evacuation times increase somewhat to about 1 and 0.5 hr for respective shelter-exit times of 1 and 2 hr, assuming a 3-hr cloud exposure period. The increase in allowable transit time, T_T, is primarily due to a larger dose incurred in the shelter structure with the higher air change rate.

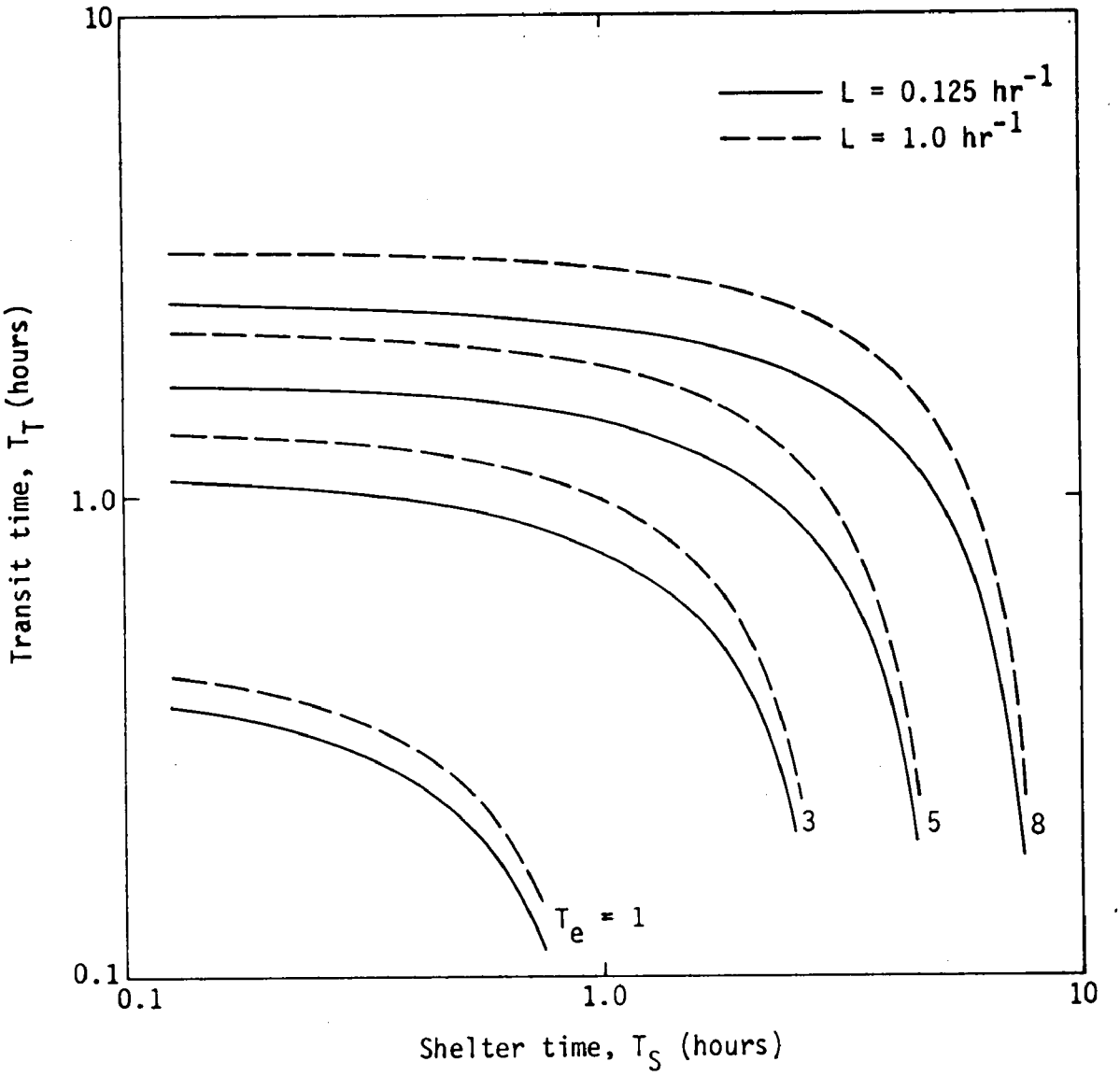

Fig. 33--Sheltering with evacuation, WB, SS--transit time versus shelter time (T_a=0.5)

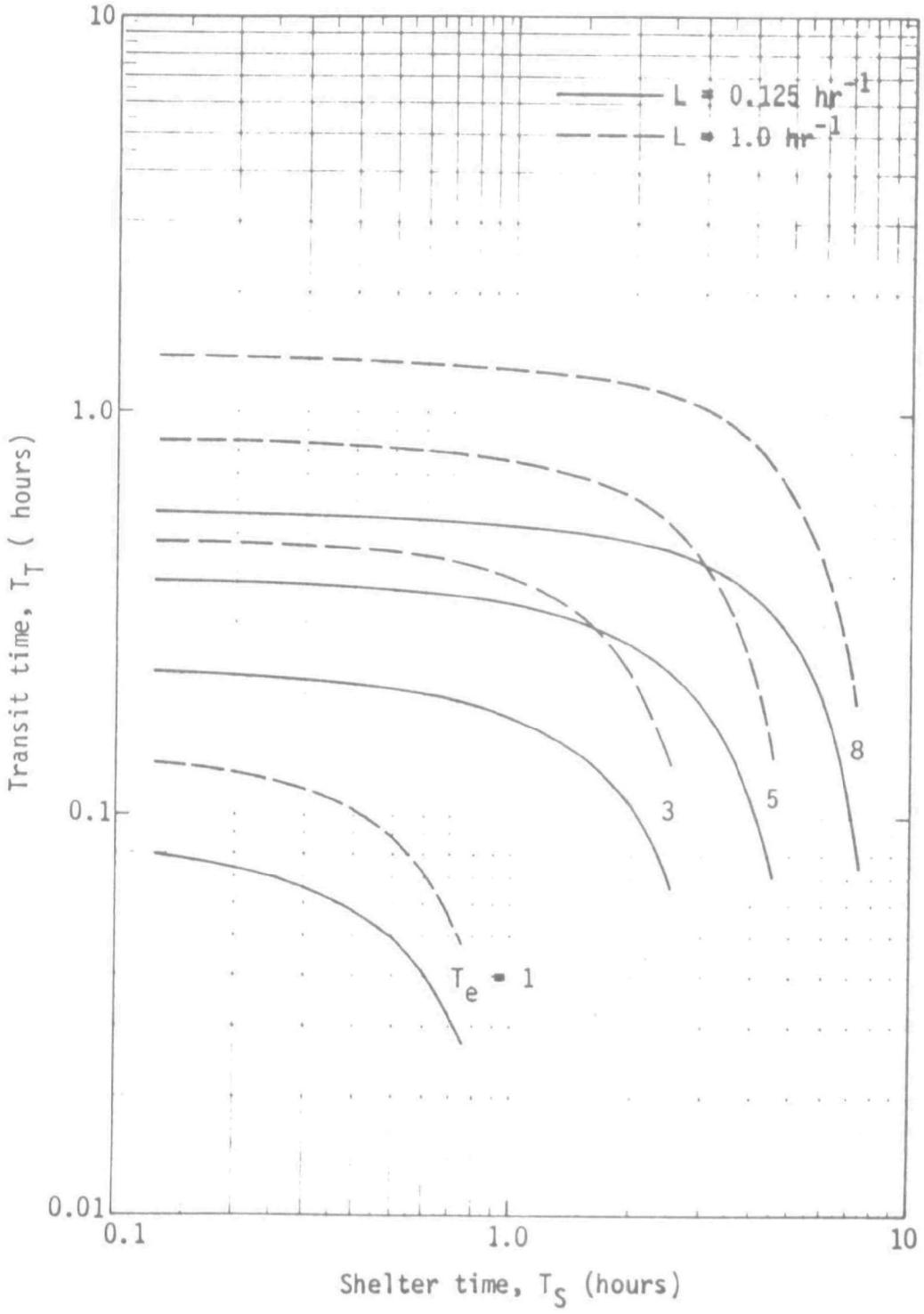

Fig. 34--Sheltering with evacuation, WB, LS--transit time versus shelter time (T_a=0.5)

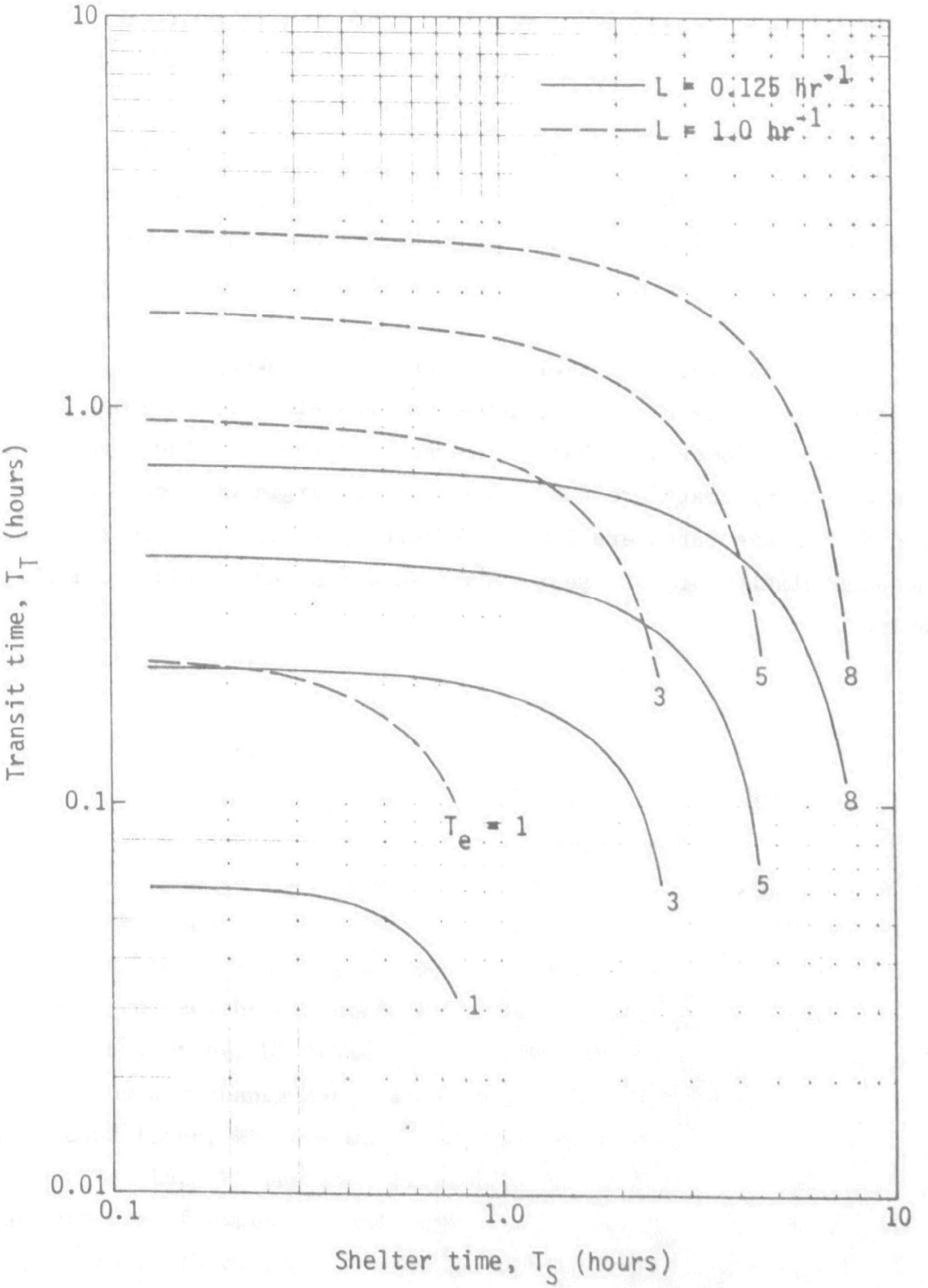

Fig. 35--Sheltering with evacuation, thyroid--transit time versus shelter time (T_a=0.5)

Figure 34 gives shelter evacuation break-even times for the LS shelter. For low air-change rate conditions, much less time is allowed for evacuation from the LS shelter area than from the SS for a given shelter-exit time, T_S, because of the significantly greater margin of protection (lower DRF) offered by the LS. For the higher representative air change rate of $L = hr^{-1}$, the allowable transit time from the LS shelter again is less than that for the SS shelter; but the time difference is not as great as compared with that for the low air-change rate situation.

Figure 35 gives the shelter evacuation break-even time points for thyroid dose protection. The lower maximum allowable evacuation transit times for the lower air change rate as compared with the higher representative air change rate are due to the larger margin of protection provided when air change rates are low and accordingly less time is required for the accumulation of the break-even dose during evacuation from the shelter.

IV. CONCLUSIONS AND RECOMMENDATIONS

Shelter protection provided by a large variety of public structures can provide a significant reduction in WB and thyroid dose from exposure to radioactive gaseous fission products that might be released during a nuclear power plant accident. Protective sheltering is attractive if shelter-access timing is ideal, but its effectiveness diminishes almost linearly with access delay time after cloud arrival.

Sheltering protection against inhalation exposures that result in thyroid dose depends on the number of air changes taking place over the period of exposure to airborne radioactive cloud material. Sheltering protection for WB exposures depends on the attenuation of gamma radiation originating from the airborne cloud source, the number of air changes during cloud exposure, and (to a lesser extent) the attenuation of gamma radiation originating from the ground fallout about the shelter structure. Accordingly, optimum ventilation control (low air-change rates during cloud passage) is more effective for reducing thyroid dose than WB dose. Albeit, ventilation control is relatively more effective for reducing WB dose in LS than in SS.

Large structures such as office buildings, multistory apartment complexes, department stores, etc., generally would provide significantly more sheltering for WB exposures than smaller structures such as single-family dwellings--a factor of about 4.5 more during low air-change rate conditions and 3 more for nominal air change rates. That is, WB doses would be reduced by a factor of 2.5 to 3 for SS sheltering; whereas for LS sheltering, WB doses would be reduced by a factor of about 12 during low air-change rate conditions. For representative air change rate conditions, WB dose would be reduced by about 2.3 for SS and from 6 to 9 for LS. WB dose can be further reduced in a shelter structure through use of expedient filtration; e.g., by stuffing cracks and openings with cloth or paper materials, which would reduce radioactive material ingress (discussed above, p. 10 ff.) and/or the natural ventilation rate. Similarly, another means of respiratory protection is to cover the nose

and mouth area with such common items as towels, handkerchiefs, or toilet paper: e.g., a crumpled handkerchief (or one with eight or more folded layers), a towel of three or more folded layers, or toilet paper of three or more folded layers can reduce inhaled radioactive material (particulate iodine in this study) by a factor of about 10 [35]. The reduction of WB dose in a SS, however, is not appreciable--about 2.5 percent for low ventilation rates and about 15 percent for representative ventilation rates. The reduction in WB dose in a LS would be more appreciable--about 13 percent for low ventilation rates and about 70 percent for representative ventilation rates.

The difference in thyroid dose protection between SS and LS shelters is not as apparent as for WB dose, because of the more nebulous correlation of building air change rate than gamma radiation-attenuation properties with the general type of structure. The degree of variability in the air change rate--an important parameter affecting the thyroid exposure--prevents meaningful estimates of the thyroid DRF for SS as opposed to LS shelters. Accordingly, LS may not necessarily have any protective advantage for thyroid dose reduction over SS or vice versa, due to any number of factors--open portals, filtering action, air conditioning, structural integrity, etc. Sheltering protection for either SS or LS, however, can result in thyroid dose reduction by a factor of from about 20 to 70 for low air-change rates, and from 4 to 10 for representative air change rates. These ranges are primarily due to the corresponding range of cloud-exposure periods of from 0.5 to 3 hr, where the DRF increases, although not linearly with the air change rate (or number of air changes). Another important parameter affecting the thyroid DRF value (also the WB DRF to a lesser extent) is the ingress fraction, which is treated like an effective filtering action in this study. For that parameter, a value of 0.51 was assumed for the radioiodines, based on review of limited experimental work discussed above (p. 10 ff.). The thyroid DRF values given would then scale linearly with whatever value is assumed. The use of expedient filtration discussed above for WB dose can be even more effective in reducing thyroid dose (i.e., reducing radioiodine ingress and/or ventilation by stuffing openings and cracks or

using such common items as handkerchiefs and towels for respiratory protection). Such expedient filtration could reduce thyroid dose by a factor of about 10 [35].

The protection against WB dose decreases linearly with the amount of radioiodine penetrating to the occupied spaces of a shelter structure. The decrease is more apparent for LS than SS, because of the relative differences in the gamma ray attenuation from sources outside the shelter, and is also related to the number of air changes that take place during the cloud-exposure period. For this analysis, an ingress fraction of 0.51 is assumed for making DRF calculational estimates. This assumption implies that radioiodine sources collect at certain locations in the shelter structures. Therefore, insofar as these locations could represent "hot spots," local exposure of individuals who may be adjacent to these collection points could result in dose increase. No attempt has been made here, however, to deal with that problem other than to make note of it. In view of current uncertainty regarding penetration of radioiodine into structures that could be used as shelters, the need for more experimental results must be emphasized.

The degree of WB dose protection afforded by shelter structures as a function of cloud-exposure time depends largely on the relative contributions of the exposure modes. The larger the relative external dose contribution from penetration of gamma radiation into the shelter as compared with WB-inhalation dose, the less the effect of cloud-exposure time on shelter effectiveness. For example, for the SS where gamma ray penetration is relatively more important, the DRF would remain relatively constant for cloud-exposure periods up to several hours. For low ventilation rates, the sheltering protection may even increase somewhat--only about 15 percent or so--because of changes in the radioisotope source mix as a result of decay.

For LS shelters, where the WB dose component from gamma ray penetration is relatively less important than in SS shelters, the degree of protection still remains nearly constant for cloud-exposure periods up to several hours for low ventilation rates; but for representative ventilation rates, the relative protection for sheltering diminishes

significantly--e.g., a factor of about 1.7 for a 3-hr cloud-exposure period as compared with a 0.5-hr period. The utility of ventilation-rate control in minimizing the number of air changes during sheltering, especially for LS, is strongly supported by the results of this analysis. Maintaining low ventilation rates is even more important from the standpoint of thyroid dose reduction for either LS or SS, as the loss in protection for the same cloud-exposure periods mentioned above would amount to a factor of about 2.5 for a representative ventilation rate of one air change per hour during sheltering.

Small-structure shelter protection for WB doses tends to increase somewhat with cloud arrival time because of radioisotope decay and corresponding changes in radionuclide proportions. For LS shelters, protection remains nearly constant with cloud arrival time, because of the relatively larger inhalation dose component; this holds true even more so for thyroid dose protection.

Shelter protection for WB dose diminishes for LS to a greater extent than for SS with increasing ventilation rates. For a low ventilation rate ($L=0.125\ hr^{-1}$) as compared with a high ventilation rate ($L=4\ hr^{-1}$), SS shelter protection diminishes by a factor of $\sim$1.32, whereas LS shelter protection diminishes by a factor of $\sim$2.7; thyroid dose protection decreases by a factor of $\sim$6.

The attenuation of gamma radiation from airborne radioactive material outside the shelter structure is more important to the WB DRF than that of ground fallout about the shelter. Also, the effect of gamma ray attenuation on the DRF from sources outside the shelter is more significant for the SS than the LS, whereas the converse holds for the ventilation rate. That is, a factor-of-two increase in gamma attenuation results in about an 80-percent increase in shelter protection for the SS, whereas a factor-of-two reduction in the air change rate results in only about an 8-percent increase in shelter protection for WB dose. For the LS, a factor-of-two increase in cloud-gamma attenuation results in a 50-percent increase in shelter protection, whereas a factor-of-two reduction in the air change rate gives rise to a 20-percent increase in shelter protection.

The penalty in shelter protection for remaining in the shelter after the cloud-exposure period depends on the number of air changes taking place during cloud passage coupled with the relative contribution to the dose from inhalation. When air change rates are low, no significant loss of protection for the WB dose in either the SS or LS occurs, regardless of how long individuals remain in the shelter after cloud passage. WB-dose sheltering protection is not affected very much when remaining in a SS after cloud passage; for a LS, shelter effectiveness may be reduced from 10 to 20 percent by remaining in the shelter for a period up to about an hour after cloud passage. The sheltering protection penalty is much more pronounced for the thyroid dose, which can amount to a factor of about a 1.2 to 3 increase in the DRF, as compared with ideal shelter-timing conditions, should individuals remain in the shelter for a period up to about one hour after cloud passage.

The extent to which sheltering is attractive depends on the ratio of the projected dose to the protective action guide (PAG). Generally speaking, when that ratio is comparable to the reciprocal of the DRF, sheltering is effective as an emergency protective action. Also, for conditions where the projected dose is so large as to cause acute injury, and the predicted time of cloud arrival prevents effective evacuation, a reduction in dose by even a factor of 2 to 3 may be quite important.

The combined protective actions of sheltering followed by evacuation during cloud exposure (as opposed to only sheltering) can be an attractive option from the standpoint of total dose reduction. The advantage becomes increasingly more attractive as the degree of protection offered by a shelter structure decreases and/or the cloud-exposure period increases. That is, for WB DRF considerations, the shelter/evacuation option is generally more attractive for SS than LS and also for high air-change rate conditions than low ones. The air-rate change considerations are more important for the LS than the SS as far as the option advantage is concerned, and most important for thyroid dose protection. Logistically, the option can be attractive for cloud-time arrival conditions that would preclude effective evacuation coupled with increasing periods of cloud exposure.

The extent to which the results for shelter effectiveness developed in this study can be applied to the release of particulate airborne radioactive material from a nuclear incident can not be quantitatively estimated here for two reasons: 1) the relative contribution that radioactive particulates make to the total dose depends on the extent of their release; 2) the ingress of particulate fission-product material into shelter structures may be different from that assumed here for gaseous radionuclides. Overall, however, shelters would tend to offer more protection in varying degrees than that indicated here for the gaseous fission product. Therefore, application of the DRF values to particulate release material would be conservative. Further mention should be made for some specific considerations.

Shelter structures would be increasingly more effective in reducing dosages from inhalation exposures, for increasing proportions of particulate release, simply because of effective filtering action. For WB dosages, shelter structures would tend also to be somewhat more effective; however, the extent to which that may be the case is complicated by variations in the dose component contributions. In general, however, when the WB dose for nonshelter conditions (unprotected) becomes progressively more attributable to particulates, the more effective sheltering becomes. Also, LS shelters would offer more protection than SS shelters for equivalent particulate release situations.

Both experimental and analytical work is needed to more accurately and specifically assess the protective advantage of sheltering.

In the experimental area, the extent of radioactive ingress into potential shelter structures still remains uncertain. Therefore, some effort using representative structures (or models) under controlled shelter-structure conditions and a variety of correlated meteorological conditions should be undertaken to obtain reliable measurements. If possible, the experiment should also address representative particulate ingress.

Another experiment that could yield useful information for sheltering protection prediction is the measurement of WB external gamma dose from airborne cloud material for shelter structures on an inside/outside dose basis. Of course, such an undertaking may be difficult in view of the intentional controlled release of radioactive airborne material.

Such measurements, however, could possibly be obtained in conjunction with experimental programs carried out for verification of computer codes used to predict off-site doses (e.g., the ERDA Health and Safety Laboratory programs).

In the analytical area, it would be useful to make additional estimates of shelter protection for specific cases based on more definitive shelter characteristics that might correspond to specific locations. The principal specific parameters would be gamma ray attenuation, finite-source geometry-correction factors, air change rate, fallout deposition, and cloud arrival time. Also needed is model improvement regarding radionuclide source components. To that end, it would be useful to assess the effect on the shelter DRF when parent-daughter decay is considered along with specific attenuation and finite source-geometry correction actions for each radionuclide. Finally, additional analytical attention should be given to include estimates of sheltering protection for radioactive airborne releases that contain particulate material. Such a research effort would focus on the extent and nature of the particulates and their ingress into shelter structures. DRF estimates would also be made using the type of model for the gaseous fission-product release addressed in this study.

Appendix A

FALLOUT GAMMA SOURCE

FINITE GEOMETRY CORRECTION

Consider the following sketch for the dose calculated at a vertical distance d from a plane source of isotropic gamma-emitting material of source strength S_a (gammas/cm^2/sec):

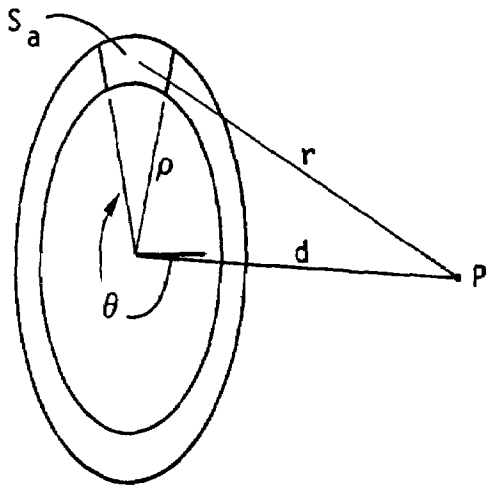

The dose rate at P from an annular source, radially bounded from R_1 to R_2, is

$$D(R_1,R_2) = kS_a \int_{R_1}^{R_2} \frac{B(\mu r)\ e^{-\mu r}}{4\pi r^2}\ 2\pi\rho\ d\rho \quad , \tag{1}$$

where k is a dose conversion constant, $B(\mu r)$ is a gamma-ray dose buildup factor, and μ is the gamma-ray absorption coefficient. The ratio of the dose $D(0,R)$ to $D(0,\infty)$ is defined here as the finite plane-source geometry correction factor given as

$$G'(R) = \frac{D(R)}{D(\infty)} = \frac{D(0,R)}{D(0,\infty)} = 1 - \frac{D(R,\infty)}{D(0,\infty)} \quad . \tag{2}$$

Assuming the Berger buildup factor form, and since $r^2 = \rho^2 + d^2$,

$$D(R,\infty) = \frac{kS_a}{2} \int_{\sqrt{R^2+d^2}}^{\infty} (1+C\mu r\ e^{D\mu r})\ \frac{e^{-\mu r}}{r}\ dr$$

$$= \frac{kS_a}{2} \left[\int_{\sqrt{R^2+d^2}}^{\infty} \frac{e^{-\mu r}}{r}\ dr + C\mu \int_{\sqrt{R^2+d^2}}^{\infty} e^{-(1-D)\mu r}\ dr \right] \quad . \tag{3}$$

Substituting $u = \mu r$ for the first integral, and evaluating:

$$D(R,\infty) = \frac{kS_a}{2} \left[\int_{\mu\sqrt{R^2+d^2}}^{\infty} \frac{e^{-u}}{u}\ du - \frac{C\mu\ e^{-(1-D)\mu r}}{(1-D)\mu} \Bigg|_{\mu\sqrt{R^2+d^2}}^{\infty} \right]$$

$$= \frac{kS_a}{2} \left[E_1\left(\mu\sqrt{R^2+d^2}\right) + \frac{C}{(1-D)}\ e^{-(1-D)\mu\sqrt{R^2+d^2}} \right] \quad , \tag{4}$$

where $E_1(x)$ is the first-order exponential integral function. Then, since $D(0,\infty) = \lim_{R \to 0} D(R,\infty)$,

$$D(0,\infty) = \frac{kS_a}{2} \left[E_1(\mu d) + \frac{C}{(1-D)}\ e^{-(1-D)\mu d} \right] \quad . \tag{5}$$

Appendix B*

DOSE REDUCTION FACTOR

DOSE COMPONENTS--UNSHELTERED

WB Fallout Gamma Source

The outside-fallout deposition rate is assumed to be

$$\frac{dF(t)}{dt} = V_g \chi_o \, e^{-\lambda t} - \lambda F(t) \quad . \tag{1}$$

Multiplying (1) by the integrating factor $e^{\lambda t}$,

$$e^{\lambda t} \frac{dF(t)}{dt} + \lambda \, e^{\lambda t} \, F(t) = V_g \chi_o \quad ,$$

which can be written as the total differential,

$$\frac{d}{dt} [e^{\lambda t} \, F(t)] = V_g \chi_o \quad . \tag{2}$$

Then, integrating

$$\int_0^t d \, [e^{\lambda t'} F(t')] = V_g \chi_o \int_0^t dt' \quad ,$$

we have

$$e^{\lambda t} \, F(t) = V_g \chi_o t$$

and then

$$F(t)_{out} = V_g \chi_o t \, e^{-\lambda t} \qquad Ci/m^2 \quad . \tag{3}$$

---

*Terms used in this appendix are listed on p. 102.

The fallout dose during cloud passage where $\chi_o \neq 0$, over the interval $(0,T_e)$, is

$$K_4 \int_0^{T_e} F(t)_{out}\, dt = V_g K_4 \chi_o \int_0^{T_e} t\, e^{-\lambda t}\, dt \qquad (4)$$

Integrating by parts,

$$\int_0^{T_e} t\, e^{-\lambda t}\, dt = -(\lambda t+1)\, \frac{e^{-\lambda t}}{\lambda^2} \Bigg|_0^{T_e} = \frac{1}{\lambda^2}\left[1-e^{-\lambda T_e}\,(\lambda T_e+1)\right] \quad . \qquad (5)$$

After cloud passage, the residual ground fallout is

$$F'(t)_{out} = F(T_e)_{out}\, e^{-\lambda t} \quad .$$

The WB gamma dose accumulated over the period (T_2+T_v) after cloud passage from residual fallout is

$$K_4 \int_0^{T_e} F'(t)_{out}\, dt = K_4 F(T_e)_{out} \int_0^{(T_2+T_v)} e^{-\lambda t}\, dt$$

$$= K_4 F(T_e)_{out}\, \frac{1}{\lambda}\left[1-e^{-\lambda(T_2+T_v)}\right] \quad . \qquad (6)$$

The outside reference fallout WB gamma dose (unprotected) due to ground-fallout deposition as given by Eqs. (5) and (6) above is

$$FD_o = V_g \chi_o K_4 \left\{ \frac{1}{\lambda^2} \left[1 - (\lambda T_e + 1)\, e^{-\lambda T_e} \right] + \frac{T_e\, e^{-\lambda T_e}}{\lambda} \left[1 - e^{-\lambda (T_2 + T_v)} \right] \right\} \quad \text{rem} \quad . \tag{7}$$

DOSE COMPONENTS--SHELTERED

Airborne Source--Inside

The rate of change of the airborne concentration in the shelter structure during cloud passage is

$$\frac{dC(t)}{dt} = \varepsilon L \chi_o\, e^{-\lambda t} - KC(t) \quad . \tag{8}$$

Choosing e^{Kt} as the integrating factor and rewriting as the total differential,

$$\frac{d}{dt}[e^{Kt} C(t)] = \varepsilon \chi_o L\, e^{(K-\lambda)t} \quad , \tag{9}$$

where $K = L+\lambda+K_f$ and $K-\lambda = L+K_f$. Integrating over the interval (0,t) where $C(0) = 0$,

$$e^{Kt}\, C(t) = \varepsilon \chi_o L \int_0^t e^{(L+K_f)t'}\, dt' = \frac{\varepsilon \chi_o L}{L+K_f} \left[e^{(L+K_f)t} - 1 \right] \quad ,$$

and the concentration is

$$C(t) = \frac{\varepsilon \chi_o L}{L+K_f} \left(e^{-\lambda t} - e^{-Kt} \right) \qquad \text{Ci/m}^3 \quad . \tag{10}$$

The dose in the shelter structure is given by integrating the concentration (10) over the interval (T_1, T_e) and multiplying by the appropriate

dose conversion and finite-source correction factors designated here by κ:

$$D = \kappa \int_{T_1}^{T_2} C(t)\, dt$$

$$= \frac{\kappa \varepsilon \chi_o L}{(L+K_f)} \left[\frac{1}{\lambda} \left(e^{-\lambda T_1} - e^{-\lambda T_e} \right) - \frac{1}{K} \left(e^{-KT_1} - e^{-KT_e} \right) \right] \quad \text{rem} \quad . \qquad (11)$$

After cloud passage, the concentration in the shelter structure as a function of time is

$$C'(t) = \frac{\varepsilon \chi_o L}{L+K_f} \left(e^{-\lambda T_e} - e^{-KT_e} \right) e^{-Kt} \qquad \text{Ci/m}^3 \quad , \qquad (12)$$

and the dose accumulated in the shelter structure over the period T_2 after cloud passage is

$$D = \kappa \int_{0}^{T_2} C'(t)\, dt$$

$$= \frac{\kappa \varepsilon \chi_o L}{(L+K_f)K} \left(e^{-\lambda T_e} - e^{-KT_e} \right) \left(1 - e^{-KT_2} \right) \qquad \text{rem} \quad . \qquad (13)$$

Surface Source--Inside

In the shelter structure, the rate of change of surface-fallout deposition (assumed on the floor space) is

$$\frac{dF(t)}{dt} = V_g' C(t) - \lambda F(t) = \frac{V_g' \varepsilon \chi_o L}{(L+K_f)} \left(e^{-\lambda t} - e^{-Kt} \right) - \lambda F(t) \quad . \qquad (14)$$

Again, choosing the integrating factor $e^{\lambda t}$ and rewriting as the total differential,

$$\frac{d}{dt}\left[e^{\lambda t}F(t)\right] = \frac{V_g \varepsilon \chi_o L}{(L+K_f)}\left(1 - e^{-K't}\right) \quad , \tag{15}$$

where $K' = (L+K_f)$.

Then, integrating where $F(0) = 0$,

$$e^{\lambda t}F(t) = \frac{V_g' \varepsilon \chi_o L}{(L+K_f)} \int_0^t \left(1 - e^{-K't'}\right) dt'$$

$$= \frac{V_g' \varepsilon \chi_o L}{(L+K_f)}\left[t - \frac{1}{K'}\left(1 - e^{-K't}\right)\right] \quad ,$$

giving the inside fallout deposition as

$$F(t)_{in} = \frac{V_g' \varepsilon \chi_o L}{(L+K_f)}\left[te^{-\lambda t} - \frac{1}{K'}\left(e^{-\lambda t} - e^{-Kt}\right)\right] \qquad Ci/m^2 \quad . \tag{16}$$

The WB external gamma dose accumulated over (T_1, T_e) is

$$FD_1 = G'K_4 \int_{T_1}^{T_e} F(t)_{in}\, dt$$

$$= \frac{G'V_g' \varepsilon \chi_o L K_4}{(L+K_f)}\left[\int_{T_1}^{T_e} t\, e^{-\lambda t}\, dt - \frac{1}{K'}\int_{T_1}^{T_e}\left(e^{-\lambda t} - e^{-Kt}\right) dt\right] \quad . \tag{17}$$

Integrating Eq. (17) above (first integral by parts) gives

$$FD_1 = \frac{V_g'G'\varepsilon\chi_o LK_4}{(L+K_f)}\left\{\frac{1}{\lambda^2}\left[(\lambda T_1+1)\ e^{-\lambda T_1} - (\lambda T_e+1)\ e^{-\lambda T_e}\right]\right.$$

$$\left. - \frac{1}{K'\lambda}\left(e^{-\lambda T_1} - e^{-\lambda T_e}\right) + \frac{1}{K'K}\left(e^{-KT_1} - e^{-KT_e}\right)\right\} \quad \text{rem} \quad . \ (18)$$

After cloud passage, the accumulated fallout level at T_e is given by Eq. (16) evaluated at T_e $(F(T_e)_{in})$, which diminishes by radioactive decay. The WB external gamma dose accumulated over interval T_2 after cloud passage is

$$FD_2 = G'K_4F(T_e)_{in}\int_0^{T_2} e^{-\lambda t}\ dt$$

$$= \frac{V_g'G'\varepsilon\chi_o LK_4}{(L+K_f)}\left[\frac{T_e\ e^{-\lambda T_e}}{\lambda} - \frac{1}{K'\lambda}\ (e^{-\lambda t} - e^{-Kt})\right]\left(1 - e^{-\lambda T_2}\right) \quad \text{rem} \quad (19)$$

After cloud passage, the continuing fallout rate in the shelter structure due to residual airborne radioiodine is

$$\frac{dF(t)}{dt} = V_g'C'(t) - \lambda F(t) \quad , \qquad (20)$$

where C'(t) is given by Eq. (12). Choosing $e^{\lambda t}$ as the integrating factor and rewriting as the total differential,

$$\frac{d}{dt}\ [e^{\lambda t}F(t)] = \frac{V_g'\varepsilon\chi_o L}{(L+K_f)}\left(e^{-\lambda T_e} - e^{-KT_e}\right)e^{-K't} \quad . \qquad (21)$$

Integrating, where F(0) = 0,

$$e^{\lambda t}F(t) = \frac{V'_g \varepsilon \chi_o L}{(L+K_f)} \left(e^{-\lambda T_e} - e^{-KT_e}\right) \int_0^t e^{-K't'}\, dt$$

$$\frac{V'_g \varepsilon \chi_o L}{(L+K_f)K'} \left(e^{-\lambda T_e} - e^{-KT_e}\right) (1 - e^{-K't}) \quad ,$$

giving the inside-fallout deposition after cloud passage as

$$F'(t)_{in} = \frac{V'_g \varepsilon \chi_o L}{(L+K_f)K'} \left(e^{-\lambda T_e} - e^{-KT_e}\right) (e^{-\lambda t} - e^{-Kt}) \quad \text{rem} \quad . \quad (22)$$

The WB external gamma dose due to $F'(t)_{in}$ accumulated over interval T_2 after a cloud passage is

$$FD_3 = G'K_4 \int_0^{T_2} F'(t)_{in}\, dt$$

$$= \frac{V'_g G' \varepsilon \chi_o L K_4}{(L+K_f)K'} \left(e^{-\lambda T_e} - e^{-KT_e}\right) \int_0^{T_2} (e^{-\lambda t} - e^{-Kt})\, dt$$

$$= \frac{V'_g G' \varepsilon \chi_o L K_4}{(L+K_f)} \left(e^{-\lambda T_e} - e^{-KT_e}\right) \left[\frac{1}{K'\lambda}\left(1 - e^{-\lambda T_2}\right) - \frac{1}{K'K}\left(1 - e^{-KT_2}\right)\right] \text{rem} \quad (23)$$

Surface Source--Outside

The WB external gamma dose accumulated over T_1 is

$$FD'_o = K_4 \int_0^{T_1} F(t)_{out}\, dt = V_g K_4 \chi_o \int_0^{T_e} t\, e^{-\lambda t}\, dt \quad .$$

Integrating by parts,

$$FD'_o = \frac{V_g \chi_o K_4}{\lambda^2} \left[1 - (T_1+1) \, e^{-\lambda T_1} \right] \quad \text{rem} \quad . \tag{24}$$

Similarly, the WB external gamma dose inside the shelter structure accumulated over interval (T_1, T_e) from outside-fallout deposition is

$$FD'_1 = A' K_4 \int_{T_1}^{T_e} F(t)_{out} \, dt$$

$$\frac{A' V_g \chi_o K_4}{\lambda^2} \left[(\lambda T_1+1) \, e^{-\lambda T_1} - (\lambda T_e+1) \, e^{-\lambda T_e} \right] \quad \text{rem} \quad . \tag{25}$$

SHELTERING AND EVACUATION--VEHICLE AIRBORNE CONCENTRATION

The rate of concentration change in the vehicle is

$$\frac{dC(t)}{dt} = \varepsilon \chi_o L_v \, e^{-\lambda t} - K_v C(t) \quad , \tag{26}$$

where $K_v = L_v + \lambda$.

Choosing $e^{K_v t}$ as the integrating factor and rewriting,

$$\frac{d}{dt} \left[e^{K_v t} \, C(t) \right] = \varepsilon \chi_o L_v \, e^{L_v t} \quad . \tag{27}$$

Integrating where $C(0) = 0$,

$$e^{K_v t} \, C(t) = \varepsilon \chi_o \left(e^{L_v t} - 1 \right)$$

and the concentration is

$$C(t) = \varepsilon\chi_o\left(e^{-\lambda t} - e^{-K_v t}\right) \qquad Ci/m^3 \quad . \qquad (28)$$

DEFINITION OF TERMS

$F(t)$ = fallout (per unit area)

$C(t)$ = inside airborne concentration (per unit volume)

χ_o = outside airborne concentration (per unit volume)

V_g = deposition velocity outside

V'_g = deposition velocity inside

λ = radioactive decay constant (per unit time)

K_4 = fallout dose conversion constant

κ = dose conversion constant

T_e = cloud exposure period

T_1 = shelter entrance delay period

T_2 = shelter period after cloud passage

T_v = evacuation period away from shelter

L = ventilation turnover rate (per unit time)

$K_f = V'_g/\ell$ (per unit time)

ℓ = mean fall distance for iodine inside

$K = L + \lambda + K_f$

ε = ingress fraction

G' = finite-source correction factor for fallout

L_v = ventilation turnover rate for vehicle (per unit time).

REFERENCES

1. *Reactor Safety Study, Appendix VI: Calculation of Reactor Accident Consequences*, WASH-1400 (Draft), U.S. Atomic Energy Commission, August 1974.

2. Bell, M. J., *ORIGEN--The ORNL Isotope Generation and Depletion Code*, ONRL-4628, May 1973.

3. *Nucleonics*, Data Sheets No. 1-30, March 1955-February 1959.

4. *The Potential Radiological Implications of Nuclear Facilities in the Upper Mississippi River Basin in the Year 2000*, WASH-1209, U.S. Atomic Energy Commission, January 1973.

5. *Radiological Health Handbook*, PB-1211784R, U.S. Department of Health, Education and Welfare, Public Health Service, September 1960 (Rev. Ed.).

6. Sabersky, R. H., D. A. Sinema, and F. H. Shair, *Environ. Sci. Technol.*, *7*, 1973, p. 347.

7. Handley, T. H., and C. J. Barton, *Home Ventilation Rates: A Literature Survey*, ONRL-TM-4318, September 1973.

8. Private communication with Dennis Latham, Los Angeles City Building and Safety Department, Health Division.

9. Yocum, J. E., W. L. Clink, and W. A. Cote, "Indoor/Outdoor Air Quality Relationships," *J. Air Poll. Contr. Assoc.*, *21*, May 1971, pp. 251-259.

10. *ASHRAE Handbook of Fundamentals*, American Society of Heating, Refrigeration, and Air Conditioning Engineers, New York, 1967.

11. Coblentz, C. W., and P. R. Achenbach, *ASHRAE Journal*, *5*, 1963, p. 69.

12. Megaw, W. J., *Intl. J. Air Wat. Poll.*, *6*, 1962, pp. 121-128.

13. Kabat, M.J., "Iodine Forms and Removal Efficiencies," panel Discussion (Radioiodine Behavior Related to Power Reaction), *Trans. Amer. Nucl. Soc.*, *21*, 1975, p. 86.

14. Private communication with M. J. Kabat, Ontario Hydro, Pickering, Ontario, Canada.

15. Hawley, C. A., Jr., *et al.*, *Controlled Environmental Radioiodine Tests at the National Reactor Testing Station, 1965 Progress Report*, IDO-12047, February 1966.

16. Bigger, M. M., R. J. Crew, and R. K. Fuller, *Non-Ingested Dose Associated with Particulate Ingress into a Prototype Shelter Via the Ventilation System*, USNRDL-TR-815, January 1965.

17. Burson, Z. G., and A. E. Profio, *Structure Shielding from Cloud and Fallout Gamma-Ray Sources for Assessing the Consequences of Reactor Accidents* (Draft), E.G.&G., Las Vegas, Nevada, March 1975.

18. Chabot, G. E., and K. W. Skrable, "A Simple Formula for Estimation of a Surface Dose and Photons Emitted from a Finite Cloud," *Health Physics, 27*, July 1974, pp. 153-155.

19. *Design and Review of Structures for Protection from Fallout Gamma Radiation*, PM-100-1, Department of Defense, Office of Civil Defense, February 1965.

20. Auxier, J. A., J. O. Buchanan, C. Eisenhauer, and H. E. Menker, *Experimental Evaluation of the Radiation Protection Afforded by Residential Structures Against Distributed Sources*, CEX-58.1, January 1969.

21. Burson, Z. G., D. Parry, and H. Borella, *Experimental Evaluation of the Fallout Radiation Protection Afforded by a Southwestern Residence*, CEX-60.5, February 1962.

22. Burson, Z. G., *Experimental Radiation Measurements in Conventional Structures, Part I*, CEX-59.7B, July 1966.

23. Strickler, T. D., and J. A. Auxier, *Experimental Evaluation of the Radiation Protection Afforded by Typical Oak Ridge Homes Against Distributed Sources*, CEX-59.13, April 1960.

24. Summers, R. L., and Z. G. Burson, *Experimental Evaluation of Techniques for Improving Fallout Protection in Home Basements*, CEX-65.5, December 1966.

25. *DCPA Attach Environment Manual*, Chapter 6, "What the Planner Needs to Know About Fallout," CPG-2-1A6, Defense Civil Preparedness Agency, Department of Defense, June 1973.

26. Burson, Z. G., *Experimental Evaluation of the Fallout Radiation Protection Provided by Structures in the Control Point Area of the Nevada Test Site*, CEX-69.5, October 1970.

27. Burson, Z. G., *Experimental Evaluation of the Fallout-Radiation Protection Provided by Selected Structures in the Los Angeles Area*, CEX-61.4, February 1963.

28. Borella, H., Z. G. Burson, and J. Jacovitch, *Evaluation of the Fallout Protection Afforded by Brookhaven National Laboratory Medical Research Center*, CEX-60.1, October 1961.

29. Stevens, P. N., and D. K. Trubey, *Weapons Radiation Shielding Handbook*, Chapter 3, "Methods for Calculating Neutron and Gamma-Ray Attenuation," DNA-1892-3, Rev. 1, March 1972.

30. Ramsey, W., and P. R. Reed, *Land Use and Nuclear Power Plants, Case Studies of Siting Problems*, WASH-1319 (no date).

31. *Manual of Protective Action Guides and Protective Actions for Nuclear Incidents*, U.S. Environmental Protection Agency, Office of Radiation Programs, Environmental Analysis Division, September 1975.

32. Dickerson, M. H., and R. C. Orphan, *Atmospheric Release Advisory Capability (ARAC): Development and Plans for Implementation*, UCRL-51839, June 1975.

33. Burson, Z. G., *Health Physics, 26*, January 1974, pp. 41-44.

34. Petersen, G. A., and R. H. Sabersky, *J. of the Air Poll. Contr. Assoc., 25*, October 1975, pp. 1028-1032.

35. Guyton, H. G., *et al., A.M.A. Arch. Indus. Health, 20*, August 1959, pp. 91-95.

★ U.S. GOVERNMENT PRINTING OFFICE: 1978—720-335/6098